공학박사학위논문

Studies on the Synthesis of Novel Structured Polyamides by Reactive Extrusion and Their Physical Properties

반응압출을 통한 새로운 구조의 폴리아미드 합성 및 물성에 관한 연구

2015년 2월

서울대학교 대학원

재료공학부

오 경 환

Studies on the Synthesis of Novel Structured Polyamides by Reactive Extrusion and Their Physical Properties

반응압출을 통한 새로운 구조의 폴리아미드 합성 및 물성에 관한 연구

지도교수 서 용 석

이 논문을 공학박사학위논문으로 제출함

2015년 2월

서울대학교 대학원

재료공학부

오 경 환

오경환의 박사학위논문을 인준함

2015년 2월

위 원 장	윤 재 륜 (인)
부위원장	서 용 석 (인)
위 원	홍 성 현 (인)
위 원	유 웅 렬 (인)
위 원	곽 순 종 (인)

Abstract

Studies on the Synthesis of Novel Structured Polyamides by Reactive Extrusion and Their Physical Properties

Kyunghwan Oh

Department of Materials Science and Engineering

The Graduate School

Seoul National University

Reactive extrusion (REX) is an attractive polymer processing, in order to carry out melt blending as well as various chemical reactions including polymerization, grafting, branching and functionalization simultaneously. In addition, REX involves introducing reactive agents in the reaction sequence, homogenizing the ingredients and allowing sufficient time for the completion of the reactions. It can be performed that melt blending and chemical reaction at the same time through REX process, compared to typical extrusion which is only used in mixing or blending. Therefore, production and processing can be carried out in one-stage processing. According to its unique characteristic features, REX has provided different types of chemical reactions such as polymerization of monomers, modification of polymer by grafting or crosslinking and coupling reaction between homopolymer. Many researches have been carried out for

polymerization or modification, but two or more chemical reactions took place simultaneously in REX process has been scarcely reported yet. Also, obtaining the high-performance polymer from the monomers by REX has been very difficult due to the extreme high-sensitivity of chemical reactions which are affected by temperature, composition, residence time and so on.

In this study, Polyamide 6 (PA6, Nylon 6) based composites had been in-situ polymerized well through REX from monomers with bifunctional additives (diepoxy and diamine). In extruder, both polymerization of PA6 and modification reaction were taken place simultaneously. Both type of additives acted as chain extender resulted in increasing the molecular weight of PA6 polymer and enhancing the physical properties. Polymerization reaction and performance of composites were very sensitive to the composition of reactants and reaction condition, so precious control was needed.

We also produced thermotropic liquid crystalline epoxy (LCE) based liquid crystalline polymer (LCP) with various monoamines through REX. Epoxy groups of LCE had been reacted linearly with primary monoamine, and successfully polymerized to form thermotropic LCPs. Unfortunately, we failed to obtain high molecular weight and narrow PDI LCPs. However, it is worth that we suggested the possibility of manufacturing thermotropic LCPs through in-situ REX process.

KEYWORDS: Polyamide 6, Nylon 6, Ring opening polymerization, Anionic polymerization, In-situ, Reactive extrusion, Diepoxy, Diamine, Chain extender, Liquid crystalline epoxy, Primary monoamine, Liquid crystalline polymer

Student Number: 2007-20723

Contents

Chapter 3

Modification of Polyamide 6 with diamine chain extenders through in-situ polymerization by reactive extrusion and its properties.

Chapter 4

In-situ polymerization of epoxy based thermotropic liquid crystalline polymers by reactive extrusion and its liquid crystalline behaviors.

List of Tables

List of Schemes

List of Figures

N at 170℃ (c) LCE3-A at 220℃ (d) LCE3-N at 190℃

Chapter 1

Introduction

1.1 Reactive extrusion

Reactive extrusion (REX) is an attractive polymer processing, in order to carry out melt blending as well as various chemical reactions including polymerization, grafting, branching and functionalization simultaneously. In addition, REX involves introducing reactive agents in the reaction sequence, homogenizing the ingredients and allowing sufficient time for the completion of the reactions. It can be performed that melt blending and chemical reaction at the same time through REX process, compared to typical extrusion which is only used in mixing or blending. The REX instrument is illustrated briefly in Figure 1.1. The reactants are fed into the extruder, usually through a feed hopper, but sometimes fed into specific points in the extrusion sequence. The reactive mixture is conveyed through the extruder, and the reaction is driven to the desired degree of completion. After removing any volatile by-products through vent port, the molten polymeric product is pumped out through a die and subsequently quenched, solidified, and pelletized. Therefore, production and processing can be carried out in one-stage processing and hence REX is very cost and time efficient process.

REX has some advantages as follows. First, the high viscous materials can be

handled without any solvents by REX. Polymers are produced by REX in ready-to-used form from the monomers, therefore the cost and total processing time are reduced dramatically. Also, chemical reactions such as polymerization, crosslinking and grafting are carried out during mixing in extruder simultaneously. Second, REX can be one of the solutions for heat and mass transfer problems that arise when viscosity of the reaction medium increases in batch polymerization process. In batch reactor, as the polymerization proceeds, the viscosity increases and the materials become unmanageable in terms of mixing and heat transfer at certain point. But, in extruder, new thin surface layers are continuously created that can increase the degree of mixing and minimize temperature gradients. Finally, the residence time can be controlled by REX via operating conditions and geometry of screw extruders. Generally, long exposure to high temperature causes polymer degradation. However, this problem can be overcomed by using REX because the residence time is substantially lower as compared to that in a batch reactor.

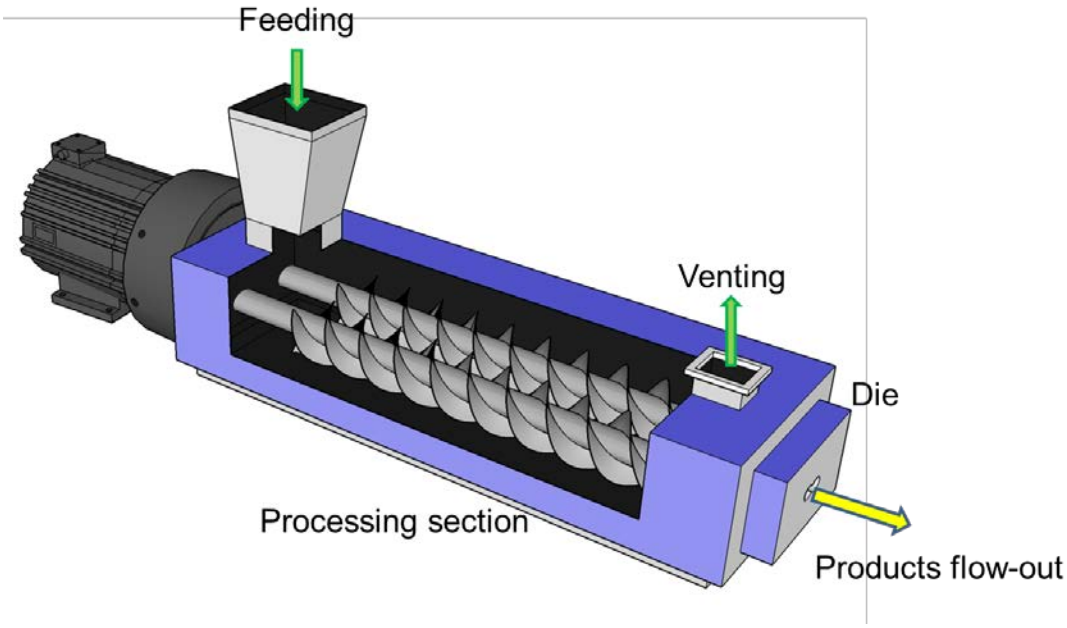

Figure 1.1 Reactive extrusion.

1.2 Objectives

According to its unique characteristic features, REX has provided different types of chemical reactions as follows.

- ✓ Free radical, anionic, cationic, condensation polymerizations of monomers to high molecular weight polymers.
- ✓ Polymer modification by grafting or crosslinking of materials onto the backbone of polymers for improving various properties.
- ✓ Coupling reactions that involves reaction of homopolymer with another polymer or multifunctional coupling agent in the preparation of high-performance products.

Many researchers have been applied REX process on various polymerization reactions. Kim et al. reported bulk ring opening polymerization (ROP) of caprolactone carried out in a twin-screw extruder.[1,2] ROP of caprolacone was investigated through REX processing for various ratio of monomer to initiator as well as under a range of different processing conditions. Nylon 6 had been successfully synthesized through anionic ring opening polymerization of caprolactam in a twin-screw extruder.[3,4] Tang et al. researched about the PET-block-PCL block copolymer fibers which have been developed through REX.[5] The synthesis of PET-block-PCL block copolymers was carried out by ROP of caprolactone initiated by hydroxyl terminated PET with catalyst. Also, modification of polymers has been carried out in many researches. Polypropylene

(PP) and Polyethylene (HDPE, LDPE, LLDPE) have been modified by radical-induced grafting of monomers in REX process such as maleic anhydride (MAH) resulted in MAH-PE or MAH-PP grafting polymers.[6-9] Nylon, polyester, polyether and polycarbonate have been blended with various coupling agents or polymers which had reactive functional groups on it. Seadan et al. have examined a one-step process in which polyolefin (PP or PE), MAH, peroxide and Nylon are combined in an extrusion process to form a compatibilized polyolefin–nylon blend.[10] Phan et al. have examined the compounding of low molecular weight α,γ-diamino-poly(propyleneoxide) with blends of MAH–PP and MAH–EPDM with the aim of achieving compatibilization of the PP and rubber phases by forming linkages between the two polymers.[11]

In most cases, either polymerization of monomers or modification of polymer has been carried out respectively. However, there are little researches have been carried out two or more chemical reactions took place simultaneously in REX process. Also, obtaining the high-performance polymer from the monomers by REX have been very challengeable because it is hard to control the molecular weight and molecular weight distribution due to the extreme high-sensitivity of chemical reactions which are affected by temperature, composition, residence time and so on.

In this study, we tried to synthesize the high-performance polymer by in-situ REX process. Simultaneously, modification and enhancement of polymer were also performed in REX process with reactive additives which had reactive functional groups and designed chemical structure. In order to achieve both polymerization and modification of polymer at the same time in extruder, we adopted a new reactive system which has been not reported yet. Furthermore, we synthesized thermotropic liquid crystalline polymer from the monomer by using REX. Also we investigated the reaction

mechanism as well as physical properties of the polymers.

1.3 References

[1] Kim, B. J.; White, J. L. J Appl Polym Sci 2004, 94, (3), 1007-1017.

[2] Kim, B. J.; White, J. L. Int Polym Proc 2002, 17, (1), 33-43.

[3] Tang, W. M.; Murthy, N. S.; Mares, F.; McDonnell, M. E.; Curran, S. A. J Appl Polym Sci 1999, 74, (7), 1858-1867.

[4] Kye, H.; White, J. L. J Appl Polym Sci 1994, 52, (9), 1249-1262.

[5] Hornsby, P. R.; Tung, J. F.; Tarverdi, K. J Appl Polym Sci 1994, 53, (7), 891-897.

[6] Shi, D.; Yang, J. H.; Yao, Z. H.; Wang, Y.; Huang, H. L.; Jing, W.; Yin, J. H.; Costa, G. Polymer 2001, 42, (13), 5549-5557.

[7] Oliphant, K. E.; Russell, K. E.; Baker, W. E. Polymer 1995, 36, (8), 1597-1603.

[8] Kelar, K.; Jurkowski, B. Polymer 2000, 41, (3), 1055-1062.

[9] Pesetskii, S. S.; Jurkowski, B.; Krivoguz, Y. M.; Kelar, K. Polymer 2001, 42, (2), 469-475.

[10] Seadan, M.; Graebling, D.; Lambla, M. Polym Netw Blen 1993, 3, (3), 115-124

[11] Phan, T. T. M.; DeNicola, A. J.; Schadler, L. S. J Appl Polym Sci 1998, 68, (9), 1451-1472.

Chapter 2

In-situ polymerization of Polyamide 6 with 1,4-di(2,3-epoxypropyloxy) benzene in reactive extrusion and its properties.

2.1 Introduction

Polyamide 6 (PA6), known as Nylon 6, is one of the widely used engineering polymers in film, fiber, textile and packaging industry because of their excellent advantages on ductility, toughness, durability and price. Besides, PA6 can be polymerized from ε-caprolactam monomer through ring opening anionic polymerization (ROP) within several minutes with various activators.[1-3] This attractive advantage makes possible that anionic polymerization of PA6 applied in in-situ processing field such as reactive injection molding (RIM) and reactive extrusion (REX).[4-6]

Another remarkable feature of PA6 is the excellent reactivity. Amine and carboxylic acid groups at the end of PA6 chain as well as amide linkage can become active easily. They can react with various functional groups of organic/inorganic materials. Especially, epoxide can reacts well with both amide linkage and amine end group of PA6 chain, so many researchers had focused on the reactive PA6/epoxy blends.[7,8] Gorton reported that amide linkage of PA6 reacted with epoxy group in PA6/epoxy adhesive blends.[7] He found that the epoxy resin crosslinks the nylon through the reaction of oxirane group

with amide nitrogen in nylon chain. Zhong et al investigated the miscibility and cure kinetics of PA/epoxy reactive blends with various compositions.[8]

A lot of PA6/epoxy reactive blends have been studied. But, investigations of reactive PA6/epoxy blends from in-situ polymerization of ε-caprolactam rarely reported. Gupta et al. synthesized reactive blends of epoxy resin and PA6 through the anionic polymerization of ε-caprolactam.[9] They successfully synthesized PA6/epoxy blends in the flask or mold and optimized the synthesis condition. But, within our knowledge, no researches are reported that combines PA6/epoxy blends with in-situ REX process yet.

In this study, we performed in-situ polymerization of the PA6/epoxy composites from monomers through reactive extrusion process. Also, reaction conditions optimized and expected mechanisms were proposed. Rheological and mechanical properties of PA6/epoxy composites were investigated with this study.

2.2 Experimental

2.2.1 Materials

ε-caprolactam used in this study was procured from Capro Corporation (Korea). Sodium hydride, N-acetyl caprolactam, hydroquinone, 3-bromopropene and 3-chloroperoxybenzoic acid were purchased from Aldrich. 1,4-di(2,3-epoxypropyloxy) benzene (HQEP1, Figure 2.1 (a)), which acted as diepoxide reactant in our system, was synthesized in laboratory.

2.2.2 Synthesis

2.2.2.1 Synthesis of sodium caprolactam (Na-CL)

Before synthesis, ε-caprolactam was dried at 100℃ oven for 24 hours and 50℃ vacuum oven for 48 hours to completely remove the moisture. 1mol of dried ε-caprolactam was put in the round flask under an argon atmosphere. After ε-caprolactam was completely melted at 70℃, 0.05 mol of sodium hydride was added with stirring. When hydrogen emission was stopped, the mixture was stirred under an argon atmosphere for 10 min to react. The mixture was cooled to room temperature and pulverized. Obtained sodium caprolactam (Figure 2.1 (b)) powder was stored in argon charged container.

2.2.2.2 Synthesis of 1,4-di(2,3-epoxypropyloxy) benzene (HQEP1)

Synthetic scheme was reported by Jun Yeob Lee.[10] HQEP1 was purified by column chromatography using CH_2Cl_2 as an eluent solvent. After evaporation of solvent, the HQEP1 product recrystallized in Chloroform.

Melting temperature: 117℃. Yield: 55%. H-NMR spectrum ($CDCl_3$): δ (ppm) 6.86 (4H, s), 4.16 (2H, dd), 3.90 (2H, dd), 3.33 (2H, m, CH of epoxy), 2.89 (2H, dd, CH_2 of epoxy), 2.74 (2H, dd, CH_2 of epoxy).

2.2.3 In-situ polymerization of PA6/epoxy composites by reactive extrusion

The whole polymerization process illustrates briefly in Figure 2.2. Reactant mixtures were composed of ε-caprolactam, sodium caprolactam, N-acetyl caprolactam and HQEP1 which were monomer, initiator, activator and epoxy additives each. The mol ratio of monomer : initiator : activator was optimized as 50 : 1 : 1 in terms of both high polymer yield and short polymerization time by pre-experimental. The mol ratio of HQEP1 contents to 1mol of initiator was 0.05, 0.1, 0.15, 0.2 mol for each sample. The reactant mixtures were fed into twin screw extruder (BA-19, Bau tech), with flowing an argon to prevent the quenching of anionic initiator by moisture. The temperature profiles from feeding zone to die were set 140/160/180/210/210/210/230℃ and screw speed was set to 50 rpm. Extruded PA6/HQEP1 composite fiber was pelletized and dried at 60℃ vacuum oven for sufficient time before characterization.

2.2.4 Characterization

Differential scanning calorimetry (DSC, DSC 823e, METTLER TOLEDO) was used to analyze the thermal properties of PA6/HQEP1 composites. Under a nitrogen atmosphere, samples were first heated from 25℃ to 280℃ at 10 ℃/min, cooled to 25℃ and heated to 280℃ again at same heating rate. The degree of crystallinity (X_c) was obtained by following equation.

$$X_c(\%) = \frac{\Delta H_m}{\Delta H_{100}} \times 100$$

ΔH_m is the specific enthalphy of melting, and ΔH_{100} is the enthalphy of melting with fully crystalline PA6 which is 190 J/g in this study.[11] The Fourier transform infrared spectrometer (FT-IR) spectra analysis was also carried out. Before measurement, the extruded PA6/HQEP1 pellets were hot pressed at 240℃ and cooled to room temperature to obtain films. To check both polymerization of ε-caprolactam and reaction of oxirane ring, FT-IR (Nicolet 6700, Thermo Scientific(USA)) with ATR accessory was used. The spectra were recorded with 32 scans at 8 cm^{-1} resolution. Intrinsic viscosity (η) was measured to calculate the viscosity average molecular weight (M). By using Ubbelohde viscometer, the time for polymer solution passed through capillary was checked at 25℃ in 90% formic acid solution. Molecular weights of PA6/HQEP1 composites were calculated by Mark-Houwink equation.

$$[\eta] = K(M)^a$$

The Mark-Houwink constants are K = 22.6 x 10^3 (mL/g) and a = 0.82 for PA6 at 25℃ in 90% formic acid solution.[12] Rheological properties were studied through Advanced Rheometric Expansion System (ARES, Rheometric Scientific). Samples were prepared

in mold with diameter 25 mm and thickness 1mm at 240℃ by injection molding. Storage, loss modulus and complex viscosity were measured between parallel plates at 250℃, applied strain 10% and angular frequency from 0.05 to 500 rad/s. For tensile test, specimens were prepared according to ASTM D638 by injection molding at 240℃. The mechanical properties were tested through Instron (5567, Instron) with crosshead speed of 10 mm/min. The values of various mechanical properties were determined the average of 10 tested values for each PA6/HQEP1 sets.

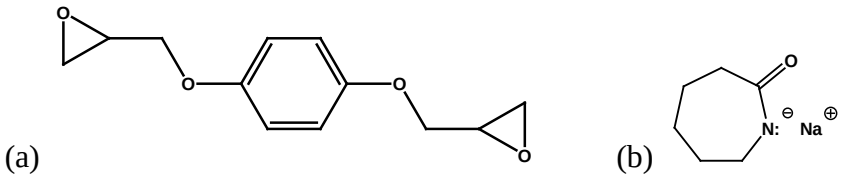

Figure 2.1 Structures of materials. (a) HQEP1 (b) sodium caprolactam

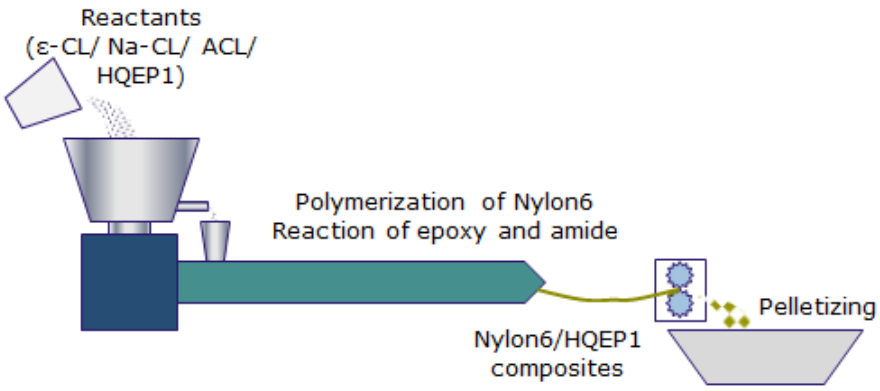

Figure 2.2 Polymerization process. The composition of reactant mixture was controlled to set as monomer : initiator : activator : HQEP1 = 50 : 1 : 1 : (0, 0.05, 0.1, 0.15, 0.2) mol.

2.3 Results and discussion

2.3.1 Reaction mechanism

The mechanisms of major possible reactions are shown in Scheme 2.1. In Scheme 2.1 (a), N-acetyl caprolactam reacts with sodium caprolactam anion and caprolactam ring is opened. Then living anion attacks a ε-caprolactam monomer and extracts a proton, generating a new living anion. This new anion acts as nucleophile, opening the caprolactam ring of dimer. As a result, trimer with living anion is formed and this anion reacts with another ε-caprolactam monomer. The chain propagation continues until the anion is quenched and high molecular PA6 was polymerized. Crosslinking mechanism of PA6 with HQEP1 is exhibited in Scheme 2.1 (b). It is reported in other researches on PA6/DGEBA curing reaction.[8,9,13] The oxirane ring is opened by nucleophilic attack to the living anion of PA6. As a result, crosslinking between two PA6 chains was formed, quenching the living anion. When small amount of HQEP1 is existed, polymerization is more predominant than crosslinking reaction due to the low probability of quenching the anion with oxirane ring. On the other hand, above adequate amount of HQEP1 is added, total polymerization reaction is depressed because of reaction (b). There is another reaction existed during curing in Scheme 2.1 (c) at high temperature and long reaction time. In our study, this type of reaction scarcely occurred during the polymerization because of the small amount of diamine and short residence time in extruder.

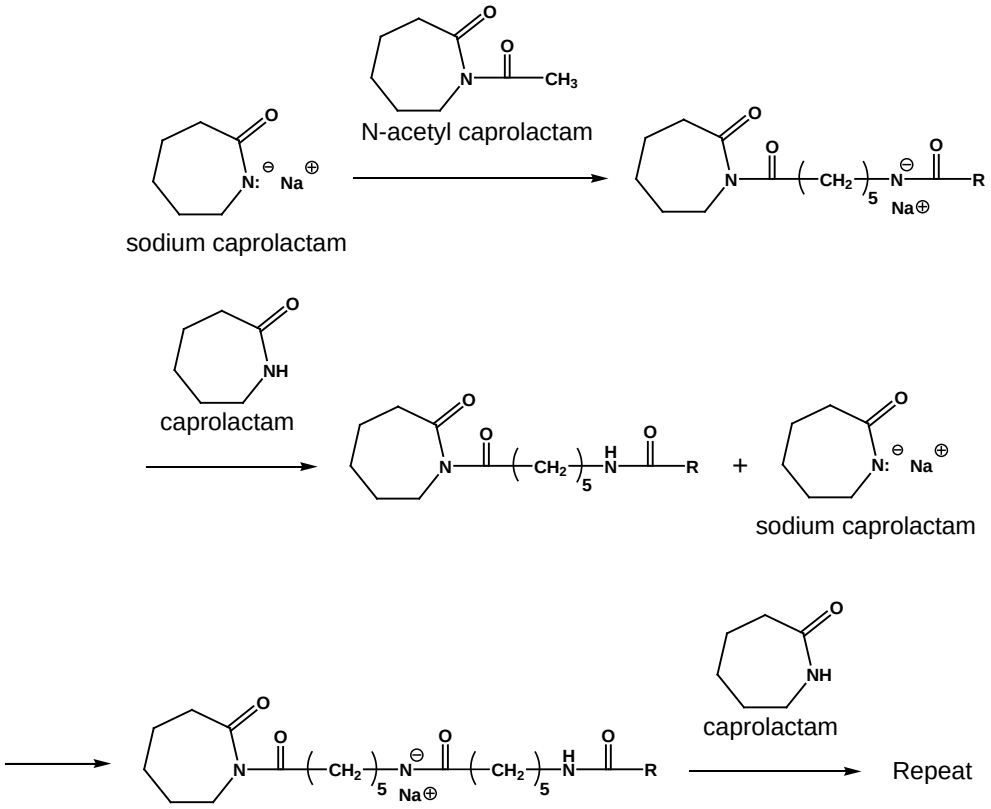
N-acetyl caprolactam
sodium caprolactam
caprolactam
sodium caprolactam
caprolactam
Repeat

(a)

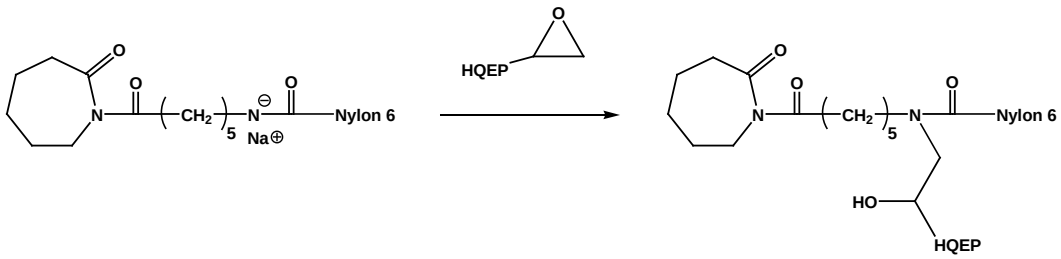

(b)

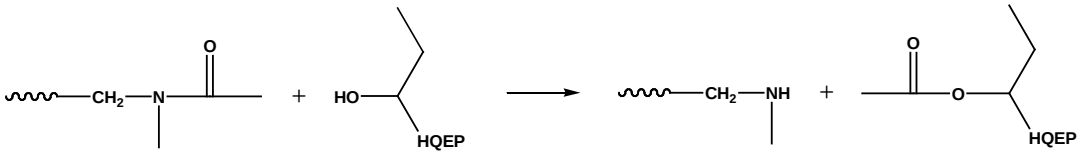

(c)

Scheme 2.1 Reaction schemes. (a) polymerization of ε-caprolactam to form PA6 (b) crosslinking reaction of PA6 with HQEP1 (c) formation of ester

2.3.2 Polymerization of PA6/epoxy composites by reactive extrusion

The heating DSC scanning result of PA6/HQEP1 composites is exhibited in Figure 2.3. Exact values of melting temperature, enthalpy of melting and crystallinity are given in Table 2.1. All composites show only one exothermic peak between 212 and 214℃ which have known as melting point of PA6 except the mol ratio of epoxy 0.25 composite. It means that all monomers reacted completely and PA6 had been well polymerized up to the mol ratio of epoxy 0.2. On the contrary, two broad exothermic peaks existed around 70℃ and 190℃ for mol ratio of epoxy 0.25 sample, each are the melting temperature of residual ε-caprolactam and very low molecular weight polyamide (maybe oligomer). Over the mol ratio of 0.2 HQEP1 added, the polymerization of ε-caprolactam was incomplete and an amount of monomers remained. Because the large amount of epoxy could quench the active anions during the polymerization. So in this study, we investigated composites content under 0.2 mol ratio of HQEP1.

Both enthalpy of melting (ΔH_m) and crystallinity (X_c) was reduced upon epoxy introduction during the melting temperature did not show any remarkable difference. It is indicated that the crystallization of PA6 was hindered by epoxy molecules. It is supposed that the part of lightly crosslinked PA6 chains with epoxy were hard to crystallize because of low chain mobility. A similar result already had been reported with different kind of epoxy chain extender.[14] Generally, crystallinity drop with chain extender concentration which was attributed to the increase of the molecular weight that hinders the arrangement of the macromolecules in a crystalline phase. In our research,

the crystallinity drop was largely affected by the hindrance of lightly crosslinked chains and increase of molecular weight.

To investigate the reaction of epoxy with PA6, we analyzed FT-IR spectra (Figure 2.4). For both PA6 and the mol ratio 0.1 composite, the sharp absorption peaks were exhibited at 3300, 2934 and 2865 cm^{-1}. Theses peaks are due to the hydrogen bonded NH stretching, asymmetric and symmetric stretching of CH_2 respectively. Peaks at 1635 and 1540 cm^{-1} belongs to absorption of amide, and peak at 1170 cm^{-1} can be attributed to CONH skeletal motion.[15] This means that ε-caprolactam completely polymerized to form PA6 with or without HQEP1 additives. But, as HQEP1 added, absorption of broad shoulder peak at about 3450 cm^{-1} increased which was attributed to the stretching vibration of the OH group due to the reaction between oxirane ring with amide. Also, no peaks observed at 914 cm^{-1} in PA6/HQEP1 composite, which was ascribed to the absence of the vibration of oxirane ring (Figure 2.4 (b)). It confirms that epoxy groups were completely reacted with amide linkage. Back to the reaction Scheme 2.1 (c), if the side reaction occurred during crosslinking, the ester group was formed. As a result, there should be existed the absorption of the carbonyl of ester. Zhong et al and Gupta et al reported that a new peak appeared at 1720 cm^{-1} after curing with the high concentration of PA6/epoxy blends.[8,9] Due to the secondary amine group could react further with the epoxide groups. However, in our case, small amounts of epoxide crosslinked with PA6 in the twin screw extruder within short residence time. So there are no further side-reactions with epoxides and amide linkage.

The molecular weight of PA6/HQEP1 composites calculated from intrinsic viscosity, and the values are given in Figure 2.5 and Table 2.1. Neat PA6 was well polymerized and its molecular weight is 25,200 g/mol. The molecular weight of composites were

increased with mol ratio of 0.05 HQEP1 contents, but decreased with increasing HQEP1 composition. It seemed that PA6 chain lengthened due to the reaction with diepoxide. Epoxy groups of HQEP1 reacted with amide linkage of PA6, affecting to whole molecular weight in two ways. First, it increased molecular weight by connecting two PA6 chains. Simultaneously, it decreased molecular weight by quenching the living anion. So the more HQEP1 was added, the molecular weight drop was shown. Beyond the mol ratio of HQEP1 0.15 added, molecular weights were even smaller than neat PA6. We supposed that some amount of epoxide ring quenched the anionic polymerization of PA6 (Scheme 2.1 (b)). Consequentially, to obtain high molecular weight PA6 composite, controlled composition of epoxy additives is required.

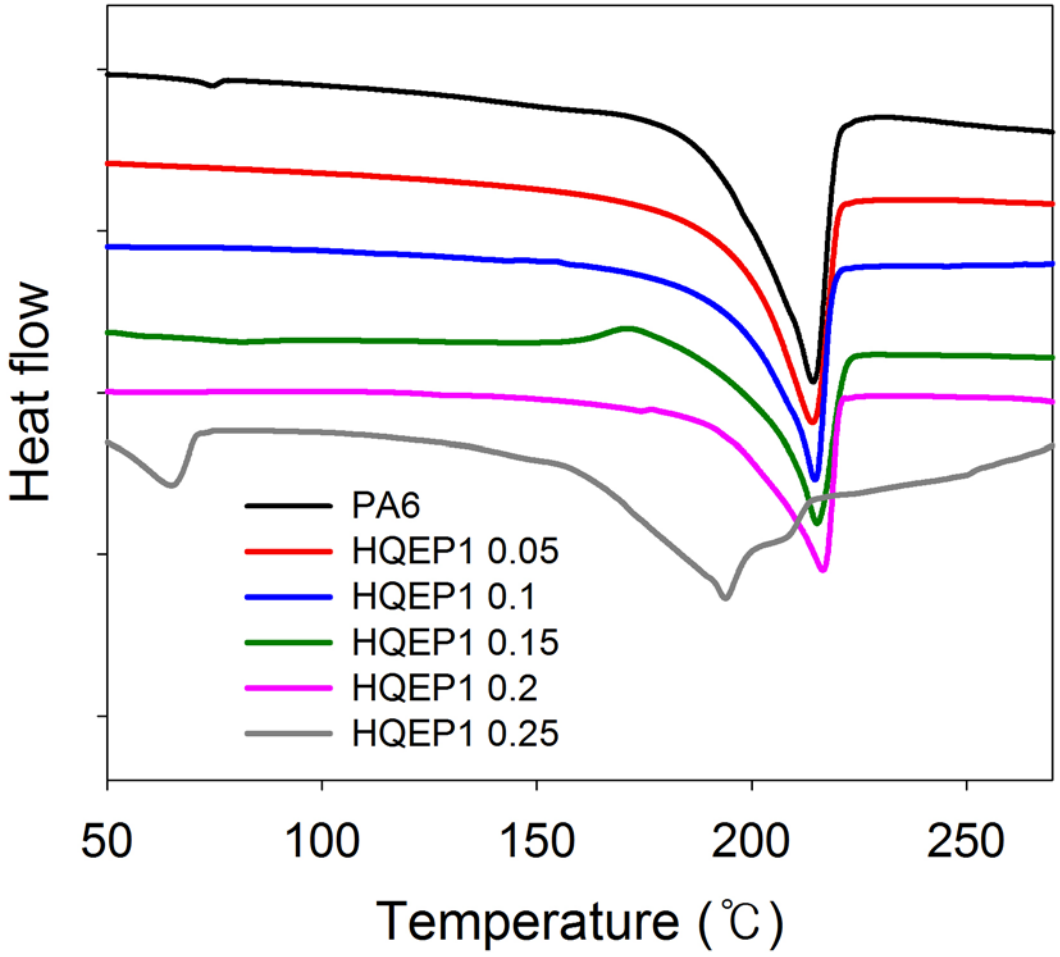

Figure 2.3 DSC heating thermogram curves.

Mol ratio of HQEP1 to initiator	T_m (℃)	ΔH_m (J/g)	X_c (%)	Molecular weight (g/mol)
0	213.6	68.02	35.8	25,200
0.05	212.8	61.18	32.2	29,200
0.1	213.5	59.66	31.4	27,500
0.15	213.7	53.77	28.3	23,900
0.2	214.2	48.83	25.7	20,200

Table 2.1 Melting temperature, enthalphy of melting and molecular weight of PA6/HQEP1 composites.

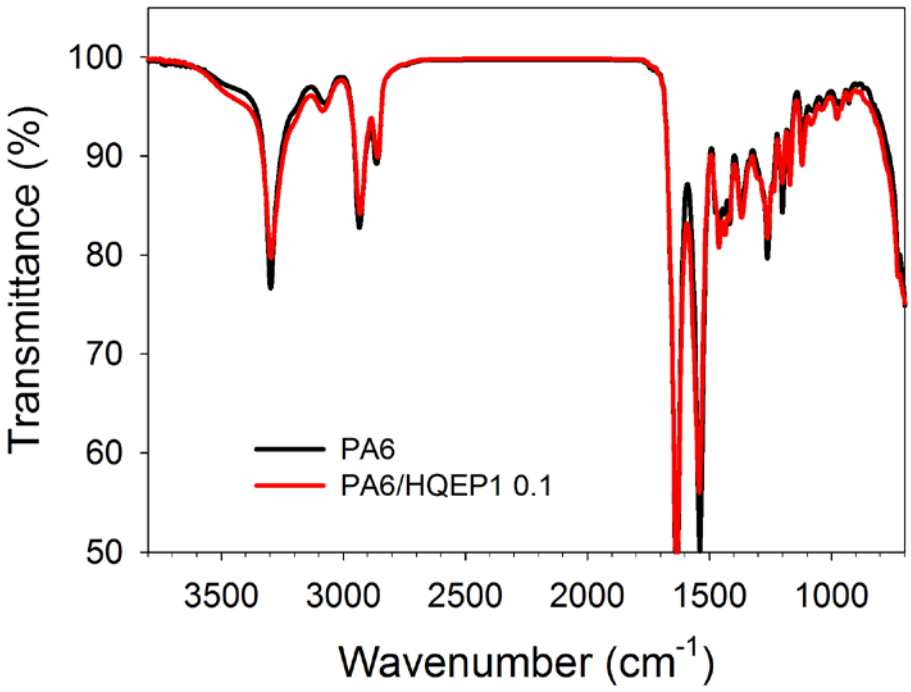

(a)

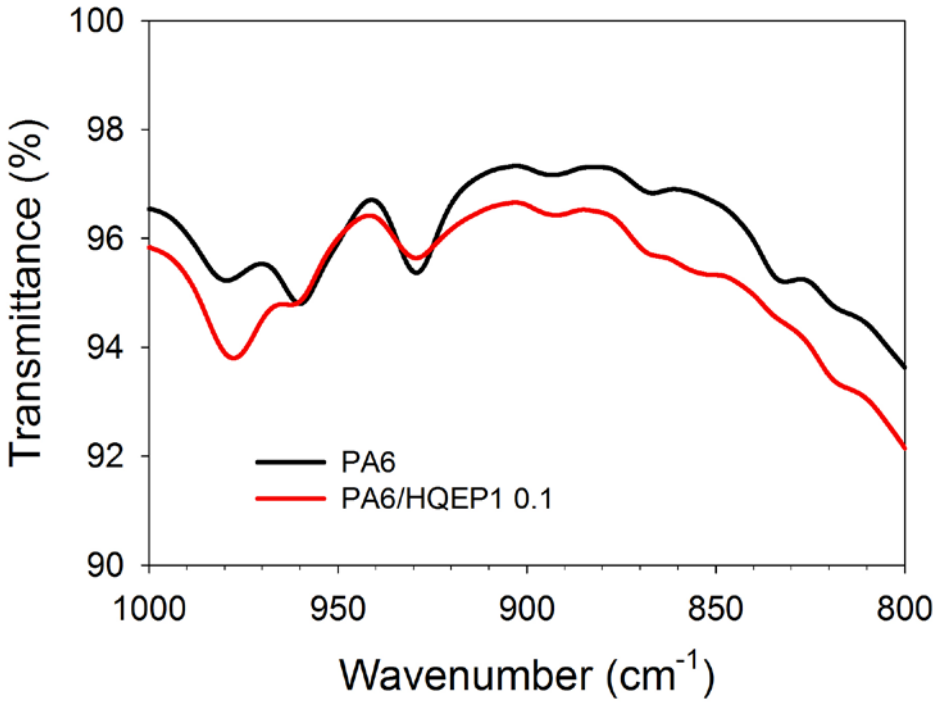

(b)

Figure 2.4 FT-IR transmittance spectra of PA6 and 0.1 mol ratio of PA6/HQEP1 composite. (a) whole range IR spectra (b) enlarged spectra range from 800 to 1000 cm^{-1}

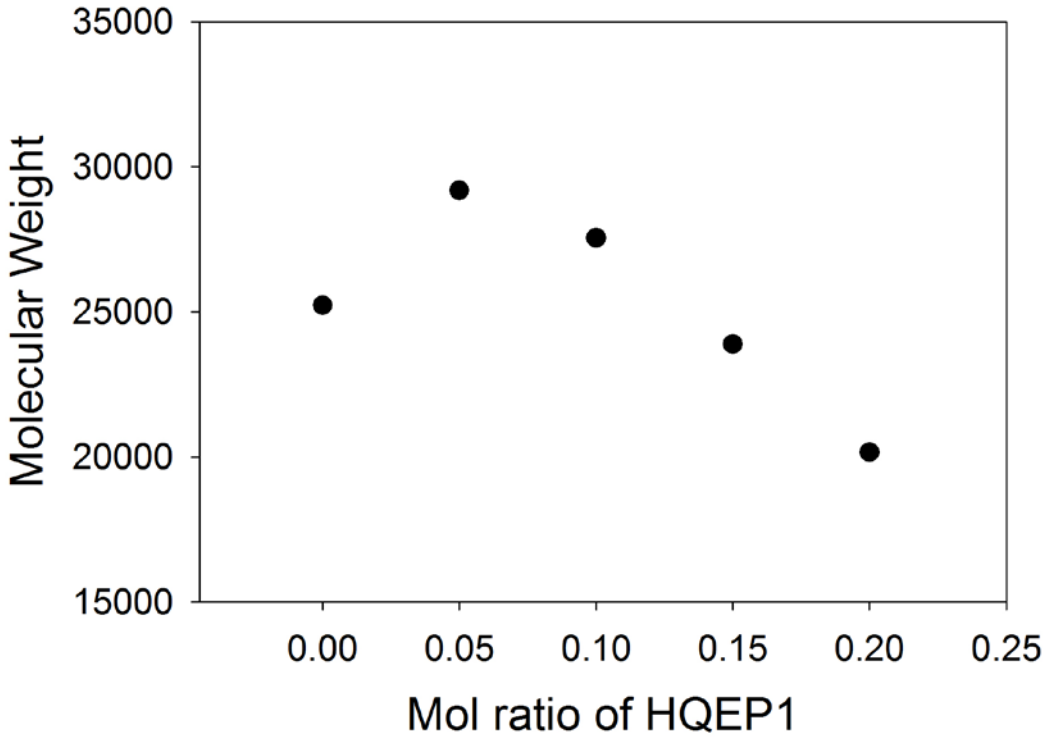

Figure 2.5 Molecular weights of PA6 and its composites which were calculated from intrinsic viscosity.

2.3.3 Rheological properties

Figure 2.6 shows the dependency of viscosity, storage and loss modulus on frequency with varying the HQEP1 amount. All PA6/HQEP1 composites show higher values of viscosity and modulus than neat PA6 through the whole range of frequency. This tendency is remarkable at low frequency range and PA6/HQEP1 composites show strong shear thinning behavior. It is observed in Figure 2.6 (a) that melt viscosity increases with the more amount of HQEP1 added up to the mol ratio of HQEP1 0.1, because the entanglement molecular weight increased through HQEP1 crosslinked the PA6 chain. On the other hand, viscosity decreases mol ratio of HQEP1 0.15 and 0.2, showing weaker shear thinning behavior than the mol ratio 0.05 and 0.1 relatively. These phenomena are related to the molecular weight and crosslinking of polymer chains. The more HQEP1 added, the larger molecular weight is due to the crosslinking. So polymer chains show rubber-like behavior and strong shear thinning effect is observed at low frequency range. But over the mol ratio of HQEP1 0.15 added, the probability that the active anions quenched with oxirane ring increased so that the molecular weight decreased. As a result, PA6/HQEP1 composites show weaker shear thinning behavior than low amount of HQEP1 contents. In Figure 2.6 (b) and (c), the slopes of PA6/HQEP1 composites are steeper than PA6 and dramatically changed in storage modulus rather than on loss modulus. Especially in the mol ratio of HQEP1 0.1, loss modulus increased about 16 times than PA6 while storage modulus increased over 1000 times than PA6 at low frequency. In general linear polymer melts, storage modulus is proportional to the square of frequency and loss modulus is proportional to frequency, following viscoelastic motion. But in our research, modulus of PA6/HQEP1 composites

was largely deviated from linear viscoelastic motion and G’ is larger than G” in all frequency range. It implied that polymer chains of composites were almost solid-like behavior and crosslinked. It implies that PA6/HQEP1 composite melt has more solid-like viscoelastic behavior due to the crosslinking and chain entanglement.

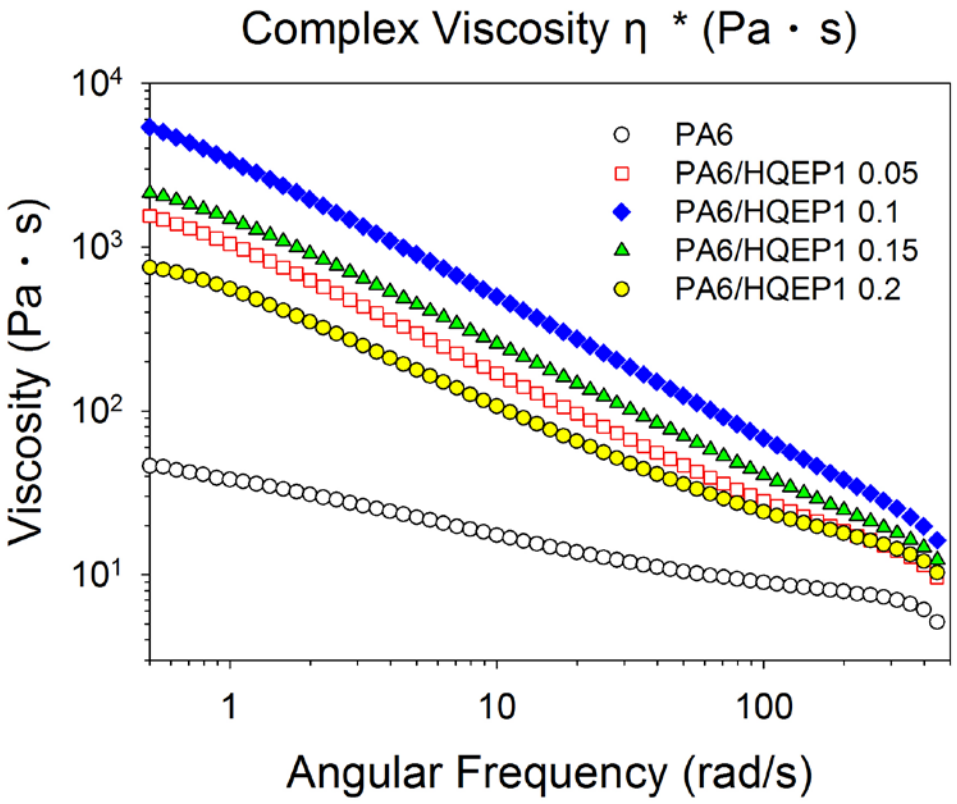
Complex Viscosity η * (Pa · s)
Viscosity (Pa · s)
10⁴
10³
10²
10¹
1
10
100
Angular Frequency (rad/s)
PA6
PA6/HQEP1 0.05
PA6/HQEP1 0.1
PA6/HQEP1 0.15
PA6/HQEP1 0.2

(a)

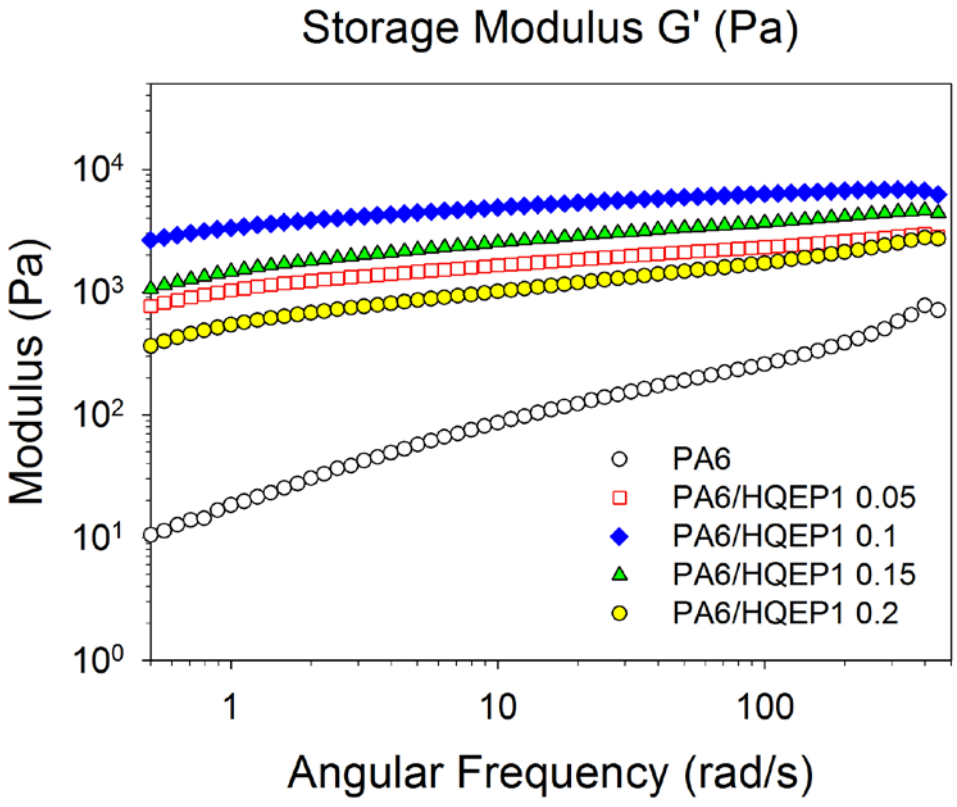
Storage Modulus G' (Pa)
Modulus (Pa)
10⁴
10³
10²
10¹
10⁰
1
10
100
Angular Frequency (rad/s)
PA6
PA6/HQEP1 0.05
PA6/HQEP1 0.1
PA6/HQEP1 0.15
PA6/HQEP1 0.2

(b)

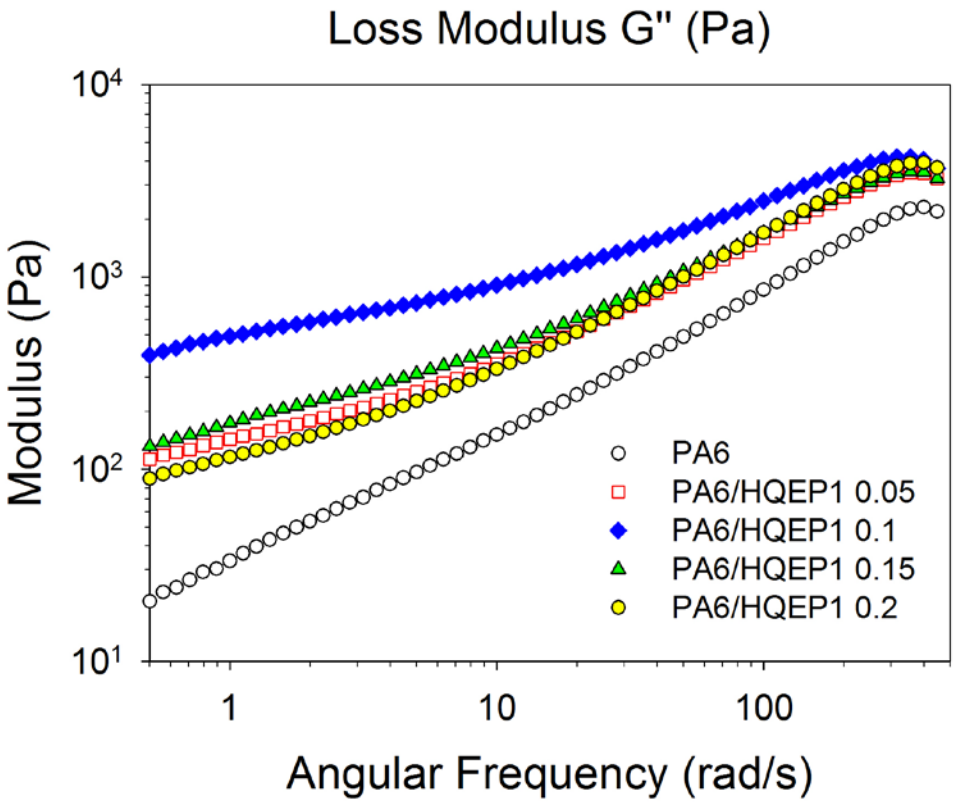

(c)

Figure 2.6 Rheological properties of PA6 and its composites measured by ARES. (a) complex viscosity (b) storage modulus (c) loss modulus

2.3.4 Mechanical properties

Some important mechanical properties are summarized in Figure 2.7 and Table 2.2. The elastic modulus and tensile strength increased with HQEP1 added until the mol ratio of HQEP1 0.1, probably because of the higher molecular weight. Generally, for linear polymer, modulus and tensile strength are declined with the crystallinity drop. On the other hand in our study, despite the reduction of crystallinity, the modulus and tensile strength were improved with introducing epoxy additives because the molecular weight had increased and the PA6 chains had been crosslinked. Especially, the elongation dramatically changes with the contents of HQEP1, about 72% improved yielding property observed at the mol ratio of HQEP1 0.1 rather than neat PA6. Also, energy absorbed to break was doubled, which is related to toughness of materials. Improved ductility refers to lightly crosslinked structure of PA6/HQEP1 composite as well as increased molecular weight. Increased chain entanglement by crosslinking, leads to strong resistance to shear force and deformation. However, above mol ratio of HQEP1 0.15, both crosslinking and termination occurred frequently so that molecular weight drastically decreased. As a result, mechanical properties decline. What was worse, mechanical properties of the mol ratio 0.2 composite are more worsen than neat PA6, because of the large amount of HQEP1 quenched lots of propagation reactions and the molecular weight is too small to reveal good performance.

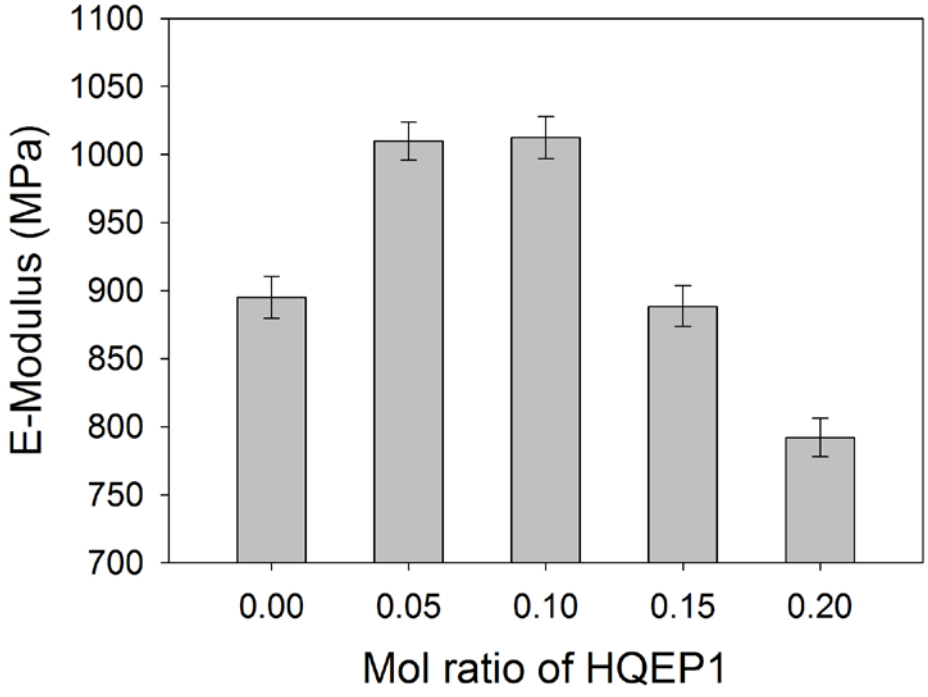
E-Modulus (MPa)
1100
1050
1000
950
900
850
800
750
700
0.00
0.05
0.10
0.15
0.20
Mol ratio of HQEP1

(a)

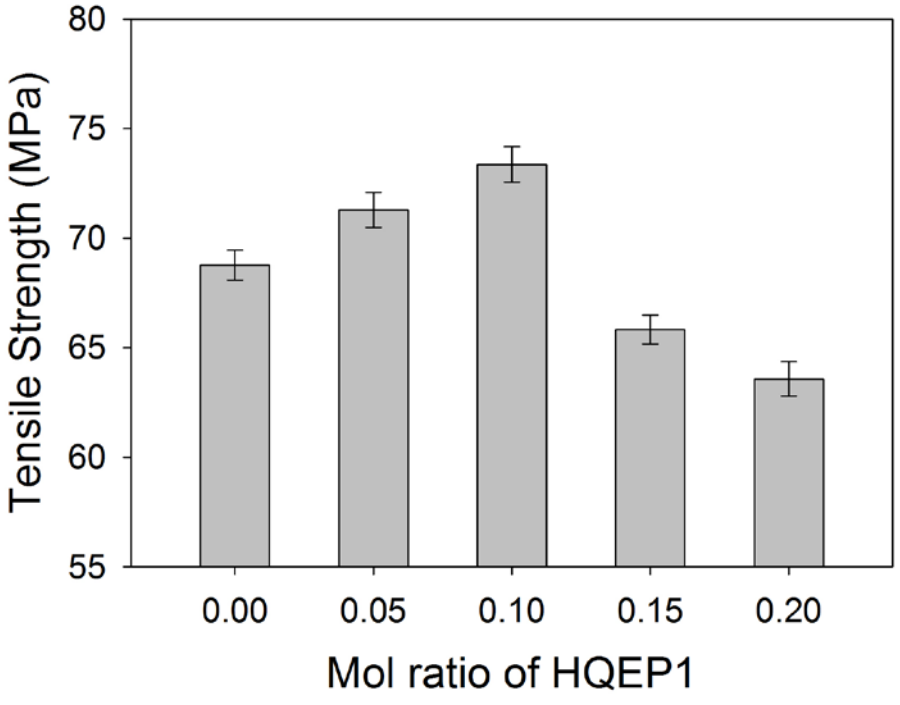
Tensile Strength (MPa)
80
75
70
65
60
55
0.00
0.05
0.10
0.15
0.20
Mol ratio of HQEP1

(b)

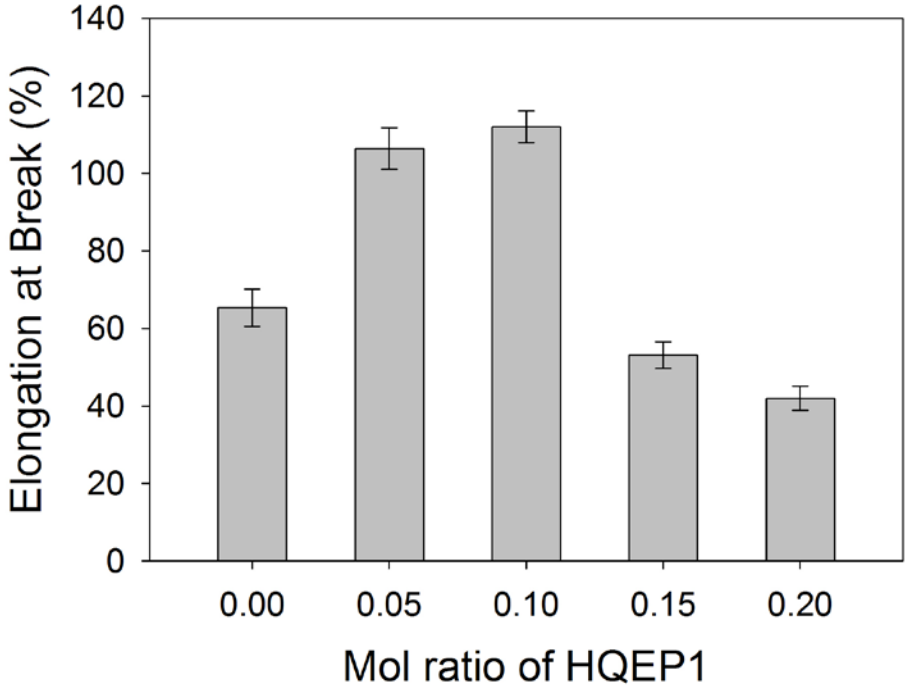

(c)

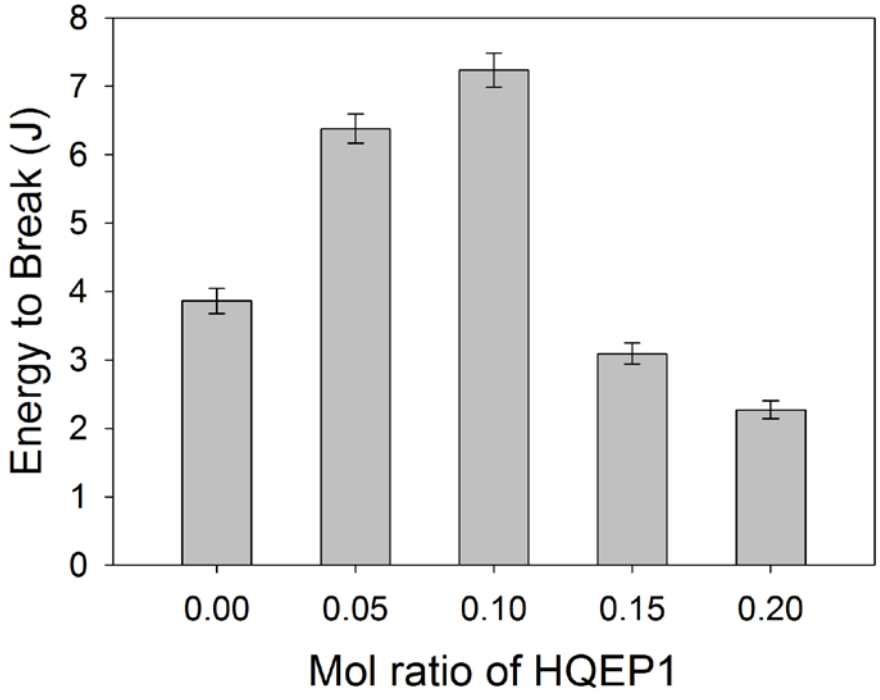

(d)

Figure 2.7 The results of tensile test. (a) elastic modulus (b) ultimate tensile strength (c) elongation at break (d) energy to break

Mol ratio of HQEP1	E-modulus (MPa)	Tensile strength (MPa)	Elongation (%)	Energy to break (J)
0	895	68.8	65.3	3.86
0.05	1010	71.3	106.4	6.38
0.1	1013	73.4	112.0	7.24
0.15	889	65.8	53.2	3.09
0.2	792	63.6	42.0	2.27

Table 2.2 The values of mechanical properties of PA6/HQEP1 composites.

2.4 Conclusion

In this study, we successfully polymerized PA6 and its composites through reactive extrusion from monomers. In the extruder, ε-caprolactam completely reacted to form PA6 polymer without any residual monomers. In reactive extrusion, diepoxy additive reacted with amide linkage of PA6 chain and extended it by crosslinking. It is supported by the DSC scanning and FT-IR analysis. Produced composites showed well known melt behavior of PA6 in DSC thermogram. Also, there are no unreacted oxirane ring and carbonyl group of ester peak in FT-IR transmittance curve of composites. Crystallinity dropped with HQEP1 concentration, because HQEP1 hindered the crystallization of PA6 chains. The molecular weight increased by adding the small amount of HQEP1, but decreased with more amount of HQEP1 had added beyond the critical composition. During polymerization, some parts of living anions at the PA6 chain encountered oxirane ring of HQEP1. Opening the epoxide ring, anionic polymerization was quenched and crosslink was formed. As a result, lightly crosslinked chain acted as extended polymer chain and affected the molecular weight increased. Spontaneously, polymerization terminated and PA6 chain could not growth more. When a small amount of HQEP1 was added, polymerization was scarcely quenched due to the low probability of encounter anion with oxirane ring. So high molecular weight polymer could be obtained because of sufficient long PA6 chains were polymerized. On the other hand, a large amount of HQEP1 was added, polymerization was quenched at early stage of propagation due to the high probability of encounter anion with oxirane ring. Finally, the molecular weight was decreased even if the number of crosslinking sites was

increased. The results of rheological study are in agreement with expected mechanism. PA6/HQEP1 composites showed shear thinning behavior throughout measured frequency range. All composites except neat PA6 exhibited higher melt viscosity than PA6 and, solid-like or rubber-like behaviors. It was derived from increased chain entanglement and the crosslinked polymer structure. Mechanical properties were improved by adding the HQEP1. Increased molecular weight and crosslinking enhanced PA6 more resists to tensile stress. But, performances were rapidly decrease over the mol ratio of HQEP1 0.15 added. HQEP1 acted both crosslinking agent and inhibitor spontaneously in in-situ polymerization of REX. So it was affected to molecular weight, increasing by connecting two polymer chains and decreasing by quenching the propagation reaction. To obtain high performance PA6/HQEP1 composites, the controlled composition of reactants was needed.

2.5 References

[1] Bessell, T.; Shortall, J. B. J Mater Sci 1975, 10, (12), 2035-2043.

[2] Pillay, S.; Vaidya, U. K.; Janowski, G. M. J Thermoplast Compos 2005, 18, (6), 509-527.

[3] Gong, Y.; Liu, A. D.; Yang, G. S. Compos Part a-Appl S 2010, 41, (8), 1006-1011.

[4] Hedrick, R. M.; Gabbert, J. D.; Wohl, M. H. Acs Sym Ser 1985, 270, 135-162.

[5] Hornsby, P. R.; Tung, J. F.; Tarverdi, K. J Appl Polym Sci 1994, 53, (7), 891-897.

[6] Kye, H.; White, J. L. J Appl Polym Sci 1994, 52, (9), 1249-1262.

[7] Gorton, B. S. J Appl Polym Sci 1964, 8, 1287-1295.

[8] Zhong, Z.; Guo, Q. Polymer 1998, 39, (15), 3451-3458.

[9] Gupta, A.; Singhal, R.; Nagpal, A. K. J Appl Polym Sci 2003, 89, (12), 3237-3247.

[10] Lee, J. Y.; Jang, J. S. Polymer 2006, 47, (9), 3036-3042.

[11] Brandrup J., I. E. H., Polymer Handbook. 1989.

[12] Cheng, L. P.; Dwan, A. H.; Gryte, C. C. J Polym Sci Pol Phys 1994, 32, (7), 1183-1190.

[13] Prime, R. B.; Sacher, E. Polymer 1972, 13, (9), 455-&.

[14] Qian, Z. Y.; Chen, X.; Xu, J.; Guo, B. H. J Appl Polym Sci 2004, 94, (6), 2347-2355.

[15] Lee, K. H.; Kim, K. W.; Pesapane, A.; Kim, H. Y.; Rabolt, J. F. Macromolecules 2008, 41, (4), 1494-1498.

Chapter 3

Modification of Polyamide 6 with diamine chain extenders through in-situ polymerization by reactive extrusion and its properties.

3.1 Introduction

Polyamide 6 (PA6), known as Nylon 6, is one of the widely used engineering polymers in film, fiber, textile and packaging industry because of their excellent advantages on ductility, toughness, durability and price. Besides, PA6 can be polymerized from ε-caprolactam monomer through anionic ring opening polymerization (ROP) within several minutes with various activators.[1-3] This attractive advantage makes possible that anionic polymerization of PA6 applied in in-situ processing field such as reactive injection molding (RIM) and reactive extrusion (REX).[4-6] Especially, reactive extrusion is very demanding because it makes one-pot process possible through fast and well controlled reaction. Another remarkable feature of PA6 is the excellent reactivity. Amine and carboxylic acid groups at the end of PA6 chains as well as amide linkage can become active easily. They can react with various functional groups of organic/inorganic materials. This can adopt coupling agent called ‘chain extender’ to PA6. Chain extenders are generally bifunctional materials that can react with polymer end group easily, producing high molecular weight PA6. Numerous addition-type chain

extenders have been described for commercial PA6 which has amine and carboxyl acid end group. For example, bisepoxies,[7-9] biscaprolactams,[10-13] bisoxazolines [10,13,14] or diisocyanates[15] have been reported.

Despite many advantages, there have been rarely reported that chain extending of PA6 during in-situ polymerization successively. Due to the polymerization mechanism difference between typical hydrolytic PA6 and anionic ROP PA6, functional end groups are different. In typical hydrolytic process, PA6 is polymerized from condensation polymerization of aminoic acid, which was generated from hydrolysis reaction of caprolactam. On the other hand, in in-situ polymerization of PA6 through anionic ROP, nucleophilic addition reaction produces non-amine or carboxylic acid terminated polymer. Instead, caprolactam ring or functional groups of used activator are located at the end of PA6 chains. So it is necessary that another bifunctional chain extenders, which can react with caprolactam, are needed to use in in-situ polymerization of PA6.

Novitsky et al. synthesized polyamide 12, 6 block copolymer successively by the incorporation of lactams involved reactions coinitiated by N-acylcaprolactam-based macrocoinitiator (McI).[16,17] The McI, which had been synthesized from ring opening reaction of terephthaloyl biscaproactamate with diamine, had N-terephthaloyl caprolactam end groups and it could initiate anionic ring opening polymerization of PA6. In addition, lots of researches have been reported that biscaprolactams could act activator for anionic ROP as well as chain extender.[16-20] So in this research, we applied biscaprolactam as activator and diamine as chain extender on in-situ polymerization of PA6, producing high molecular weight PA6 through reactive extrusion. We performed in-situ polymerization of the PA6/diamine composites from monomers through reactive extrusion process. Also, reaction conditions optimized and

expected mechanisms were proposed. Rheological and mechanical properties of PA6/diamine composites were also investigated.

3.2 Experimental

3.2.1 Materials

ε-caprolactam used in this study was procured from Capro Corporation (Korea). Sodium hydride, terephthaloyl chloride, triethylamine, pyridine, resorcinol, 4-nitrobenzoyl chloride and activated Pd-carbon (10%) were purchased from Aldrich. Synthesized biscaprolactam type catalyst, TBC (Terephthaloyl biscaprolactamte, Figure 3.1 (a)), was used to initiate the polymerization. Two different diamine chain extenders were used in this research are presented in Figure 3.1 (c) and (d). PDA1 (p-phenylenediamine) was purchased from Aldrich and EDA3 (3-(4-Aminobenzoyloxy)phenyl 4-aminobenzoate) was synthesized in laboratory.

3.2.2 Synthesis

3.2.2.1 Synthesis of sodium caprolactam (Na-CL)

Before synthesis, ε-caprolactam was dried at 100℃ oven for 24 hours and 50℃ vacuum oven for 48 hours to completely remove the moisture. 1mol of dried ε-caprolactam was put in the round flask under an argon atmosphere. After ε-caprolactam was completely melted at 70℃, 0.05 mol of sodium hydride was added with stirring. When hydrogen emission was stopped, the mixture was stirred under an argon atmosphere for 10 min to react. The mixture was cooled to room temperature and

pulverized. Obtained sodium caprolactam (Figure 3.1 (b)) powder was stored in argon charged container.

3.2.2.2 Synthesis of terephthaloyl biscaprolactamte (TBC)

TBC was synthesized by reaction of terephthalyol chloride with caprolactam in benzene.[16] It's melting temperature is 206℃. H-NMR spectrum ($CDCl_3$): δ (ppm) 7.54 (4H, s), 3.96 (4H, t), 2.69(4H, t), 1.83(12H, m)

3.2.2.3 Synthesis of 3-(4-Aminobenzoyloxy)phenyl 4-aminobenzoate (EDA3)

EDA3 was synthesized by hydrogenation of phenyl nitrobenzoate which was obtained by reaction of resorcinol with 4-nitrobenzoyl chloride.[21] It's melting temperature is 197-199℃. H-NMR spectrum ($CDCl_3$): δ (ppm) 7.98 (4H, d), 7.41 (1H, m), 7.10 (3H, m), 6.68 (4H, d), 4.12 (4H, s, two diamines).

3.2.3 Polymerization of PA6/diamine composites

3.2.3.1 In-situ polymerization by reactive extrusion

The whole polymerization process illustrates briefly in Figure 3.2. Reactant mixtures were composed of ε-caprolactam, sodium caprolactam, TBC and diamines which were monomer, initiator, activator and chain extenders each. The mol ratio of monomer : initiator : activator was optimized as 50 : 1 : 0.5 in terms of both high polymer yield and short polymerization time by pre-experimental. The mol ratio of diamine contents to 1mol of initiator was 0.05, 0.1, 0.15, 0.2 mol for each sample. The reactant mixtures were fed into twin screw extruder (BA-19, Bau tech), with flowing an

argon to prevent the quenching of active anions by moisture during polymerization. The temperature profiles from feeding zone to die were set 140/180/200/220/220/230/240℃, screw speed was set to 50 rpm. Extruded PA6/diamine composite fibers were pelletized and dried at 60℃ vacuum oven for sufficient time before characterization.

3.2.3.2 2-steps chain extension by reactive extrusion

In in-situ polymerization, there had an upper limit amount of adding diamine existed, because diamines depressed the polymerization rate. So adding more amount of diamines than adequate amount (mol ratio of 0.2 to initiator), PA6/diamine composites were incompletely polymerized during reactive extrusion and residual monomers remained. To investigate the effect of diamine chain extender clearly, it was necessary that the analysis for more amount of diamine added composites were needed. So we designed new experimental. PA6 which had been polymerized from in-situ reactive extrusion without diamine reacted with diamine chain extender into extruder again. Experimental method was same as in-situ polymerization of PA6/diamine composites, but composition of reactant mixtures was different, only PA6 and diamine were fed. The mol ratio of diamine contents to 1mol of initiator was designed as 0.25, 0.5, 0.75, 1, 1.25 mol for each sample. The temperature profiles from feeding zone to die were set 140/180/200/220/220/230/240℃, screw speed was set to 50 rpm. All the samples and those compositions are summarized in Table 3.1.

3.2.4 Characterization

Differential scanning calorimetry (DSC, DSC 823e, METTLER TOLEDO) was used to analyze the thermal properties of PA6/diamine composites. Under a nitrogen atmosphere, samples were first heated from 25℃ to 280℃ at 10 ℃/min, cooled to 25℃ and heated to 280℃ again at same heating rate. The degree of crystallinity (X_c) was obtained by following equation.

$$X_c(\%) = \frac{\Delta H_m}{\Delta H_{100}} \times 100$$

ΔH_m is the specific enthalphy of melting, and ΔH_{100} is the enthalphy of melting with fully crystalline PA6 which is 190 J/g in this study.[22] The Wide angle X-RAY diffraction (WAXD) spectra analysis was also carried out. Before measurement, the extruded PA6/diamine pellets were hot pressed at 240℃ and cooled to room temperature to obtain films. To analyze crystalline order of PA6/diamine composites, WAXD (d8 Advance, BRUKER MILLER Co.) was used. The spectra were recorded at 25℃ through diffraction angles (2θ) 5-40˚ by CuKα radiation. Intrinsic viscosity (η) was measured to calculate the viscosity average molecular weight (M). By using Ubbelohde viscometer, the time for polymer solution passed through capillary was checked at 25℃ in 90% formic acid solution. Molecular weights of PA6/diamine composites were calculated by Mark-Houwink equation.

$$[\eta] = K(M)^a$$

The Mark-Houwink constants are K = 22.6 x 10^3 (mL/g) and a = 0.82 for PA6 at 25℃ in 90% formic acid solution.[23] Rheological properties were studied through Advanced Rheometric Expansion System (ARES, Rheometric Scientific). Samples were prepared

in mold with diameter 25 mm and thickness 1 mm at 240℃ by injection molding. Storage, loss modulus and complex viscosity were measured between parallel plates at 250℃, applied strain 10% and angular frequency from 0.05 to 500 rad/s. The degree of crosslinking was determined using solvent extraction method according to ASTM D2765 method, using m-cresol for 20 hours reflux.[24] UV spectrometer (Agilent 8453 UV-Vis system) was used to analyses of chain regularities in PA6 chains.[25] The presence of structural irregularities in PA6 chains are able to absorb in the UV region with OD_{max} at 270~280 nm, 1 wt% of PA6 solutions in formic acid had been prepared and UV absorption was measured between 250 and 400 nm (1 cm path length). For tensile test, specimens were prepared according to ASTM D638 by injection molding at 240℃. The mechanical properties were tested through Instron (5567, Instron) with crosshead speed of 10 mm/min. The values of various mechanical properties were determined the average of 10 tested values for each PA6/diamine sets.

(a)

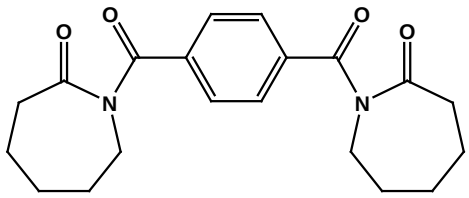

(b)

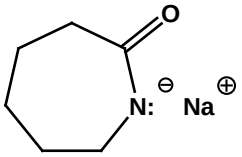

(c)

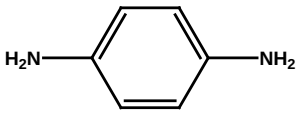

(d)

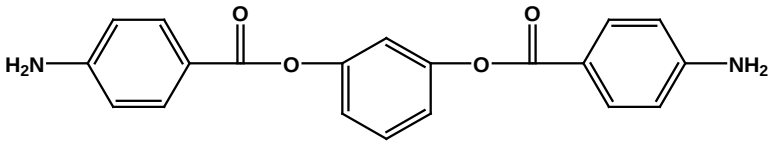

Figure 3.1 Structures of materials. (a) TBC (b) sodium caprolactam (c) PDA1 (d) EDA3

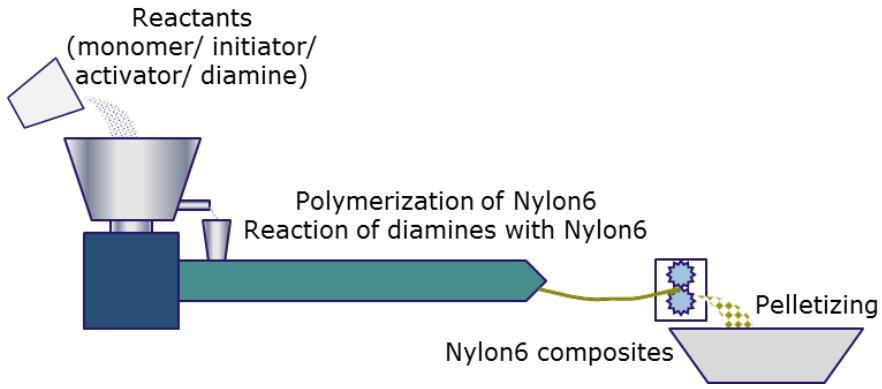

Figure 3.2 Polymerization process. The composition of reactant mixture was controlled to set as monomer : initiator : activator : chain extender = 50 : 1 : 0.5 : (0, 0.05, 0.1, 0.15, 0.2) mol.

Samples	Diamine	Mol ratio of diamine to initiator	Polymerization process
PA6 (Ny6)		0	In-situ
PDA1 0.05s	PDA1	0.05	
PDA1 0.1s		0.1	
PDA1 0.15s		0.15	
PDA1 0.2s		0.2	
EDA3 0.05s	EDA3	0.05	
EDA3 0.1s		0.1	
EDA3 0.15s		0.15	
EDA3 0.2s		0.2	
PDA1 0.25f	PDA1	0.25	2-steps
PDA1 0.5f		0.5	
PDA1 0.75f		0.75	
PDA1 1f		1	
PDA1 1.25f		1.25	
EDA3 0.25f	EDA3	0.25	
EDA3 0.5f		0.5	
EDA3 0.75f		0.75	
EDA3 1f		1	
EDA3 1.25f		1.25	

Table 3.1 Brief information of samples. The mol ratio of ε-caprolactam : sodium hydride : TBC had fixed to 50 : 1 : 0.5 for all experimental.

3.3 Results and discussion

3.3.1 Reaction mechanism

3.3.1.1 Main reaction

The mechanisms of major possible reactions are shown in Scheme 3.1. In Scheme 3.1 (a), TBC reacts with sodium caprolactam anion and caprolactam ring is opened. Then living anion attacks a ε-caprolactam monomer and extracts a proton, generating a new living anion. This new anion acts as nucleophile, opening the caprolactam ring of dimer. As a result, trimer with living anion is formed and this anion reacts with another ε-caprolactam monomer. The chain propagation continues until the anion is quenched and high molecular PA6 was polymerized. Reaction of amine with caprolactam is already known by some researches.[10,16,17] Akkapeddi and Gervasi suggested that biscaprolactam can react with amine end group of PA6 through two possible mechanisms.[10] The reaction mechanism is shown in Scheme 3.1 (b). The first mechanism is elimination of caprolactam by nucleophilic substitution reaction. This reaction forms caprolactam molecule as by-product and predominates at low temperature (under 200℃). The second mechanism is ring opening reaction of caprolactam without any by-product. At elevated temperature (over 200℃), both reactions take place. In this study, expected reaction mechanism between caprolactam end group of PA6 and diamine chain extender is exhibited in Scheme 3.1 (c). In twin screw extruder, both ring opening and elimination of caprolactam mechanisms are

possible because reaction temperature was sufficiently high (about 230℃). Caprolactam chain end groups of polymerized PA6 are connected with diamine chain extender, forming new PA6 repeating unit by ring opening of caprolactam or connecting directly with creation of caprolactam by-product.

3.3.1.2 Side reaction

In anionic ROP of PA6 with activator, there are some well-known side-reactions cause branching.[29-32] In Scheme 3.2, it briefly showed that possible reactions can generate branches during polymerization. During propagation and initial stage of polymerization, active anions on the living chain tend to react with activators rather than monomers (Scheme 3.2 (a)). As a result, bifunctional activator dangles on the side position of living PA6 chain and provides new growth site to produce branched polymer. Claisen type condensation also generates branched polymer chain. Stehlicek and Sebenda reported that two α-C next to the carbonyl group of polymer chain can attacked by lactamate anion, and this new active anion could act as branching site. (Scheme 3.2 (b))[31] Branching reaction can occur depend on the composition of reactants, structure of activators, polymerization time and temperature.[26,28,33] Ricco et al. reported that high polymerization temperature and bifunctional activator could accelerate the side-reaction of PA6.[26] Kim et al. observed that the occurrence of more branching and crosslinking reactions due to the dominant Claisen type condensation reaction for bifunctional activator than monofunctional activator.[30]

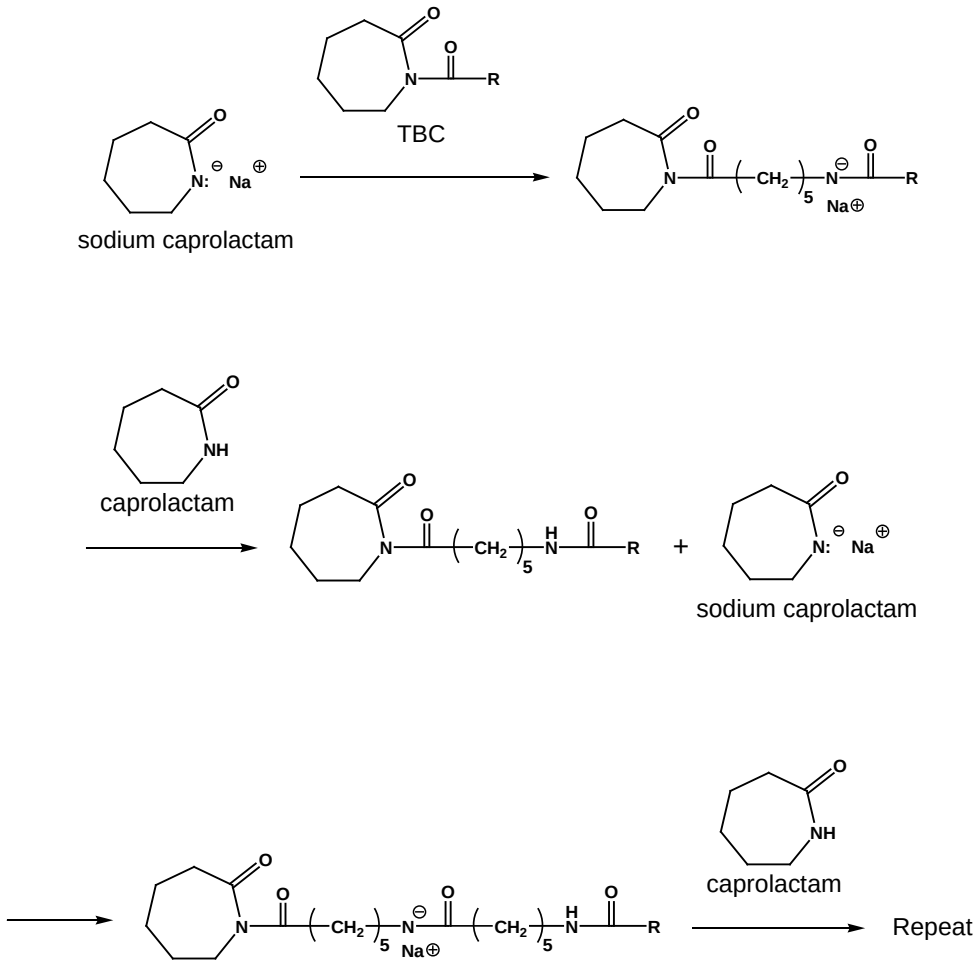
TBC
sodium caprolactam
caprolactam
sodium caprolactam
caprolactam
Repeat

(a)

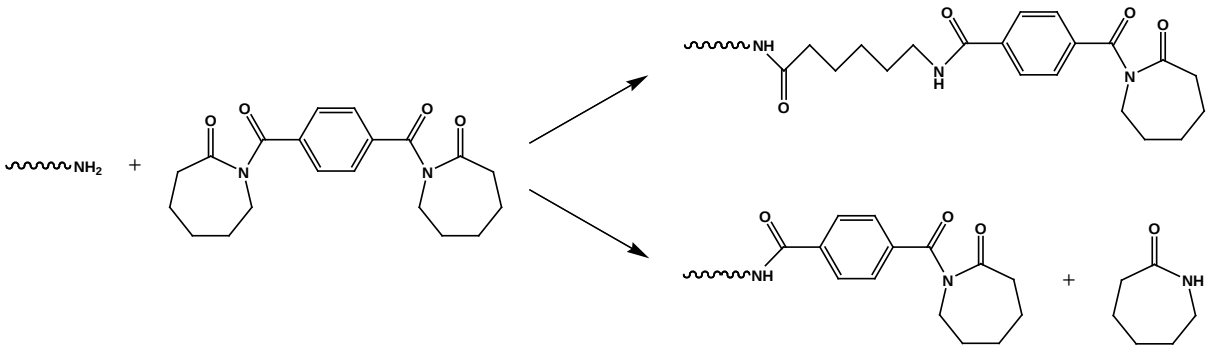

(b)

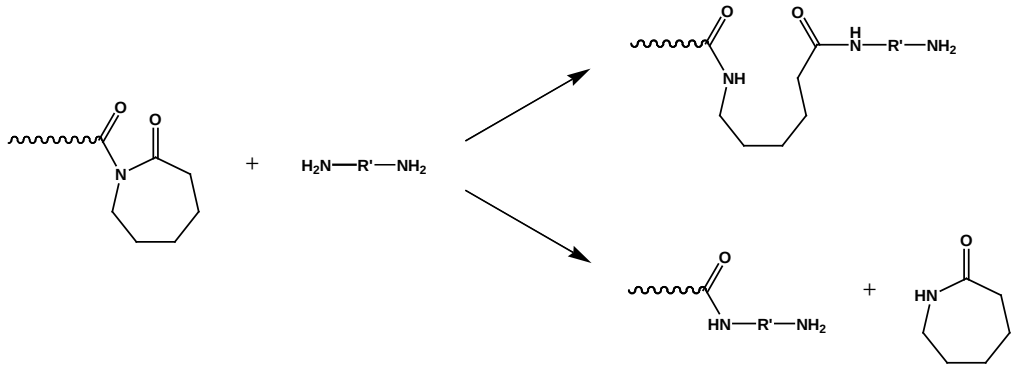

(c)

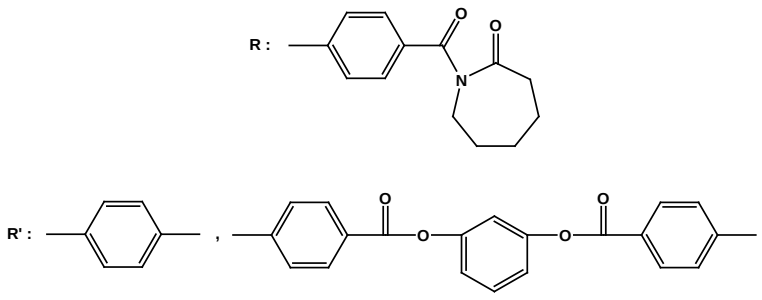

Scheme 3.1 Reaction schemes. (a) polymerization of ε-caprolactam to form PA6 (b) chain extending reaction of anime with biscaprolactam chain extender (c) chain extending reaction of caprolactam with diamine chain extender

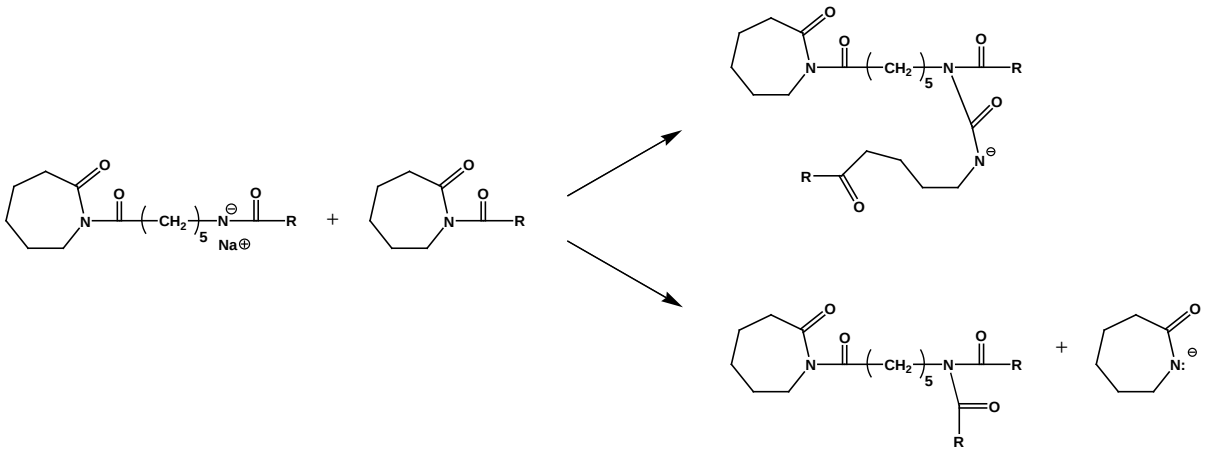

(a)

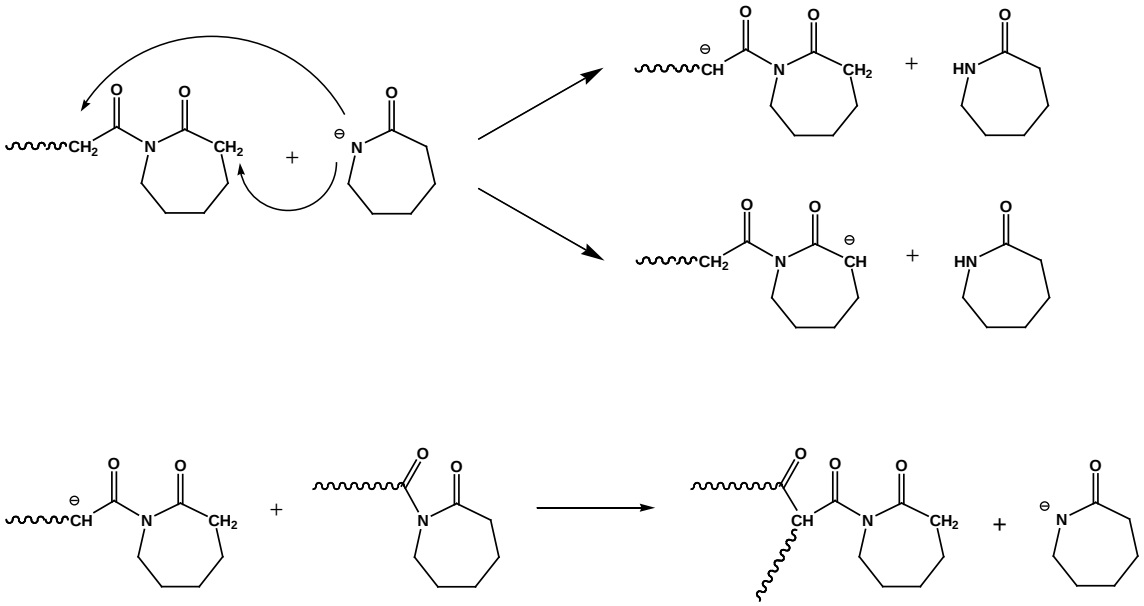

(b)

Scheme 3.2 Side reaction schemes. (a) reaction between anions on the living chain with activators (b) Claisen type condensation

3.3.2 Polymerization of PA6/diamine composites

Figure 3.3 (a) and (b), the first heating DSC scanning results of PA6/EDA3 composites produced by in-situ and 2-steps respectively. Exact values of melting temperature (T_m), enthalphy of melting (ΔH_m) and crystallinity (X_c) are given in Table 3.2. In Figure 3.3, all PA6 composites shows only one exothermic peak between 212 and 214℃ which is known as melting temperature of PA6 and no transition peaks of residual reactants, except the mol ratio of 0.25 EDA3 in in-situ polymerization. It means that all monomers had reacted each other completely and PA6 had been well polymerized up to mol ratio of 0.2 of EDA3. On the contrary, in Figure 3.3 (a), two broad exothermic peaks exists around 70℃ and 190℃ for PA6/EDA3 composite with mol ratio of diamine 0.25, each are the melt of residual ε-caprolactam and very low molecular weight PA6 (maybe oligomers). We could check the same result in PDA1 in-situ case. Over the mol ratio of diamine 0.2 added, the polymerization rate had slowed down so that the polymerization of ε-caprolactam had been incomplete in short residence time in extruder. So in this study, we investigated composites content under mol ratio of 0.2 of diamines for in-situ polymerization.

Both enthalphy of melting (ΔH_m) and crystallinity (X_c) was reduced upon diamine introduction during the melting temperature did not show any remarkable difference. It is indicated that the crystallization of PA6 was hindered by chain extenders. Similar results already have been reported with different kind of linear chain extenders.[7,12,13] In those researches, crystallinity drop was attributed to the increase of the molecular weight that hinders the arrangement of the macromolecules in a crystalline phase.

Buccella et al. also reported that the presence of caprolactam by-products due to side-reaction of chain extension (Scheme 3.1 (b)) could negatively affect the crystallinity.[13] But in our case, we supposed that the effect of by-product is not much dominance, even the caprolactam by-product could be generated from the side-reaction. Because in in-situ REX process, generated by-product caprolactam could act as new monomer for anionic ROP of PA6 (Scheme 3.1 (a)), or had been vented out during extrusion. So the crystallinity drop was largely affected by the increase of molecular weight and hindrance of the chain extender.

To investigate the crystallization, WAXD analysis was performed and the results were exhibited in Figure 3.4 and Table 3.2. Both WAXD spectra for PA6/EDA3 in-situ and 2-steps showed two sharp characteristic peaks at $2\theta = 20^\circ$ and 23°. Both peaks are corresponding to the reflection of the α-crystalline planes (200) and (002) + (202), respectively.[26] There are no other peaks observed in WAXD profiles such as γ-crystalline peak which is existed at $2\theta = 21.5^\circ$ corresponding to (001) plane. The peak intensities of α-form are reduced with EDA3 concentration and new phase induced from the adding of EDA3 does not appear. We had checked the same results for PA6/PDA1 composites. The crystallinity dropped from 43.1% for neat PA6 to 29.4 ~ 39.2% for PA6/EDA3 composites. It is indicated that diamine chain extenders hindered the crystallization of PA6 and decreased the crystallinity. It is supported by the DSC thermal analysis results from above. Also, diamine chain extender rarely affected to form new crystalline phase because it remained in inter-lamella amorphous region. Formation of γ-form of PA6 was already known as depending on the thermal history, processing conditions, annealing, crystallization conditions, existence of additives and so on.[27] Ricco et al. mentioned that the use of some bifunctional activators could lead

to form the γ-crystalline phase, but they did not investigate correlation between γ-form content and degree of crosslinking clearly.[26] Even if in our study, we had produced branched PA6 and its composites by using the bifunctional activators, there is no γ-form PA6 existed. It is supposed that polymerization conditions and process mainly affected to crystallization rather than activator.

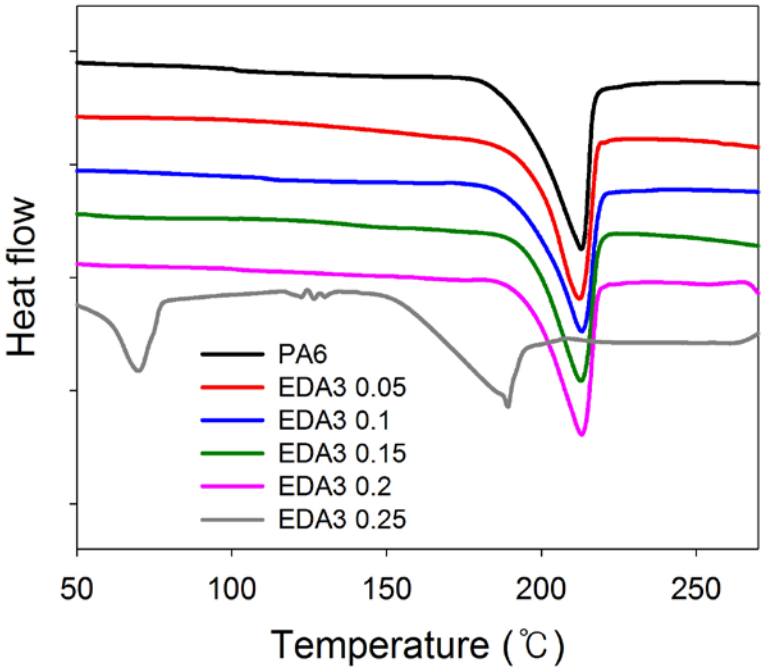

(a)

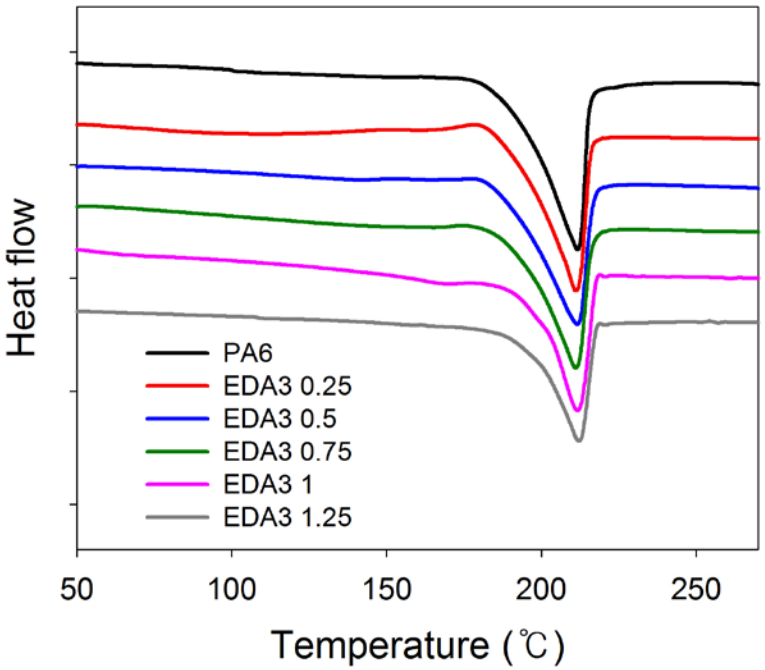

(b)

Figure 3.3 DSC heating thermograms. (a) PA6/EDA3 in-situ composites (b) PA6/EDA3 2-steps composites

Samples	T_m (℃)	ΔH_m (J/g)	X_c DSC (%)	X_c WAXD (%)	Molecular weight (g/mol)
PA6 (Ny6)	213.6	61.75	32.5	43.1	26,800
PDA1 0.05s	212.9	60.04	31.6	39.0	33,000
PDA1 0.1s	212.7	60.04	31.6	37.5	36,500
PDA1 0.15s	213.2	59.47	31.3	36.2	23,900
PDA1 0.2s	212.8	58.52	30.8	35.0	29,300
EDA3 0.05s	212.2	60.23	31.7	38.8	33,900
EDA3 0.1s	213.3	59.85	31.5	37.1	36,800
EDA3 0.15s	212.8	59.47	31.3	36.4	35,000
EDA3 0.2s	212.9	58.71	30.9	35.1	29,700
PDA1 0.25f	212.8	60.04	31.6	38.8	38,100
PDA1 0.5f	213.4	57.19	30.1	37.3	44,900
PDA1 0.75f	212.7	56.81	29.9	35.0	49,000
PDA1 1f	213.4	54.72	28.8	32.2	52,500
PDA1 1.25f	212.9	50.54	26.6	29.3	50,400
EDA3 0.25f	212.8	60.23	31.7	39.2	39,200
EDA3 0.5f	213.2	57.95	30.5	37.4	45,700
EDA3 0.75f	212.6	55.67	29.3	34.8	49,100
EDA3 1f	213.1	54.15	28.5	32.1	52,800
EDA3 1.25f	213.0	49.78	26.2	29.4	51,800

Table 3.2 Melting temperature (T_m), enthalphy of melting (ΔH_m), crystallinity (X_c) and molecular weight of PA6/diamine composites.

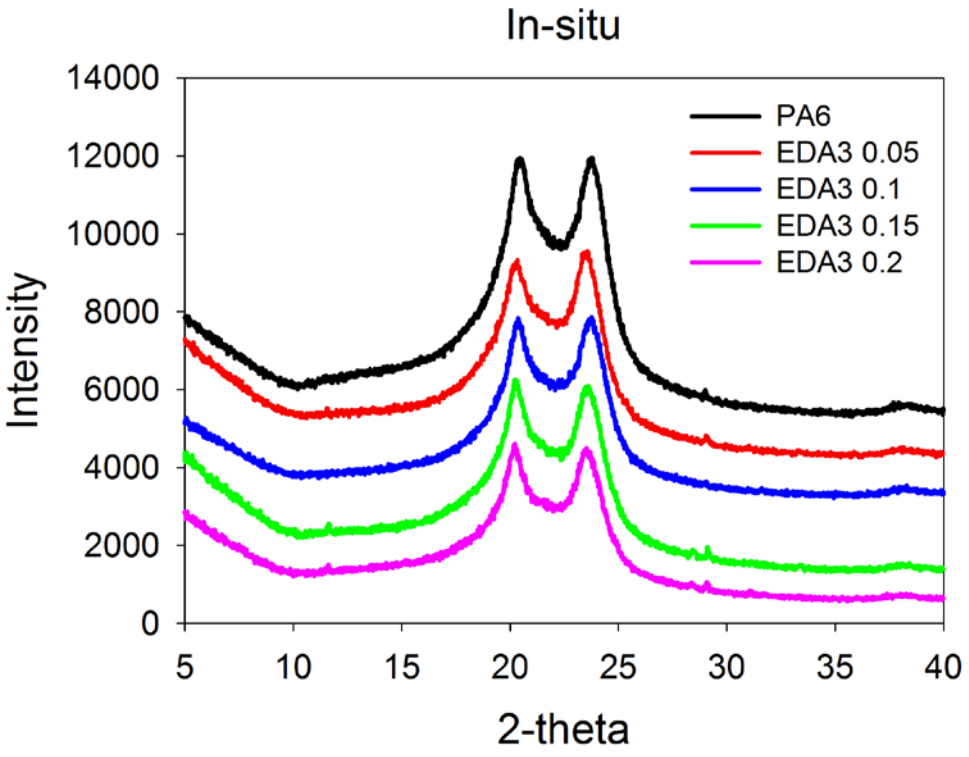

(a)

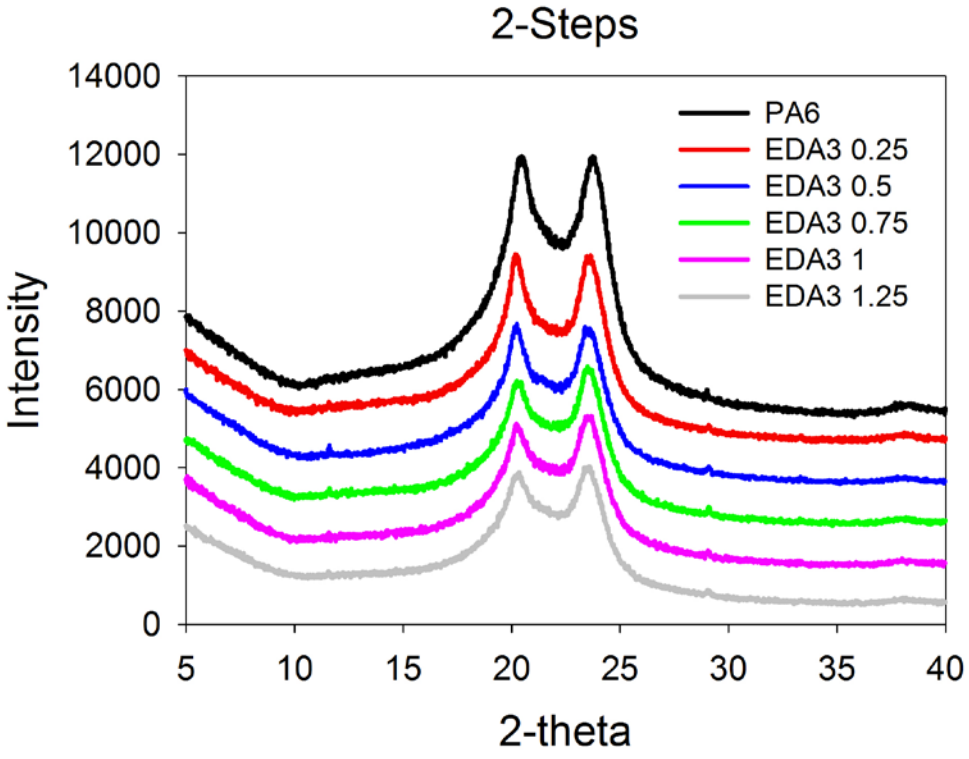

(b)

Figure 3.4 WAXD spectra. (a) PA6/EDA3 in-situ composites (b) PA6/EDA3 2-steps composites

3.3.3 Molecular weight

The molecular weight of PA6/diamine composites calculated from intrinsic viscosity, and the values are given in Figure 3.5 and Table 3.2. Neat PA6 was well polymerized and its molecular weight is 26,800 g/mol. The molecular weight of composites were increased with increasing mol ratio of diamine until 0.1, but decreased subsequently with adding more diamine. It seemed that PA6 chain lengthened due to the chain extending by diamine, because reactant composition and polymerization condition were fixed for each experimental. Amine groups of PDA1 and EDA3 reacted with caprolactam end group of PA6, affecting to whole molecular weight in two ways in in-situ polymerization. First, it increased molecular weight by connecting two PA6 chains. Simultaneously, it decreased molecular weight by termination of chain growth. In anionic polymerization (scheme 3.1 (a)), living anions on growing PA6 chain transfer to another monomer, generating new living anions. Subsequently, this new anion attacks the caprolactam ring which is located at the end of PA6 chain. As a result, PA6 chain length increases just as much as one repeating unit and anion still lives on the PA6 chain. On the other hand, PA6 chain had reacted with diamine chain extender, PA6 end group was blocked by chain extender (scheme 3.1 (c)). So transferred anion cannot attack the PA6 chain fast again, because there is no acyllactam reaction site. Finally, extended PA6 chain cannot growth more and whole PA6 molecular weight cannot increases more. Until mol ratio of chain extender reached 0.1, molecular weight increased from 26,800 to 36,500, because chain extending effect is more predominant than blocking effect. But, more diamine was added, molecular weight decreased to 29,300, because blocking

effect is more predominant than chain extending effect. Molecular weights are scarcely different between adding PDA1 and EDA3 in in-situ process. There are some kinds of reasons to explain this phenomenon, but there existed the possibility of small amount of diamine cannot make remarkable difference, so more experimental with the large amount of diamines are necessary.

Because, there is very little difference between PDA1 and EDA3 in in-situ process, more amount of diamines were added for 2-steps process to investigate the effect of diamines more clearly. The results are shown in Figure 3.5 (b). The molecular weight of composites produced by 2-steps process were increased with increasing mol ratio of diamine until 1, showing maximum value, and decreased subsequently with adding more diamine. Very high molecular weight PA6/diamine composites were produced, that almost 2 times improved at optimum condition by adding large amount of diamine. But, beyond this condition, increasing molecular weight was saturated and slightly decreased. The mol ratio of diamine reached 1.25 under extrusion condition, caprolactam reactive sites were saturated and remained amine groups were dangling at the end of polymer chains. Eventually, molecular weight stopped increasing and slightly decreased by blocking effect. Lu et al. reported that if an excess amount of TBC chain extender was added, the blocking reaction would occur predominantly.[12] Due to the excess amount of chain extender, intrinsic viscosity led to reduction in the odds of chain segment contact. Molecular weights are scarcely different between adding PDA1 and EDA3 both in in-situ condition and 2-steps condition, independent of the type of diamines. It is supposed that the chain extending mechanisms for both types of diamines were almost same. Both diamines have similar structure and same bifunctional reactive groups at the end of molecules, the only difference are length of diamine molecules. So

it is not showed any noticeable differences on the tendency of molecular weight which was closely related to chain extending mechanism.

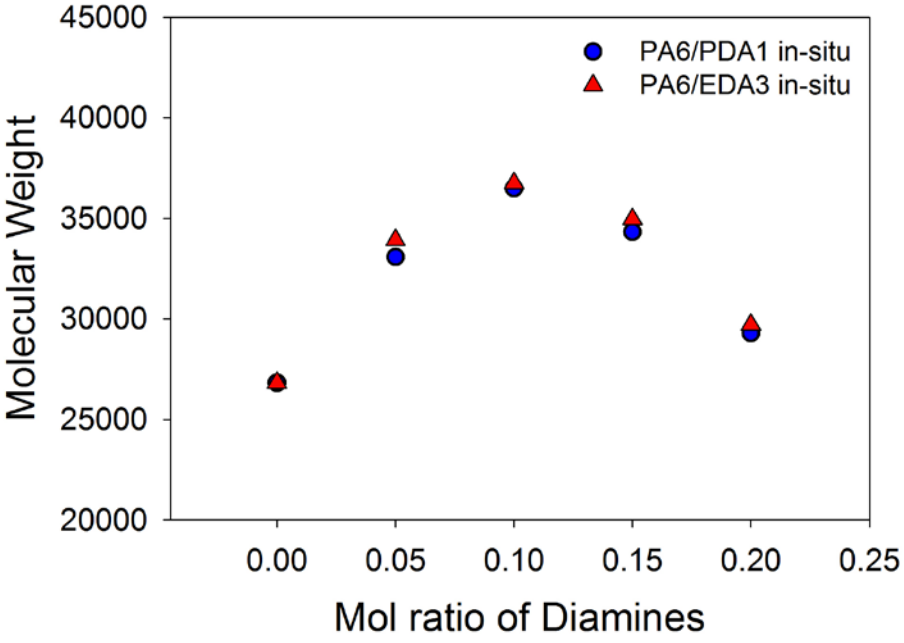

(a)

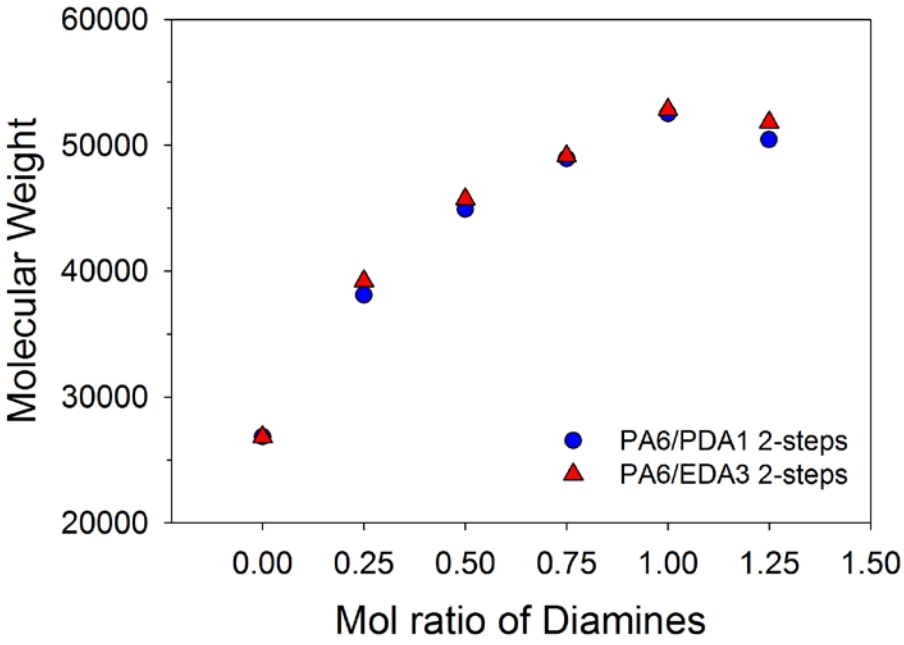

(b)

Figure 3.5 Molecular weights of PA6 and its composites which were calculated from intrinsic viscosity. (a) PA6/PDA1 and PA6/EDA3 composites prepared by in-situ reactive extrusion (b) PA6/PDA1 and PA6/EDA3 composites prepared by 2-steps reactive extrusion

3.3.4 Side reaction

To investigate the existence of crosslinking or branching, we measured the chain irregularity by UV spectrometer. The OD_{max} value of neat PA6 was 1.5 which was greatly higher than the value of a typical hydrolytic PA6 which is 0.044.[28] All the other PA6/diamine composites had shown extremely high values of OD_{max}, beyond the analysis range of UV spectrometer. It means that very high level of chain irregularity was existence in PA6 and its composites. To examine the PA6 and its composites had crosslinked or not more clearly, the gel content of PA6 and its composites had been extracted with solvent. After extraction, there had been almost nothing remained. According to the results from above two experimental, it implies that PA6 has very high level of chain irregularities but little amount of crosslinking existed, maybe almost of them are branching. In our experimental, highly branched PA6 was polymerized due to the polymerization conditions, which were relative high temperature and shear rate in the extruder as well as usage of bifunctional activator.

3.3.5 Rheological properties

Figure 3.6 shows the dependency of complex viscosity on frequency with varying the diamine amount. All PA6/diamine composites show higher values of viscosity and modulus than neat PA6 through the whole range of frequency. This tendency is remarkable at low frequency range and PA6/diamine composites show strong shear thinning behavior. It is observed in Figure 3.6 (a) and (b) that melt viscosity of in-situ

polymerized PA6/diamine composites increases with the more amount of diamine added up to mol ratio 0.1, because diamine extended the PA6 chain and entanglement molecular weight increased. On the other hand, viscosity decreases mol ratio of diamine 0.15 and 0.2, showing weaker shear thinning behavior than mol ration 0.05 and 0.1 of it relatively. These phenomena are closely related to the molecular weight and chain entanglement of composites. The more diamine added, the larger molecular weight and chain entanglement are due to the chain extending, simultaneously, the more chance was existed to block the living polymerization. So these two mechanisms counterbalanced each other and decided molecular weight, affecting to rheological properties. As a result, polymer chains show solid-like behavior and strong shear thinning effect especially at low frequency range. It is observed that the stronger shear thinning behaviors in 2-steps polymerization case than in-situ polymerization case in Figure 3.6 (c) and (d). In 2-steps process, more amount of diamine reacted to increase the molecular weight and entanglement molecular weight also increased, showing solid-like behaviors. Up to mol ration of diamine 1, melt viscosity of composites were dramatically increased, subsequently saturated and slightly decreased for mol ratio 1.25. These tendencies are same as molecular weight. In in-situ process, there are little difference between PDA1 and EDA3 because of small amount of diamine. But in 2-steps process, EDA3 has higher melt viscosity than PDA1 with large amount of diamine (Figure 3.6 (e)). It is supposed that EDA3 disrupts the PA6 chain movement because of its long ester molecular structure.

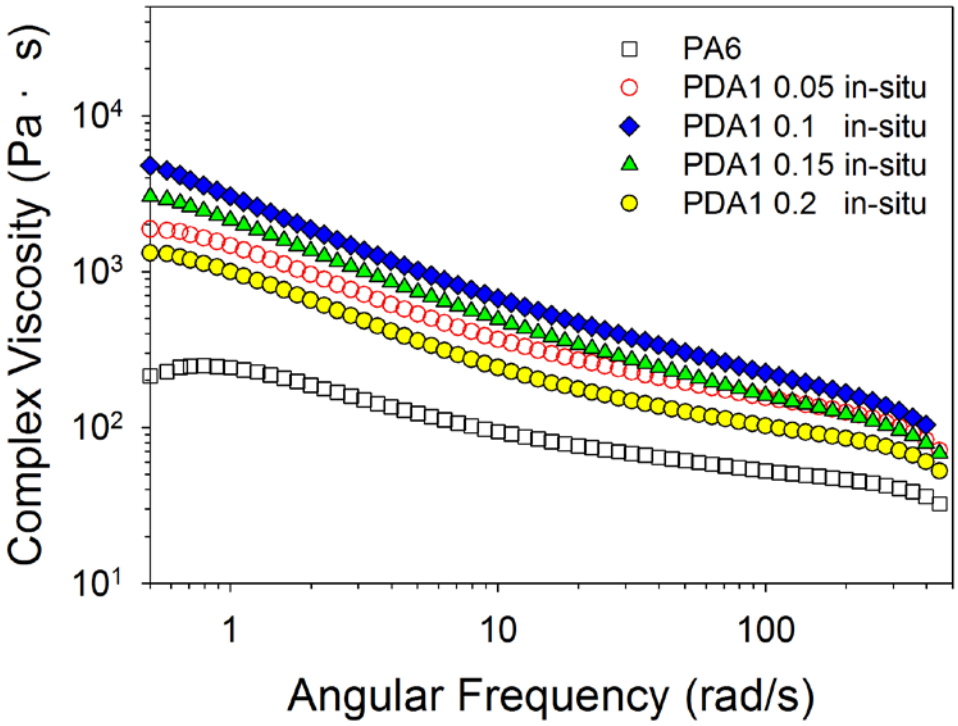
PA6
PDA1 0.05 in-situ
PDA1 0.1 in-situ
PDA1 0.15 in-situ
PDA1 0.2 in-situ
Complex Viscosity (Pa · s)
10⁴
10³
10²
10¹
1
10
100
Angular Frequency (rad/s)

(a)

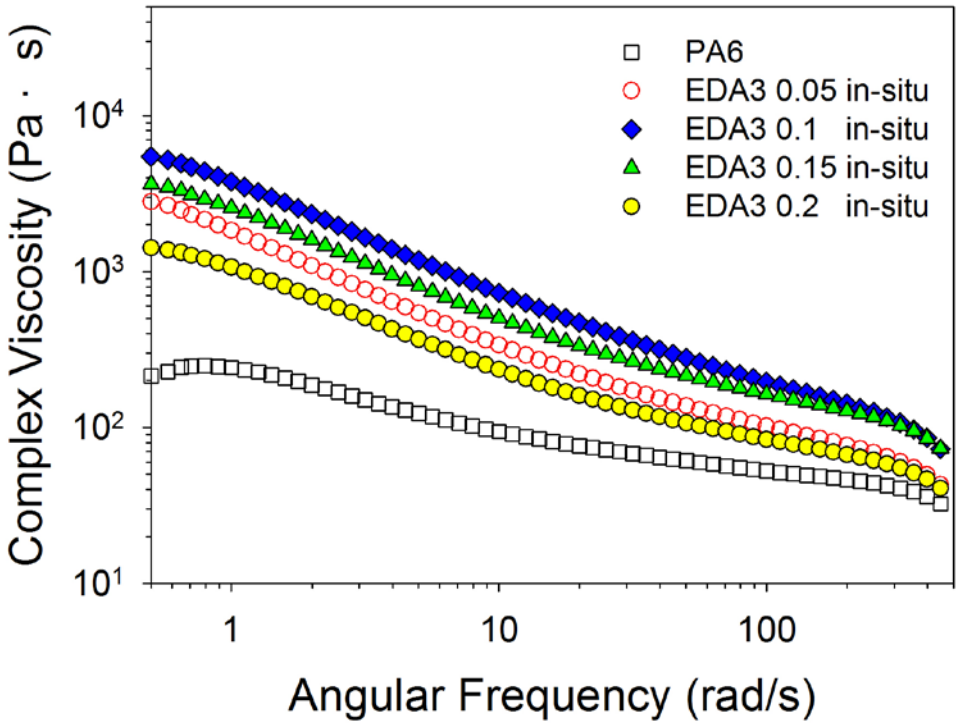
PA6
EDA3 0.05 in-situ
EDA3 0.1 in-situ
EDA3 0.15 in-situ
EDA3 0.2 in-situ
Complex Viscosity (Pa · s)
10⁴
10³
10²
10¹
1
10
100
Angular Frequency (rad/s)

(b)

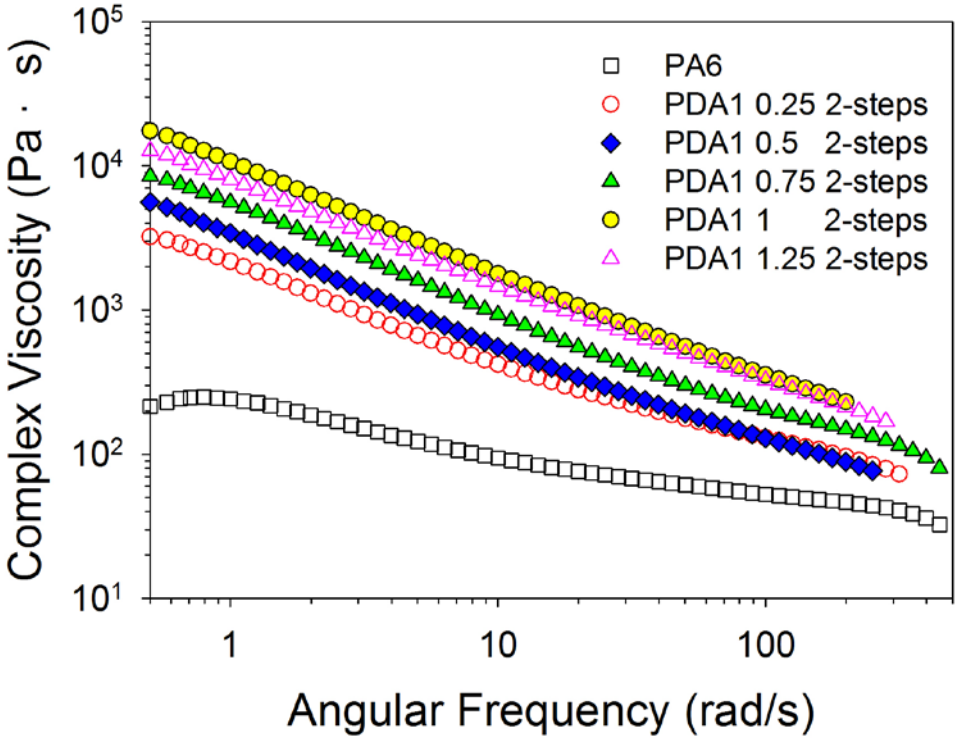
Complex Viscosity (Pa · s)
Angular Frequency (rad/s)
PA6
PDA1 0.25 2-steps
PDA1 0.5 2-steps
PDA1 0.75 2-steps
PDA1 1 2-steps
PDA1 1.25 2-steps

(c)

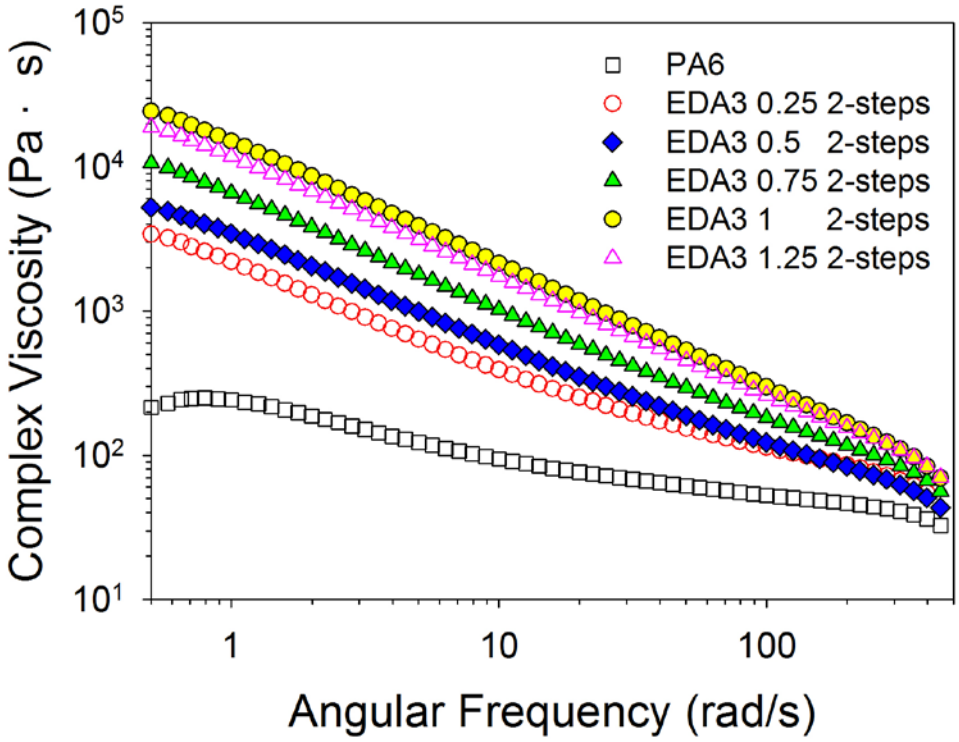
Complex Viscosity (Pa · s)
Angular Frequency (rad/s)
PA6
EDA3 0.25 2-steps
EDA3 0.5 2-steps
EDA3 0.75 2-steps
EDA3 1 2-steps
EDA3 1.25 2-steps

(d)

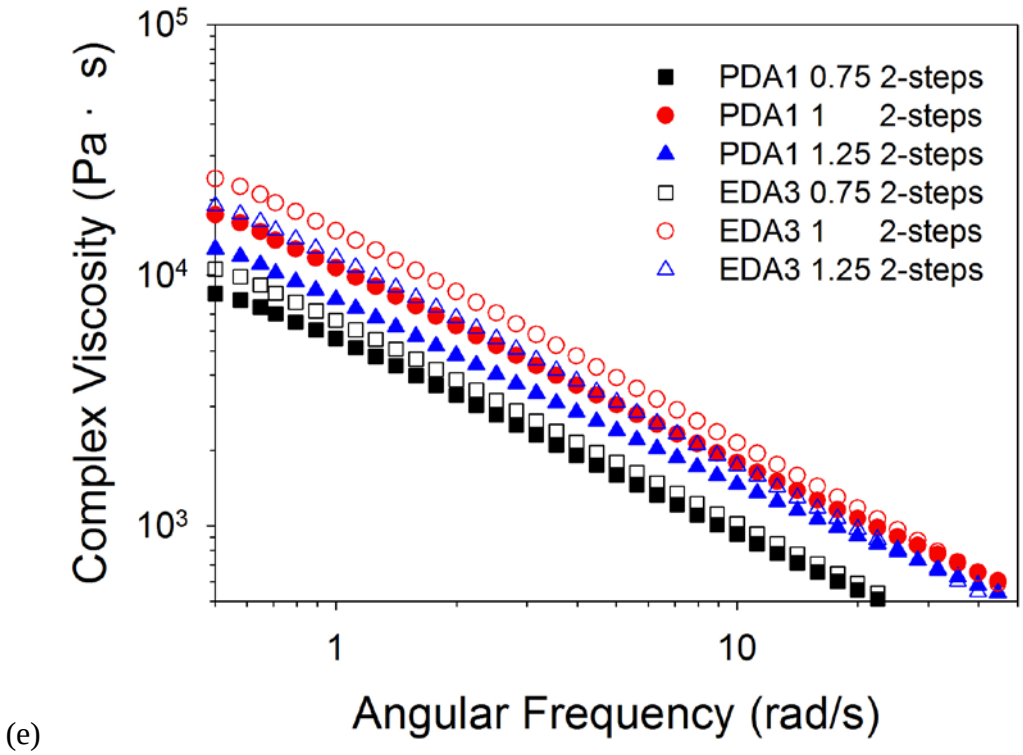

(e)

Figure 3.6 Complex viscosity of PA6 and its composites. (a) in-situ PDA1 composites (b) in-situ EDA3 composites (c) 2-steps PDA1 composites (d) 2-steps EDA3 composites (e) comparison of PDA1 with EDA3 for high concentration

In Figure 3.7 and 3.8, it is exhibited that storage and loss modulus of PA6 composites on frequency with varying the diamine amount. The slopes of PA6/diamine composites are gentler than PA6 and dramatically changed in storage modulus rather than on loss modulus. Both PDA1 and EDA3 by in-situ polymerization, storage and loss modulus increased to mol ratio of diamine 0.1, subsequently decreased mol ratio of diamine 0.15 and 0.2. It is observed in 2-steps polymerization that changing tendency of modulus also similar to in-situ polymerization and follows molecular weight. In general linear polymer melts, storage modulus is proportional to the square of frequency and loss modulus is proportional to frequency, following viscoelastic motion. But in our research, modulus of PA6/diamine composites was largely deviated from linear viscoelastic motion and G' is larger than G" in all frequency range. It implied that polymer chains of composites were almost solid-like behavior and crosslinked or branched. Especially neat PA6 also shows this non-linear viscoelastic behavior, G' is larger than G". It means PA6 composites were branched or crosslinked even without the diamine chain extender. In this study, non-linear viscoelastic and solid-like behavior can be interpreted by the branching of PA6. The branched polymers require greater strain to untangle the molecules and permit them to flow. Linear polymers are simply long polymer chains with little or no branching, and are more easily untangled when a strain is applied. The branched PA6 chains were connected and extended by diamine chain extenders, achieving high molecular branched PA6/diamine composites. In 2-steps composites are observed same tendencies. This means that diamine chain extenders reacted with caprolactam end groups located main or side chain end position and induced branched PA6. The large amount of diamine added, molecular weight increased more than in-situ cases, caused strong shear thinning and solid-like behavior.

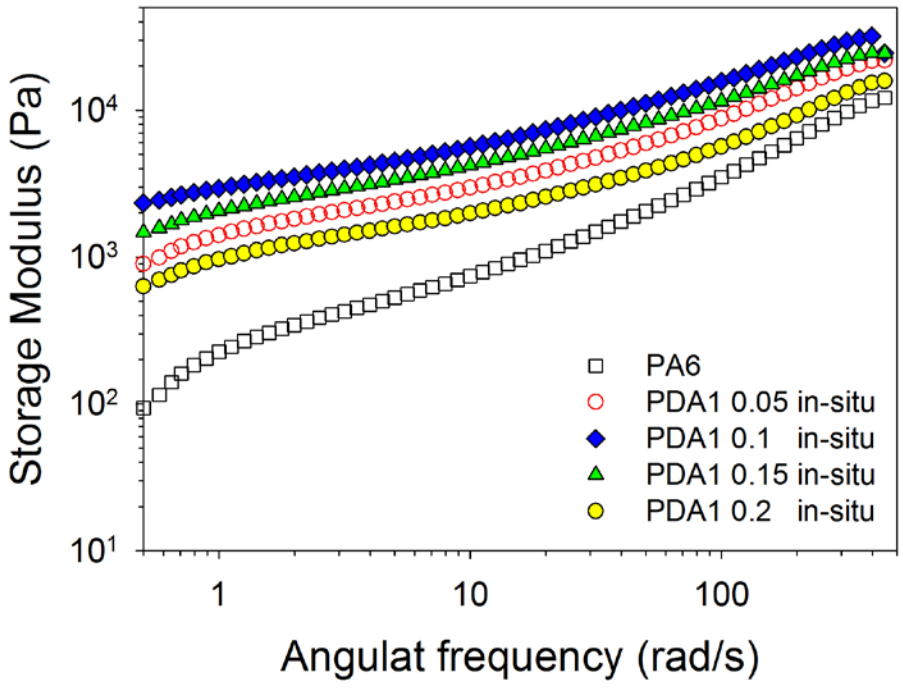
Storage Modulus (Pa)
10^4
10^3
10^2
10^1
1
10
100
Angulat frequency (rad/s)
PA6
PDA1 0.05 in-situ
PDA1 0.1 in-situ
PDA1 0.15 in-situ
PDA1 0.2 in-situ

(a)

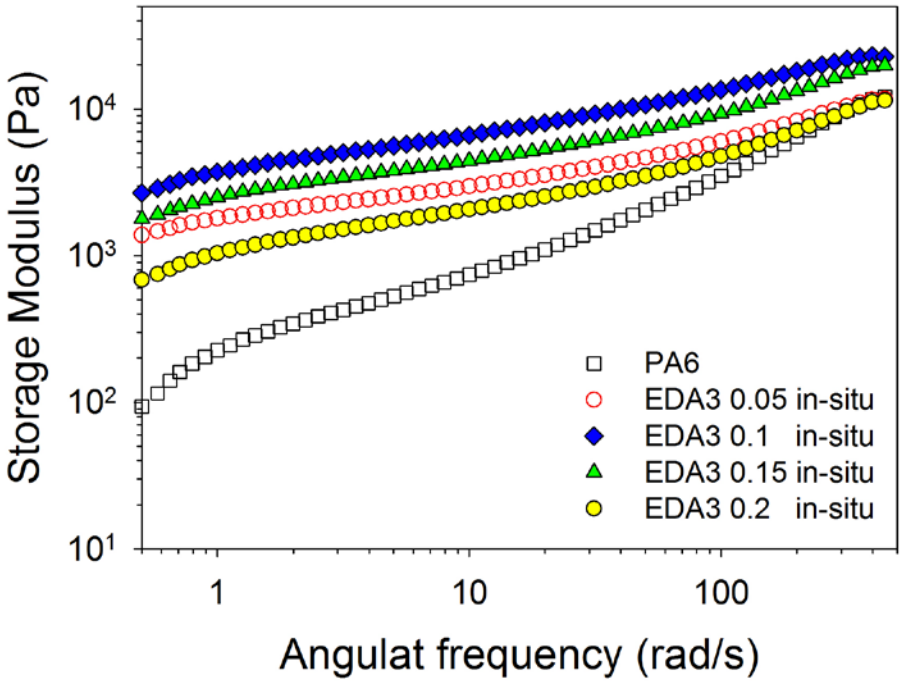
Storage Modulus (Pa)
10^4
10^3
10^2
10^1
1
10
100
Angulat frequency (rad/s)
PA6
EDA3 0.05 in-situ
EDA3 0.1 in-situ
EDA3 0.15 in-situ
EDA3 0.2 in-situ

(b)

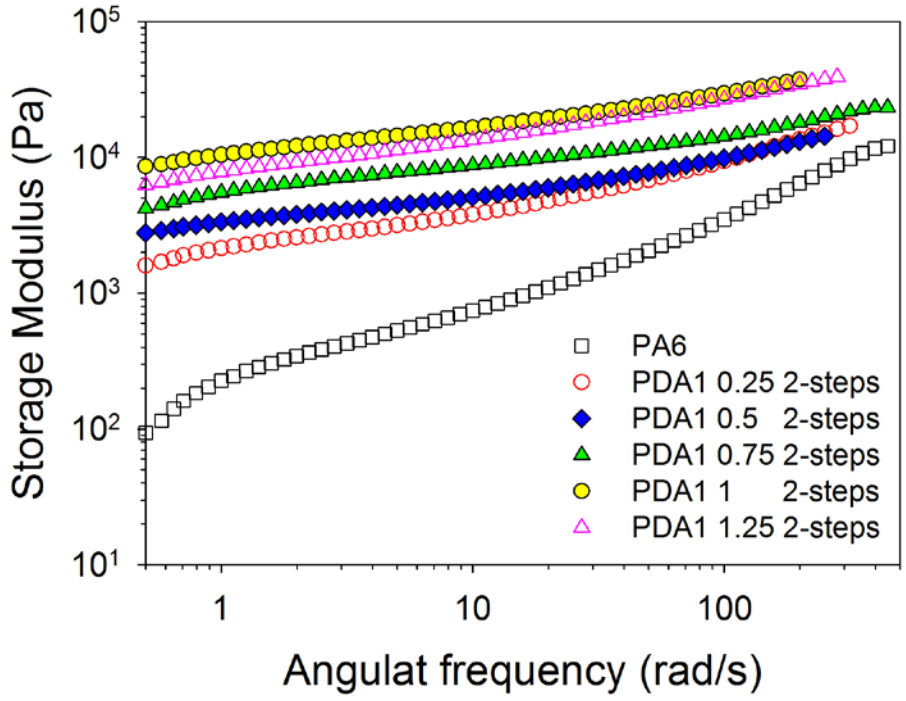

(c)

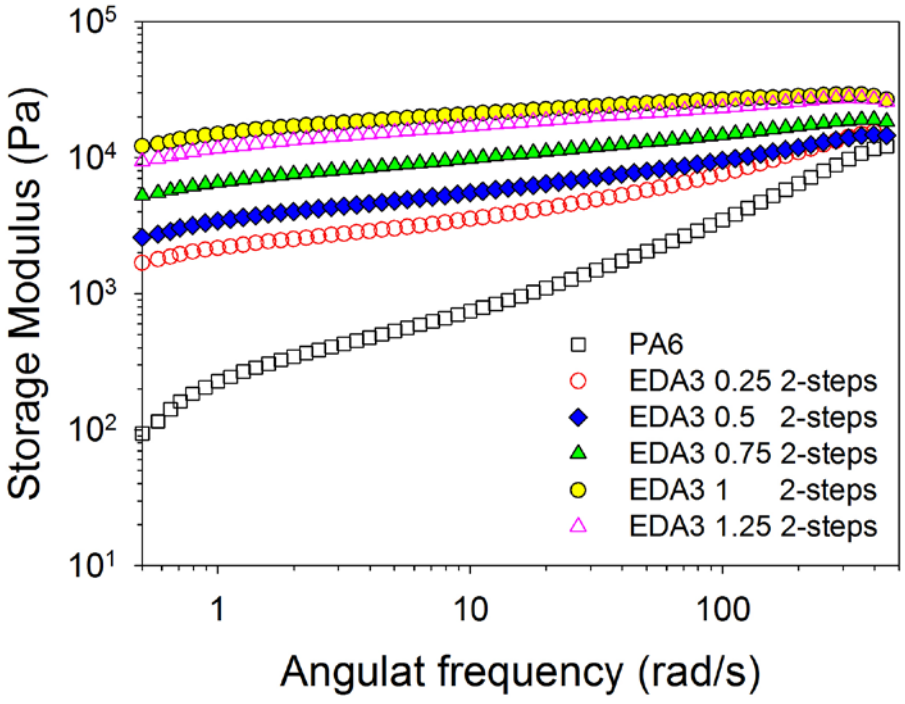

(d)

Figure 3.7 Storage modulus of PA6 and its composites. (a) in-situ PDA1 composites (b) in-situ EDA3 composites (c) 2-steps PDA1 composites (d) 2-steps EDA3 composites

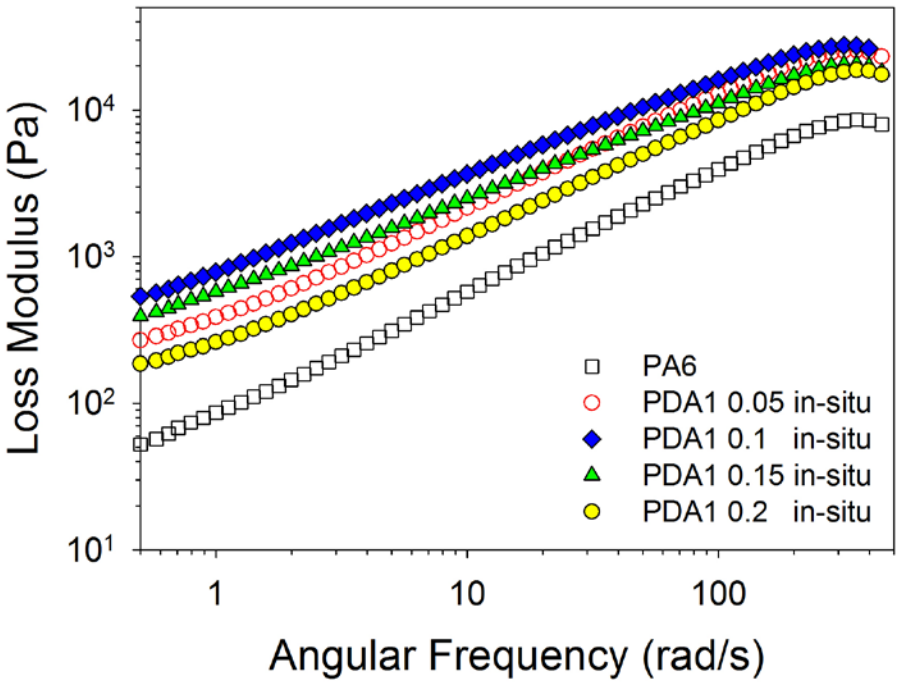
Loss Modulus (Pa)
10^4
10^3
10^2
10^1
1
10
100
Angular Frequency (rad/s)
PA6
PDA1 0.05 in-situ
PDA1 0.1 in-situ
PDA1 0.15 in-situ
PDA1 0.2 in-situ

(a)

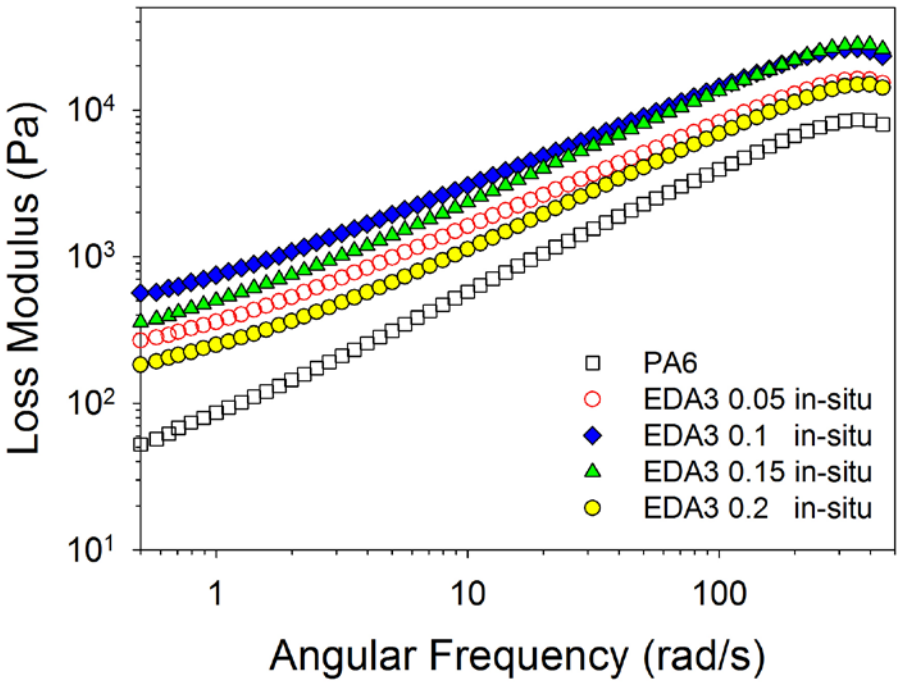
Loss Modulus (Pa)
10^4
10^3
10^2
10^1
1
10
100
Angular Frequency (rad/s)
PA6
EDA3 0.05 in-situ
EDA3 0.1 in-situ
EDA3 0.15 in-situ
EDA3 0.2 in-situ

(b)

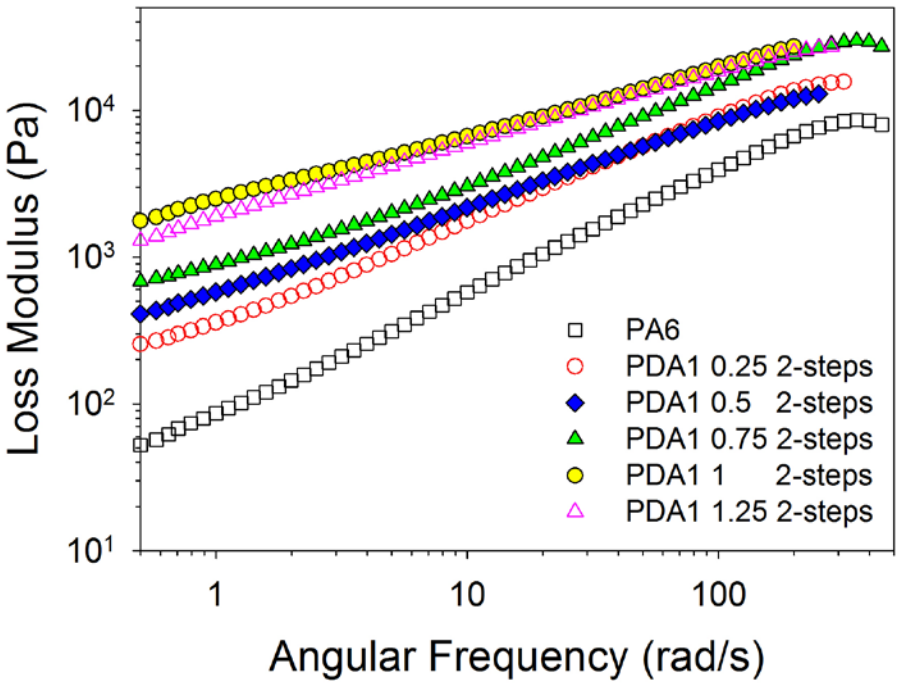

(c)

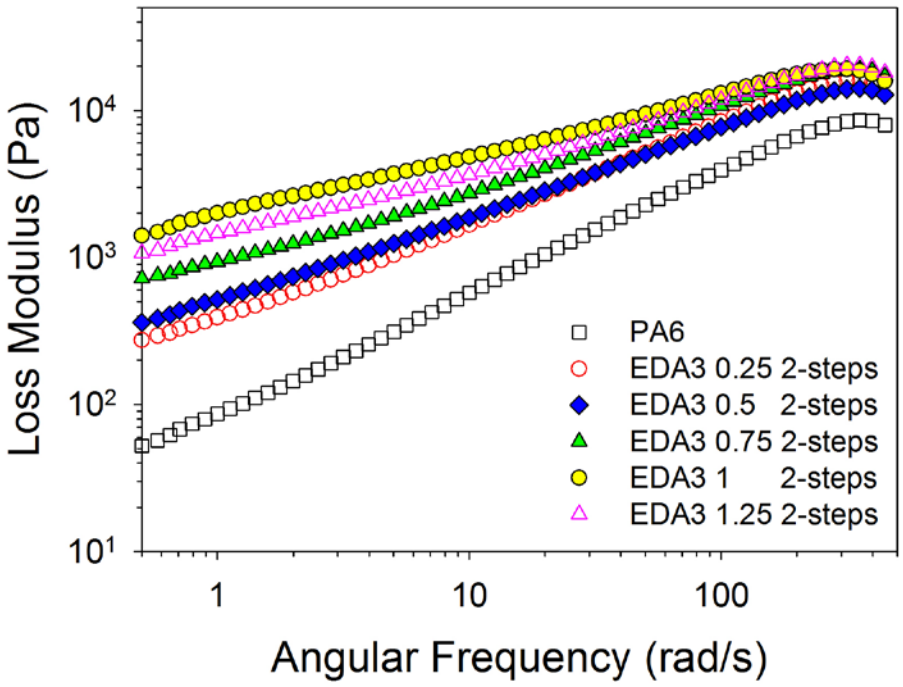

(d)

Figure 3.8 Loss modulus of PA6 and its composites. (a) in-situ PDA1 composites (b) in-situ EDA3 composites (c) 2-steps PDA1 composites (d) 2-steps EDA3 composites

3.3.6 Mechanical properties

Some important mechanical properties are summarized in Figure 3.9 and Table 3.3. It is observed that all mechanical properties were improved with introducing diamine chain extender. In in-situ process, the elastic modulus and tensile strength increased with diamine added until mol ratio 0.1 because of the high molecular weight, subsequently, decreased with more amount of diamine added. In 2-steps process, modulus and strength also increased with diamine added, above the mol ratio of diamine 1, these properties slightly decreased. (Figure 3.9 (a) and (b)) Lu et al. and Bucella et al. reported that modulus and tensile strength had slightly decreased with the chain extender concentration, because of the crystallinity reduction.[12,13,34] But in our study, the opposite tendency was observed. Despite the reduction of crystallinity, modulus and tensile strength were improved with introducing chain extender because the effect of molecular weight increasing was more dominant than the effect of crystallinity drop. It is supported by the results from molecular weight of composites.

Comparatively, elongation of composites was dramatically improved compared with modulus and strength in Figure 3.9 (c). Similar to modulus and tensile strength, elongation change was affected by molecular weight and chain entanglement of PA6 composites. Elongation was increased with diamine concentration and decreased beyond optimum amount of diamine added for both in-situ and 2-steps process. Chain extended PA6 had elongated about 2~5 times longer than neat PA6. Diamine chain extender connected PA6 chains at inter-lamella position and entangled PA6 chains when shear stress applied. So chain extender probably disrupts the PA6 chains slide toward

applied shear force direction. Even there are little difference of modulus and tensile strength between PDA1 and EDA3 both in-situ and 2-steps process, considering standard error, distinct difference of elongation between PDA1 and EDA3 in 2-steps process. In Figure 3.6 (e), melt viscosity of PA6/EDA3 composites was higher than it of PA6/PDA1 composites because EDA3 has longer ester molecular structure than PDA1, disturbing the chain movement of PA6. Likewise, chain slip and mobility disturbed by EDA3 stronger than PDA1, then PA6composite had been more elongated. Also, energy absorbed to break was progressed which is related to toughness of materials in Figure 3.9 (d). The improvement of toughness is largely depending on increasing elongation. Increased molecular weight and chain entanglement by chain extension, leads to strong resistance to deformation and absorbs more energy until fracture.

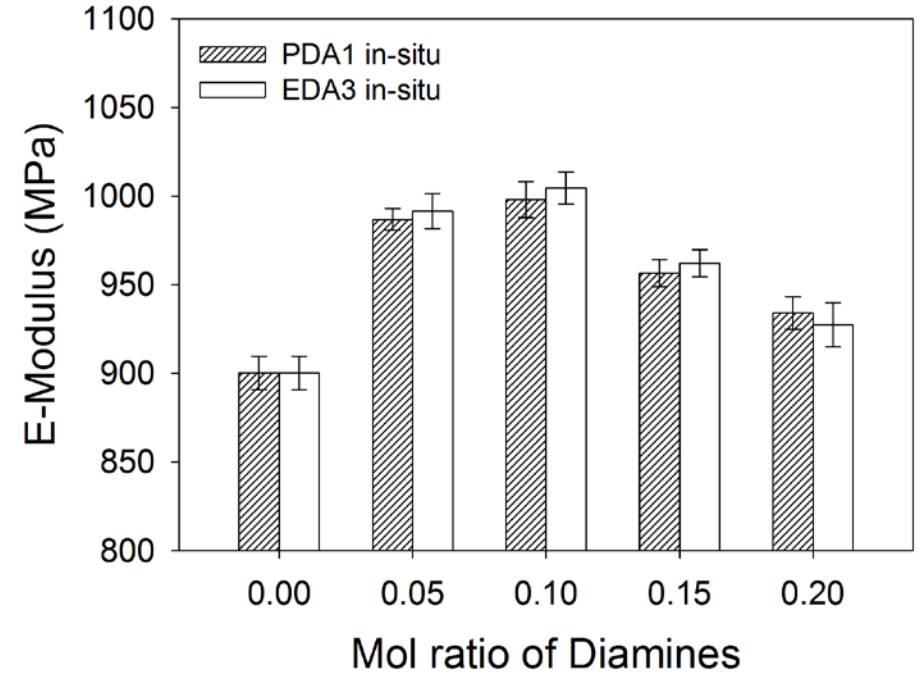
PDA1 in-situ
EDA3 in-situ
E-Modulus (MPa)
1100
1050
1000
950
900
850
800
0.00
0.05
0.10
0.15
0.20
Mol ratio of Diamines

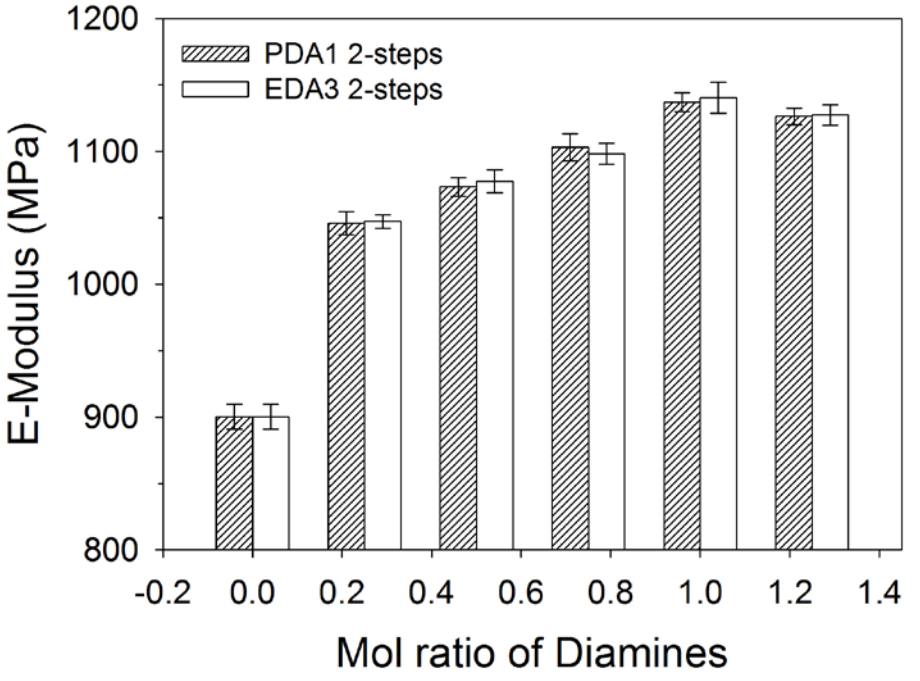
PDA1 2-steps
EDA3 2-steps
E-Modulus (MPa)
1200
1100
1000
900
800
-0.2
0.0
0.2
0.4
0.6
0.8
1.0
1.2
1.4
Mol ratio of Diamines

(a)

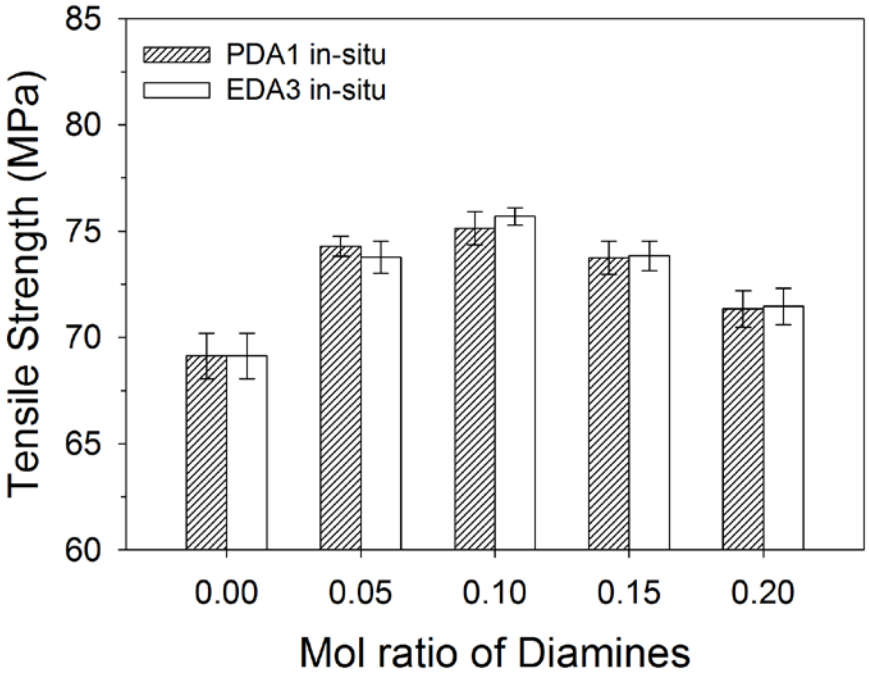
PDA1 in-situ
EDA3 in-situ
Tensile Strength (MPa)
85
80
75
70
65
60
0.00
0.05
0.10
0.15
0.20
Mol ratio of Diamines

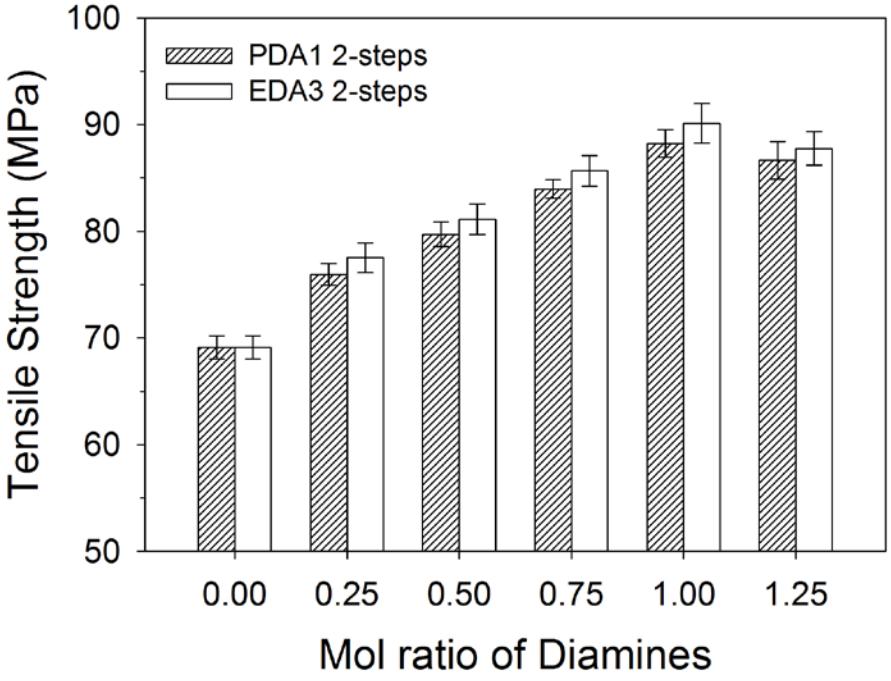
PDA1 2-steps
EDA3 2-steps
Tensile Strength (MPa)
100
90
80
70
60
50
0.00
0.25
0.50
0.75
1.00
1.25
Mol ratio of Diamines

(b)

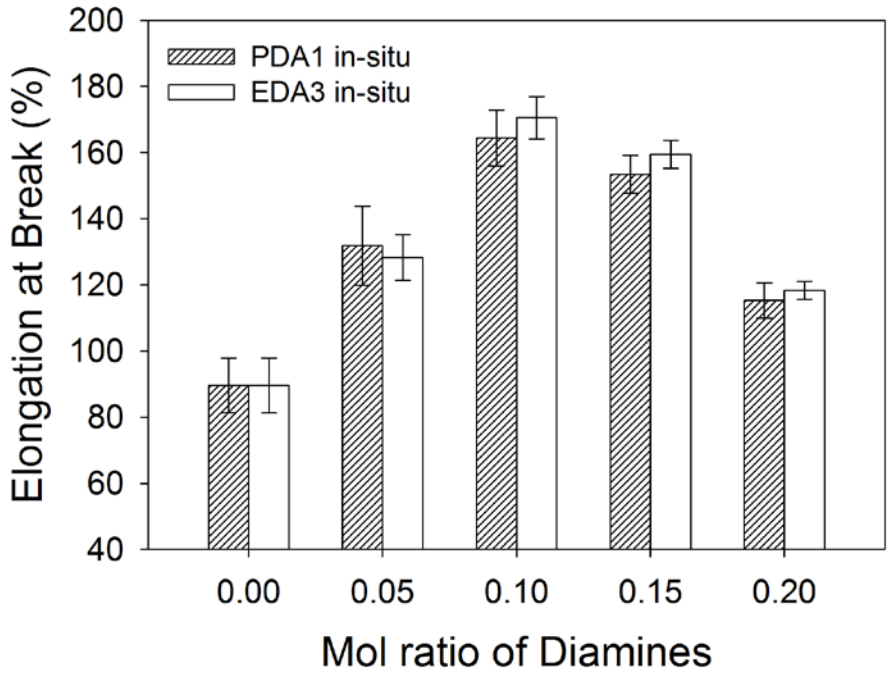
PDA1 in-situ
EDA3 in-situ
Elongation at Break (%)
200
180
160
140
120
100
80
60
40
0.00
0.05
0.10
0.15
0.20
Mol ratio of Diamines

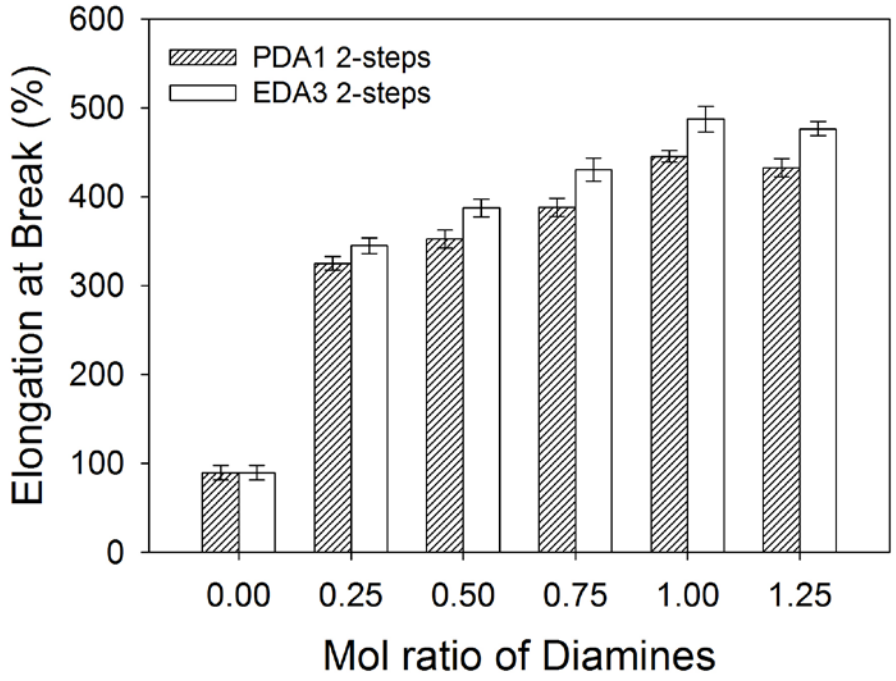
PDA1 2-steps
EDA3 2-steps
Elongation at Break (%)
600
500
400
300
200
100
0
0.00
0.25
0.50
0.75
1.00
1.25
Mol ratio of Diamines

(c)

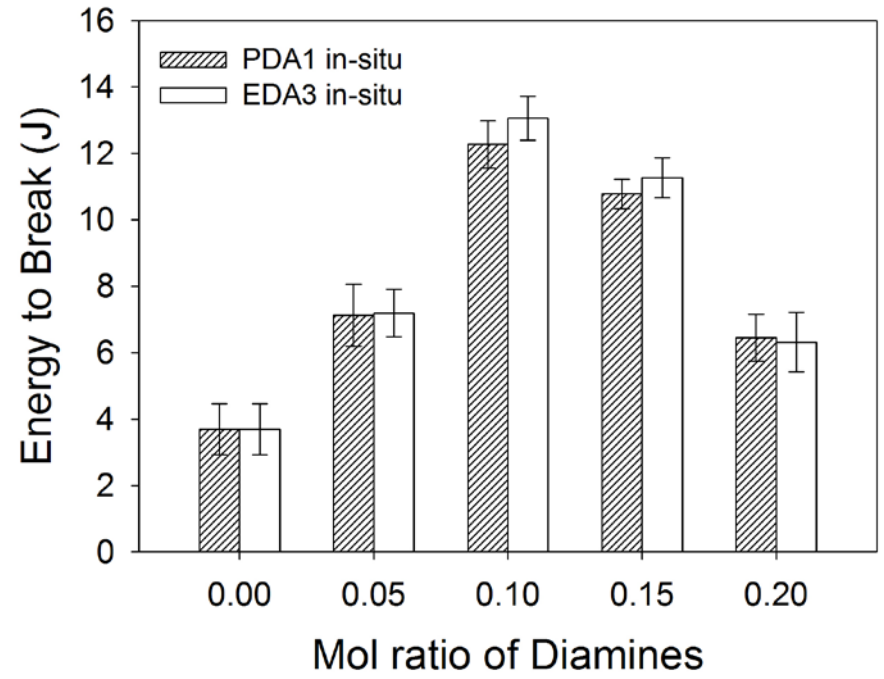

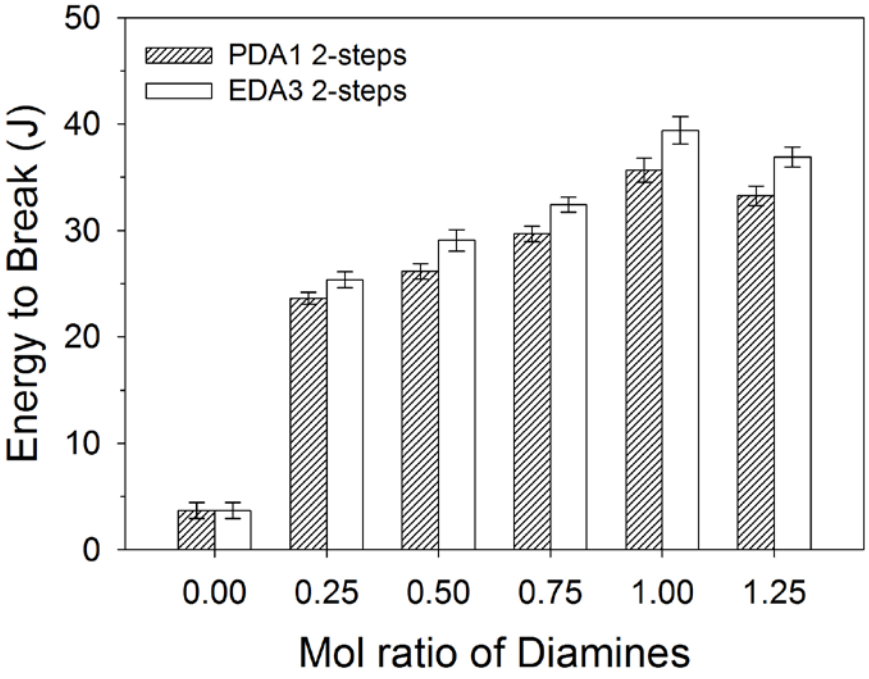

(d)

Figure 3.9 The results of tensile test. (a) elastic modulus (b) ultimate tensile strength (c) elongation at break (d) absorption energy to break

Samples	Modulus (MPa)	Tensile strength (MPa)	Elongation (%)	Energy to break (J)
PA6 (Ny6)	900	69.1	89.5	3.69
PDA1 0.05s	987	74.3	131.8	7.12
PDA1 0.1s	998	75.1	164.4	12.27
PDA1 0.15s	956	73.8	153.4	10.78
PDA1 0.2s	934	71.3	115.3	6.45
EDA3 0.05s	992	73.8	128.3	7.19
EDA3 0.1s	1004	75.7	170.6	13.07
EDA3 0.15s	962	73.8	159.4	11.27
EDA3 0.2s	927	71.5	118.3	6.32
PDA1 0.25f	1046	76.0	325.1	23.63
PDA1 0.5f	1073	79.7	352.4	26.15
PDA1 0.75f	1103	84.0	388.1	29.68
PDA1 1f	1137	88.2	445.3	35.67
PDA1 1.25f	1126	86.7	432.8	33.27
EDA3 0.25f	1047	77.5	345.0	25.38
EDA3 0.5f	1078	81.1	387.4	29.08
EDA3 0.75f	1098	85.7	430.5	32.43
EDA3 1f	1140	90.1	487.3	39.41
EDA3 1.25f	1127	87.8	476.5	36.92

Table 3.3 The values of mechanical properties of PA6/diamine composites.

3.4 Conclusion

In this study, we successfully polymerized PA6 and its composites with diamine through reactive extrusion from monomers. In the extruder, ε-caprolactam completely reacted to form PA6 polymer composite without any residual monomers. With diamine chain extender, PA6 chains connected and molecular weight was increased both in-situ and 2-steps process. For small amount of diamine added, chain extending effect is more dominant than blocking effect. So the molecular weight increased by chain extending. But, beyond optimum amount of diamine concentration (0.15 for in-situ and 1.25 for 2-steps), the molecular weight reduced because the blocking effect was more dominant than chain extending effect. Crystallinity was dropped with introducing diamine chain extenders, due to the hindrance of diamine molecules on crystallization. Even though diamine chain extenders disturbed the crystallization, did not form γ-crystalline phase or other new phase neither because chain extenders remained in inter-lamella amorphous region.

Even the crystallinity had reduced with diamine additives, elastic modulus and tensile strength were improved. It was originated from the increase of molecular weight and chain entanglement. High molecular weight highly branched PA6 composites were synthesized with connecting PA6 chains each other. Highly branched high molecular weight PA6 chains depressed the chain mobility and improved the resistance applied shear force so that elongation and toughness were advanced. It was supported by rheological properties. PA6/diamine composites exhibited extremely higher melt viscosity and strong shear thinning effect than neat PA6 through whole measured

frequency range. It has induced from the increased molecular weight and entanglement of chains. Storage and loss modulus also exhibited solid-like behavior and increased with diamine concentration subsequently decreased above critical concentration. Especially, storage modulus higher than loss modulus through the frequency range, it was because of high level of branching. PA6 had branched during the polymerization because of the high polymerization temperature, high shear rate in extruder and bifunctional activator. The molecular structure of diamine did not affect to crystallization and extending mechanism noticeably. But large amount of diamine added, EDA3 hindered the chain mobility more than PDA1 because EDA3 has long ester benzoate structure. To obtain high performance PA6 composite, the designed structure of diamine and appropriate reaction condition are needed.

3.5 References

[1] Bessell, T.; Shortall, J. B. J Mater Sci 1975, 10, (12), 2035-2043.

[2] Pillay, S.; Vaidya, U. K.; Janowski, G. M. J Thermoplast Compos 2005, 18, (6), 509-527.

[3] Gong, Y.; Liu, A.; Yang, G. Composites Part A: Applied Science and Manufacturing 2010, 41, (8), 1006-1011.

[4] Hedrick, R. M.; Gabbert, J. D.; Wohl, M. H. Acs Sym Ser 1985, 270, 135-162.

[5] Hornsby, P. R.; Tung, J. F.; Tarverdi, K. J Appl Polym Sci 1994, 53, (7), 891-897.

[6] Kye, H.; White, J. L. J Appl Polym Sci 1994, 52, (9), 1249-1262.

[7] Qian, Z. Y.; Chen, X.; Xu, J.; Guo, B. H. J Appl Polym Sci 2004, 94, (6), 2347-2355.

[8] Guo, B. H.; Chan, C. M. J Appl Polym Sci 1999, 71, (11), 1827-1834.

[9] Haralabakopoulos, A. A.; Tsiourvas, D.; Paleos, C. M. J Appl Polym Sci 1999, 71, (13), 2121-2127.

[10] Akkapeddi, M.; Gervasi, J. Polymer Preprints (ACS, Division of Polymer Chemistry) 1988, 29, (1), 567.

[11] Loontjens, T. J Polym Sci Pol Chem 2003, 41, (21), 3198-3205.

[12] Lu, C.; Ye, R.; Yang, Y.; Ren, X.; Cai, X. Journal of Macromolecular Science, Part B 2011, 50, (2), 350-362.

[13] Buccella, M.; Dorigato, A.; Caldara, M.; Pasqualini, E.; Fambri, L. Journal of Polymer Research 2013, 20, (9).

[14] Inata, H.; Matsumura, S. J Appl Polym Sci 1985, 30, (8), 3325-3337.

[15] Torres, N.; Robin, J. J.; Boutevin, B. J Appl Polym Sci 2001, 79, (10), 1816-1824.

[16] Novitsky, T. F.; Mathias, L. J. J Polym Sci Pol Chem 2011, 49, (10), 2271-2280.

[17] Novitsky, T. F.; Mathias, L. J.; Osborn, S.; Ayotte, R.; Manning, S. Macromolecular Symposia 2012, 313-314, (1), 90-99.

[18] Ross Melvin Hedrick, J. D. G. Lactam-Polyol-Polyacyl Lactam Terpolymers. 4031164, 1977.

[19] Yn, M. S.; Ma, C. C. M. J Appl Polym Sci 1994, 53, (2), 213-224.

[20] Wilfong, D. L.; Pommerening, C. A.; Gardlund, Z. G. Polymer 1992, 33, (18), 3884-3888.

[21] Yelamaggad, C. V.; Hiremath, U. S.; Nagamani, S. A.; Rao, D. S. S.; Prasad, S. K. J Mater Chem 2001, 11, (7), 1818-1822.

[22] Brandrup J., I. E. H., Polymer Handbook. 1989.

[23] Cheng, L. P.; Dwan, A. H.; Gryte, C. C. J Polym Sci Pol Phys 1994, 32, (7), 1183-1190.

[24] Dadbin, S.; Frounchi, M.; Goudarzi, D. Polym Degrad Stabil 2005, 89, (3), 436-441.

[25] Ricco, L.; Monticelli, O.; Russo, S.; Paglianti, A.; Mariani, A. Macromol Chem Physic 2002, 203, (10-11), 1436-1444.

[26] Ricco, L.; Russo, S.; Orefice, G.; Riva, F. Macromolecules 1999, 32, (23), 7726-7731.

[27] Fornes, T. D.; Paul, D. R. Polymer 2003, 44, (14), 3945-3961.

[28] Russo, S.; Biagini, E.; Bonta, G. Makromol Chem-M Symp 1991, 48-9, 31-46.

[29] Rached, R.; Hoppe, S.; Fonteix, C.; Schrauwen, C.; Pla, F. Chemical Engineering Science 2005, 60, (10), 2715-2727.

[30] Kim, K. J.; Kim, Y. Y.; Yoon, B. S.; Yoon, K. J. J Appl Polym Sci 1995, 57, (11),

1347-1358.

[31] Stehlicek, J.; Sebenda, J. Eur Polym J 1986, 22, (10), 769-773.

[32] Petit, D.; Jerome, R.; Teyssie, P. J Polym Sci Pol Chem 1979, 17, (9), 2903-2916.

[33] Russo, S.; Imperato, A.; Mariani, A.; Parodi, F. Macromol Chem Physic 1995, 196, (10), 3297-3303.

[34] Lu, C. X.; Chen, T.; Zhao, X. Z.; Ren, X. C.; Cai, X. F. J Polym Sci Pol Phys 2007, 45, (15), 1976-1982.

Chapter 4

In-situ polymerization of epoxy based thermotropic liquid crystalline polymers by reactive extrusion and its liquid crystalline behaviors.

4.1 Introduction

Thermotropic liquid crystalline polymers, TLCPs, are the polymers which exhibit liquid crystalline phase behavior depends on the temperature. TLCPs have been largely investigated due to their unique properties such as high strength, excellent dimensional and thermal stability, outstanding chemical resistance and remarkable barrier properties.[1] Generally, TLCPs have a rigid rod-like or disk-like structure or contain mesogenic groups as repeating units on their main polymer chain or side pendent groups. Because, specific properties of TLCPs are largely related with their structures, hence many characteristic structured TLCPs have been synthesized and investigated in the past decades.[2-5] For outstanding high properties, lots of TLCPs have linear and rigid mesogenic groups such as aromatic groups located in the polymer main chain.

However, the unique structures of TLCPs lead to some problems. During synthesize the TLCPs, the liquid crystalline-isotropic phase transition temperature is quickly shifted to higher temperature even at low degree of polymerization. Similarly, the melting point of TLCPs increases even rises to above the decomposition temperature. It

makes hard to apply or handle the TLCPs. In order to decrease the melting temperature, there have been some methods of modifying the rigid, rod-shaped basic structure were used, copolymerization of different monomers, inclusion of flexible chains in the main chain, and attachment of flexible side-chain or bulky substituents. Through suitable combinations of different monomer units, the linearity of macromolecule can be reduced by less symmetric comonomer unit or other structured aromatic groups.[6-10] Also, adoption of flexible spacer becomes one of the solutions.[11-16] With increasing length of the flexible chain between the mesogenic groups such as alkyl or alkoxy chain, the liquid crystalline-isotropic transition temperature is lowered. Flexible chains as well as bulky aromatic groups attach on the lateral axis of rigid mesogenic unit can help manufacturing TLCPs.[13,14,17] Substituted pendant groups reduce the polymer-polymer interactions and hence decrease the melting point. In spite of the solutions mentioned above, problems on handling were not solved completely and still remained on further compounding with other polymers.

In-situ reactive extrusion (REX) can be one of the solutions. In REX process, monomers or oligomers are fed into the extruder without any solvents or additives instead of handling TLCPs. Because, the monomers can be handled easier than polymers even at low temperature, REX process is a very attractive method to overcome the problems. Also REX process is a high shear induced process hence it can helps mixing or compounding LCPs rather than other processes such as molding, solution casting and spinning. Moreover, REX process has advantages on cost because it is one-stage and short reaction time process.

Also to accelerate the polymerization rate, epoxy functional groups attached at the mesogenic unit and reacted with amine monomers. Epoxy-amine system is well known

ultra-fast reaction system for epoxy thermosets generally as well as thermoplastic.[18,19] A number of experiments exist which describe the synthesis of linear epoxy-amine addition polymers by using primary monoamines or disecondary diamines.[20-26] Blanco et al. reacted a DGEBA based epoxy with monoamine, p-toluidine, to obtain linear epoxides with M_n of 19,400 g/mol.[25] Kawakami et al. also synthesized a 26,000 g/mol thermoplastic epoxy by reaction of DGEBA based epoxy with aniline.[26] Klee et al. employed secondary diamines to yield linear epoxides with M_n values between 8,000 to 18,000 g/mol.[24]

In this study, we adopted in-situ REX process to overcome the handling problems of TLCPs and to maximize the advantage of processability. All the processes were performed at one-stage in twin-screw extruder from the monomers to final TLCP products. Epoxy-amine reaction system was used for higher polymerization rate, introducing liquid crystalline epoxy (LCE) which has long rigid mesogenic unit located in the middle of molecules. We synthesized various structured LCEs and polymerized it with monoamines to produce epoxy based TLCPs. The relationship between chemical structure and thermal properties and LC behaviors were also investigated.

4.2 Experimental

4.2.1 Materials

Ethyl-4-hydroxybenzoate, 3-bromopropene, 5-bromopentene, hydroquinone, 3-chloroperoxybenzoic acid, aniline and 1-naphthylamine were purchased from Aldrich. p-Phenylene-di[4-(2,3-epoxypropenyloxy) benzoate] (LCE1, Figure 4.1 (a)) and p-Phenylene-di[4-(4,5-epoxypropenyloxy) benzoate] (LCE3, Figure 4.1 (b)) were synthesized in laboratory.

4.2.2 Synthesis

4.2.2.1 p-Phenylene-di[4-(2,3-epoxypropenyloxy) benzoate] (LCE1)

Synthetic scheme was reported by Jun Yeob Lee.[27] LCE1 was purified by column chromatography using CH_2Cl_2 as an eluent solvent. After evaporation of solvent, the LCE1 product recrystallized in CH_2Cl_2.

Transition temperatures are following. Crystal to nematic : 182℃, nematic to isotropic : 233℃. Yield: 55%. H-NMR spectrum ($CDCl_3$): δ (ppm) 8.13 (4H, d), 7.23 (4H, s), 6.99 (4H, d), 4.33 (2H, dd, CH_2 of glycidyl), 4.02 (2H, dd, CH_2 of glycidyl), 3.38 (2H, s, CH of epoxy), 2.92 (2H, dd, CH of epoxy), 2.78 (2H, dd, CH of epoxy).

4.2.2.2 p-Phenylene-di[4-(4,5-epoxypropenyloxy) benzoate] (LCE3)

Synthetic scheme was as same as LCE1, expect using 5-bromopentene instead of 3-bromopropene.

Transition temperatures are following. Crystal to smectic : 110℃, smectic to nematic : 139℃, nematic to isotropic : 235℃. Yield: 69%. H-NMR spectrum ($CDCl_3$): δ (ppm) 8.12 (4H, d), 7.24 (4H, s), 6.96 (4H, d), 4.11 (4H, m, CH_2 of glycidyl), 3.01 (2H, m, CH of epoxy), 2.78 (2H, m, CH of epoxy), 2.51 (2H, m, CH of epoxy), 2.01 (4H, m, CH_2 of glycidyl), 1.85 (2H, m, CH_2 of glycidyl), 1.67 (2H, m, CH_2 of glycidyl).

4.2.3 Polymerization of LCE/amine LCPs

4.2.3.1 Bulk polymerization of LCE/amine LCPs

The polymerization scheme and condition are exhibited in Scheme 4.1 and Table 4.1. LCE and amine were fed into round flask with magnetic stirrer and condenser, the mol ratio of LCE : amine was 1 : 1. LCE/amine LCP was polymerized at 250℃, 30 min in nitrogen atmosphere.

4.2.3.2 In-situ polymerization of LCE/amine LCPs by reactive extrusion

Reactant mixtures were composed of LCE and amine that the mol ratio was 1 : 1. The reactant mixtures were fed into twin screw extruder (mini extruder), with flowing nitrogen. The temperature profiles from feeding zone to die were set 200/230/240/245℃, screw speed was set to 30 rpm.

4.2.4 Characterization

H-NMR and C-NMR spectra were obtained by Bruker spectrometer (300 MHz). Samples were prepared by dissolving in THF-d8 solvent. H-NMR spectra were referenced to residual TMS (0 ppm) except D_2O (solvent reference, 4.79 ppm) and DMF-d_7 (solvent reference, 8.03 ppm). Chemical shifts of the C-NMR spectra were measured relative to DMF-d_7 (67.21 and 25.31 ppm). Thermal gravimetric Analysis (TGA, TGA/DSC1, Mettler Toledo) and Differential scanning calorimetry (DSC, DSC 823e, Mettler Toledo) were used to analyze the thermal properties, degradation temperature and transition behaviors of LCE/amine LCPs. Under a nitrogen atmosphere, samples were heated from 25℃ to 450℃ at 10 ℃/min for TGA. For DSC, samples were first heated from 25℃ to 320℃ at 10 ℃/min, cooled to 25℃ and heated to 320℃ again at same heating rate, under a nitrogen atmosphere. The Fourier transform infrared spectrometer (FT-IR) spectra analysis was also carried out. Before measurement, LCE/amine samples were hot pressed at 250℃ and cooled to room temperature to obtain films. To check the reaction between epoxide ring and amine, FT-IR (Nicolet 6700, Thermo Scientific(USA)) with ATR accessory was used. The spectra were recorded with 32 scans at 8 cm^{-1} resolution. Gel Permeation Chromatography (GPC, Viscotek model 250) was carried out with a RI750F refractive index detectoer. Waters Styragel HP 4E and Styragel HR 5E columns were used with THF as eluent as flow rate of 1 mL/min at 40℃. Approximate calibration of the column was accomplished by polystyrene standards. Transition behaviors of LCE/amine LCP were observed by Polarized light Optical Microscopy (POM, BX51, Olympus) using polarization mode. Samples were prepared by hot pressing between slide glass and

cover glass at 250℃. The measurement temperature range was from 25℃ to 320℃ with Mettler Toledo FP82HT hotstage. 2-D high temperature X-RAY Diffraction (XRD) experimental was carried out with D8 Discover (Bruker) with GADDS (General Area Detector Diffraction System) program. XRD scans were carried out from 25℃ to 230℃ with CuKα radiation.

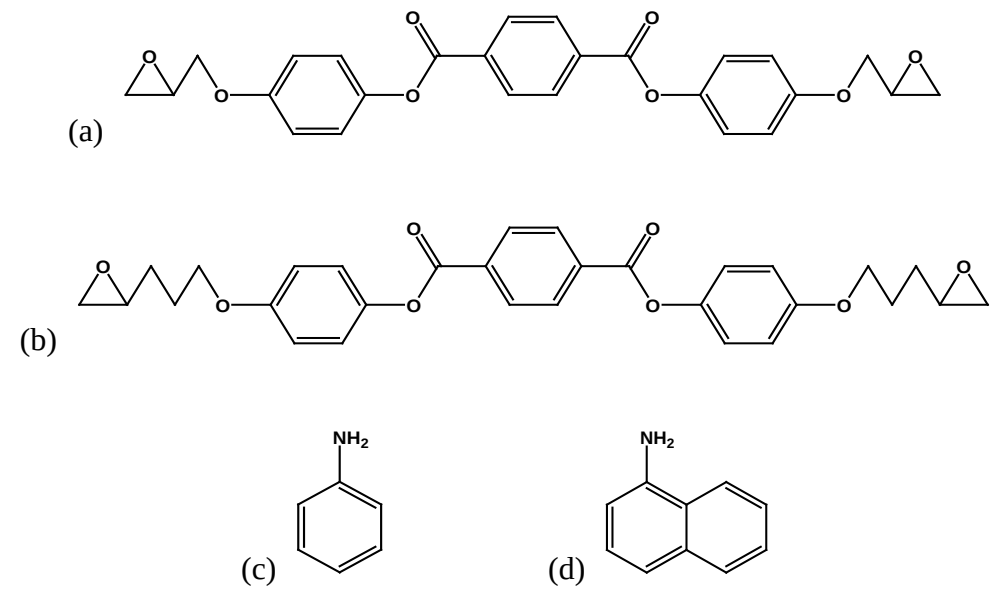

Figure 4.1 Structures of materials. (a) LCE1 (b) LCE3 (c) Aniline (d) 1-Naphthylamine

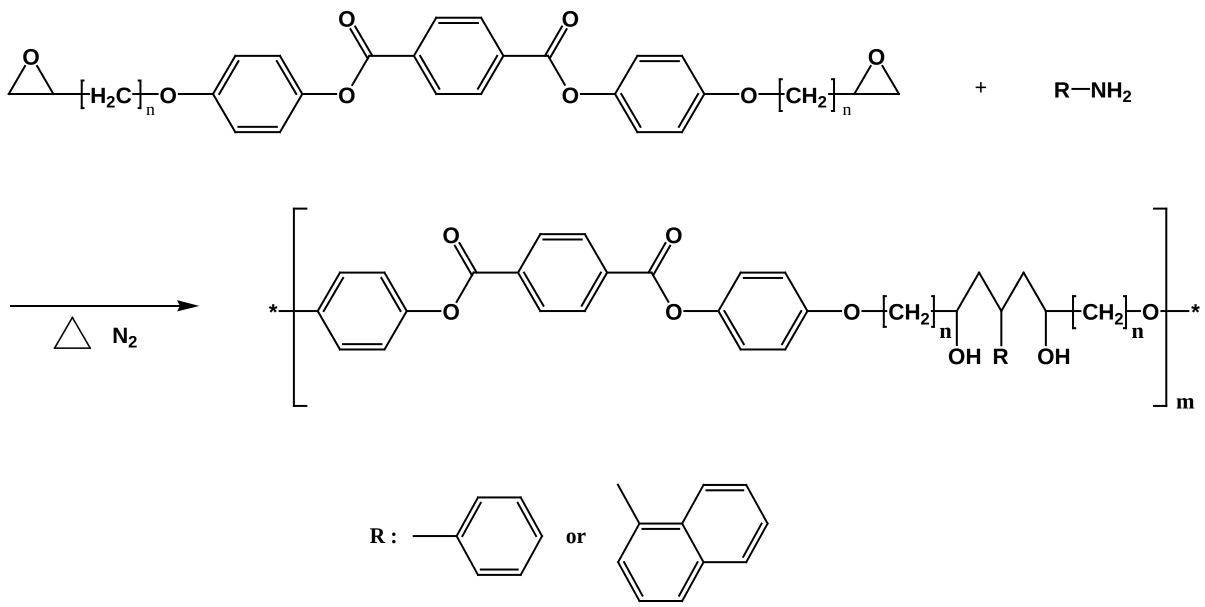

Scheme 4.1 Reaction mechanism of LCE/amine LCPs.

Samples	LCE	Amine	Polymerization	Reaction temperature (℃)
LCE1-A	LCE1		Bulk	240
LCE1-N		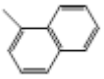	Bulk	240
LCE1-NR			REX	220~245
LCE3-A	LCE3		Bulk	240
LCE3-N		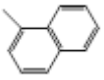	Bulk	240
LCE3-NR			REX	220~245

Table 4.1 Samples, composition and reaction condition.

4.3 Results and discussion

4.3.1 Polymerization of LCEs/amine LCPs

FT-IR spectra of LCE1 and LCE/amine LCPs are shown in Figure 4.2. For LCE, the sharp absorption peak at 914 cm^{-1} was exhibited which was ascribed to the vibration of oxirane ring. But for LCE/diamine LCPs, the intensity of peak at 914 cm^{-1} was decreased, simultaneously absorption of broad shoulder peak at about 3450 cm^{-1} appeared which was attributed to the stretching vibration of the OH group due to the reaction between oxirane ring with amine. This means that epoxide functional groups of LCEs reacted with amines and polymerized to form LCE/amine LCPs.

To investigate the reaction of epoxy with amine more clearly, we analyzed H-NMR and C-NMR spectra. The expected chemical structure is exhibited in Table 4.2 and NMR spectra for LCE1-A are observed in Figure 4.3 (a) and (b). As the LCE reacted with amine, the intensity of protons at end group epoxide ring (Figure 4.3 (a) i, j) decreased as expected. The peaks at 4.7 and 5.3 ppm appeared, the proton on the OH, resulting from the epoxide ring opening reaction via nucleophilic attack of the amine. The peaks at 1.71 and 3.57 ppm pertained to the solvent, THF and moisture appeared at approximately 2.46 ppm in spectra. Addition to LCE1-A LCP, other LCPs had been well polymerized linearly and suggested chemical structures are reasonable. It is deduced that epoxy groups of LCEs had been reacted with monoamine, resulting linear addition polymer and the expected chemical structure of LCPs, representing in Table 4.2, is

reasonable by IR and NMR results.

The molecular weight of LCE/amine LCPs measured by GPC, and the values are given in Table 4.3. All LCPs had polymerized and its number average molecular weights were from 8,600 to 24,100 g/mol. The values of PDI were very large, even over 3 for LCE3 based LCPs. It implied that lots of oligmers and low molecular weight polymers were produced during polymerization. LCE and LCP had high transition temperature thus chain mobility had been resisted with increasing viscosity during bulk polymerization. On the other hand, values of PDI were lower for REX than bulk polymerization because LCP chains had more mobility in extruder by high shear force. But, it has low molecular weight because of not enough time to polymerize due to short residence time in extruder.

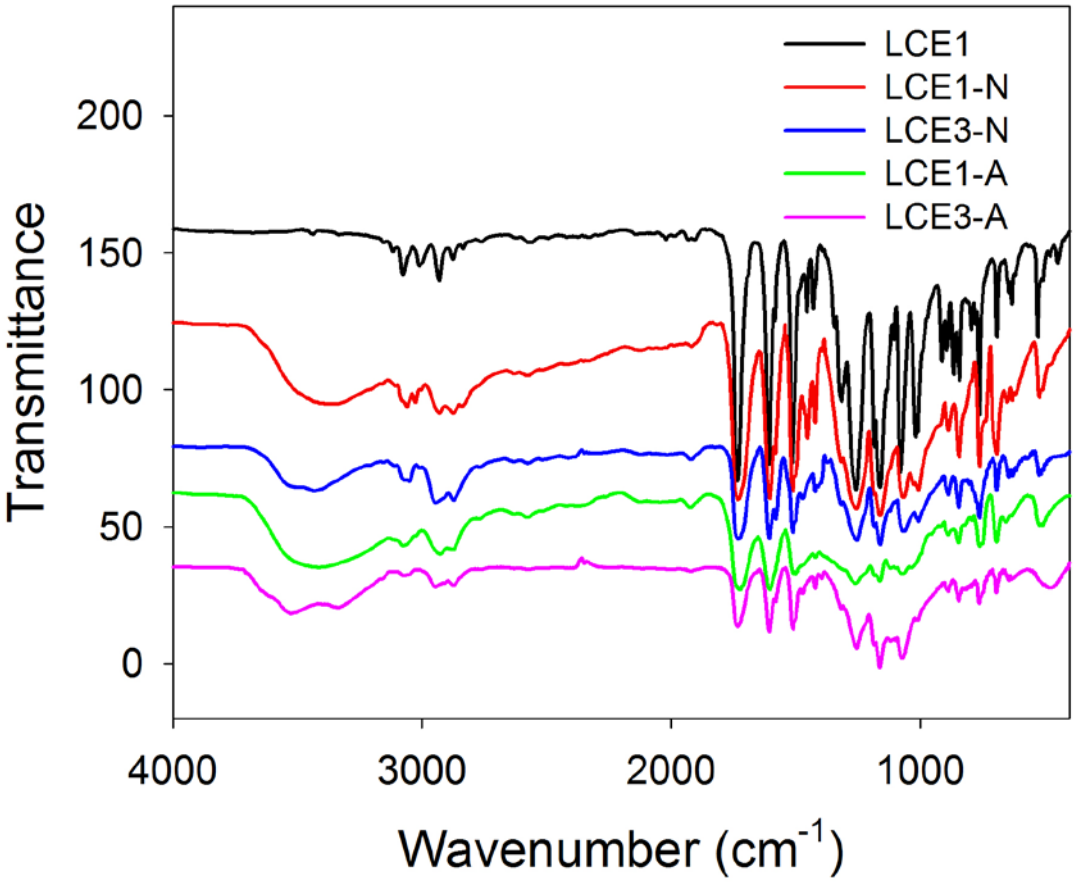

Figure 4.2 FT-IR transmittance spectra of LCE/amine LCPs.

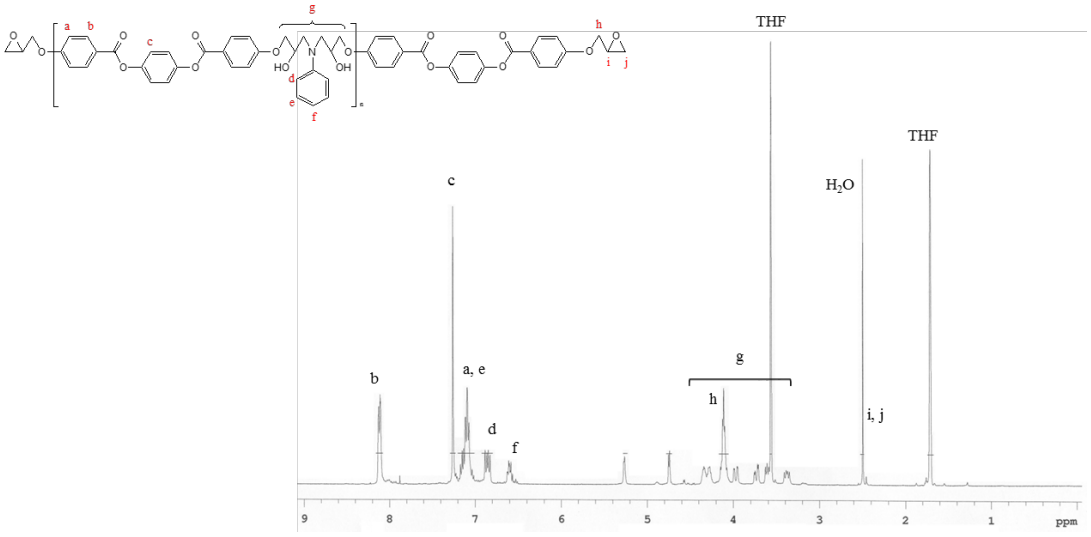

(a)

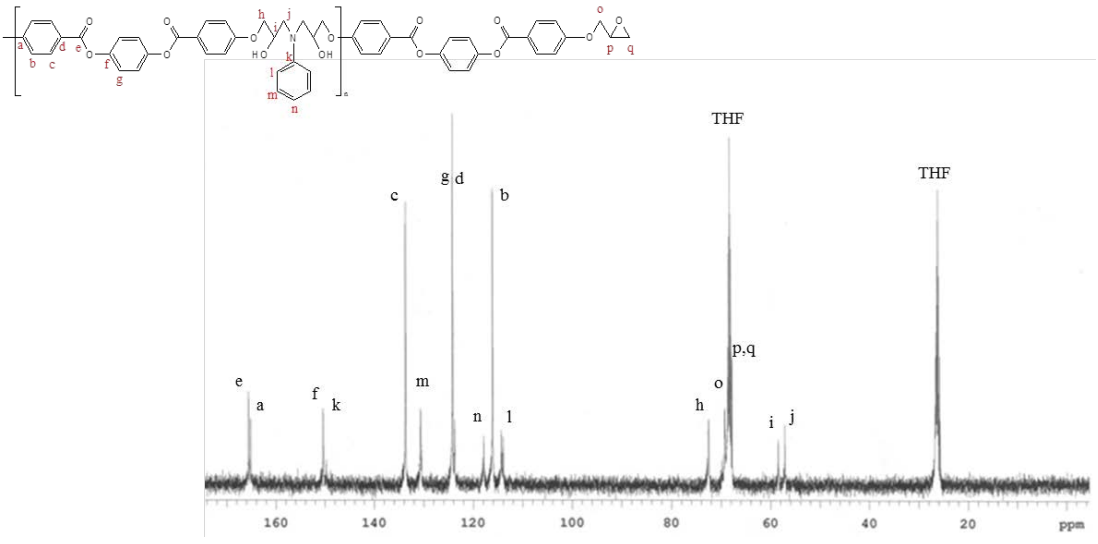

(b)

Figure 4.3 H-NMR and C-NMR spectra of LCE1/aniline LCP. (a) H-NMR (b) C-NMR

LCPs	LCE1-N, LCE1-NR	LCE3-A	LCE3-N, LCE3-NR
R_1			
C atom R_2	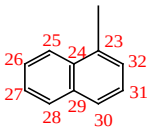	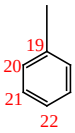	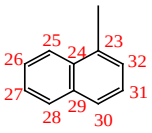
1	164.7	163.5	164.8
2	116.1	114.3	116.1
3	132.7	131.9	133.0
4	123.7	121.7	123.3
5	165.3	164.5	165.8
6	150.1	148.4	148.6
7	123.8	122.4	123.5
8	70.5	68.9	71.1
9	51.2	51.0	52.2
10	45.3	45.8	45.9
11	72.8		
12	68.3		
13	60.3		
14		68.6	69.5
15		24.5	25.8
16		31.2	31.7
17		68.0	68.8
18		66.2	65.0
19		149.2	
20		113.1	
21		128.9	
22		117.0	
23	150.1		150.5
24	132.4		132.8
25	125.7		125.0
26	127.3		127.1
27	127.5		130.0
28	129.3		131.0
29	136.4		136.5
30	124.3		124.3
31	128.1		130.3
32	117.2		117.2

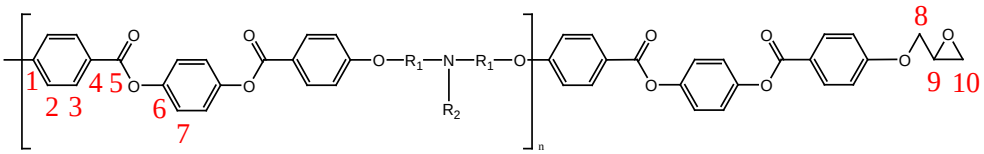

Table 4.2 C-NMR spectra of LCE/amine LCP (δ in ppm).

Samples	M_n	M_w	PDI	T_g (℃)	T_{NI} (℃)	T_{dg} (℃)
LCE1-A	24,100	56,100	2.3	99	188	358
LCE1-N	16,200	32,400	2.0	100	175	357
LCE1-NR	10,400	18,200	1.8	95	182	352
LCE3-A	10,100	31,400	3.1	57	240	355
LCE3-N	14,900	46,500	3.2	71	193	358
LCE3-NR	8,600	13,600	1.6	73	194	358

Table 4.3 Molecular weight and transition temperatures of LCE/amine LCPs. T_g : glass transition temperature, T_{NI} : nematic to isotropic temperature, T_{dg} : degradation temperature.

4.3.2 Liquid crystalline behavior of LCE/amine LCPs

The heating DSC scanning result of LCE/amine LCPs is exhibited in Figure 4.4. Exact values of glass transition temperature (T_g), nematic to isotropic transition temperature (T_{NI}) and degradation temperature (T_{dg}) are given in Table 4.3. All LCPs did not show any clear multi transition temperature during heating or cooling. Only one transition behavior except glass transition was observed which expected glassy nematic mesophase is.[28] The T_g of LCE1 based LCP were higher than that of LCE3 based LCP. And for LCE3 based LCPs, naphthylamine LCP shows higher T_g than aniline LCP. It is attributed to chemical structure of LCE that LCE3 has longer flexible alkyl chain than LCE1. Aniline LCPs showed strong LC behavior and had higher isotropic transition temperature than naphthylamine LCPs both for LCE1 and LCE3 based LCPs. The reason is that naphthylamine is more bulky than aniline, so it hindered the packing of LCP chains and formation of LC or crystalline phase.

The diffraction patterns of mesophases were obtained for the polymers by high temperature 2-D XRD (Figure 4.5). In Figure 4.5 (a) and (b), inner layer reflections for specimens are observed on a meridional scan at near TNI. The narrow inner sharp peaks are observed at diffraction angle $2\theta = 7.6^{\circ}$ which is 11.7 Å transferred by Bragg's law, corresponding to repeating unit of LCP chain. Also, the broad outer peaks are observed at diffraction angle $2\theta = 19 \sim 20^{\circ}$ which is 4.4 ~ 4.6 Å on equatorial scan. It is correspond to the typical diffraction patterns of LC lateral packing which have been known as 3 ~ 6 Å.[29,30] It can be concluded that the mesogenic units of LCP regularly packed and LC mesophase was formed. Beyond the TNI, broad outer high intensity ring

had been appeared because the LCPs were fully melted to isotropic phase, breaking the chain regularity.

Figure 4.6 gives representative POM images of LCPs near T_{NI}. Aniline LCPs exhibits (a) and (c) Shlieren-textured nematic mesophase and naphthylamine LCPs exhibits (b) and (d) marbled nematic mesophase. It is supposed that bulky pendant groups at the side chain hindered the LC behavior, so LCPs with bulky naphthylamine showed marbled texture rather than Shlieren texture.[31] Over the isotropic temperature, LC mesophase had been disappeared slowly and LC phase did not observed at 270℃.

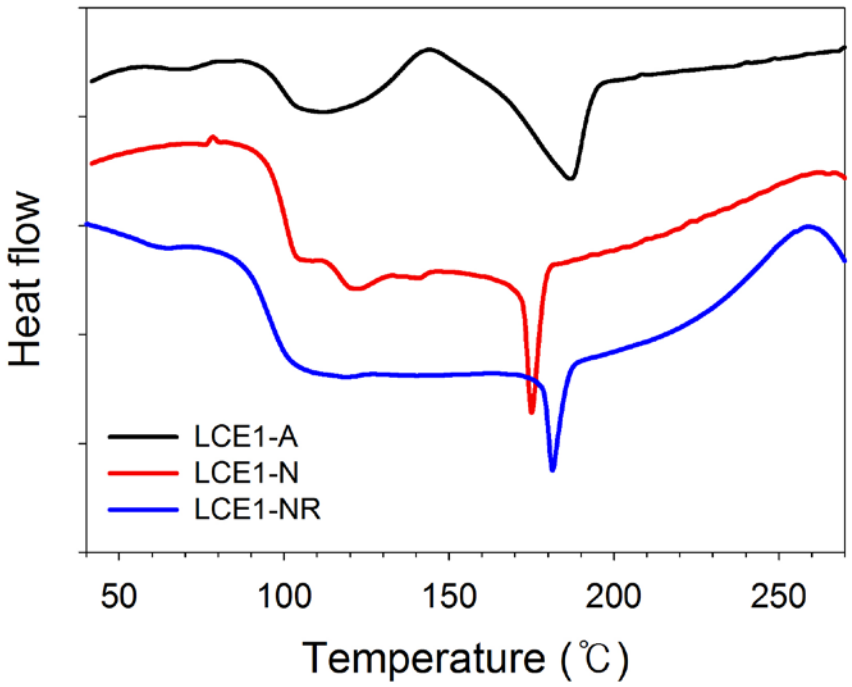

(a)

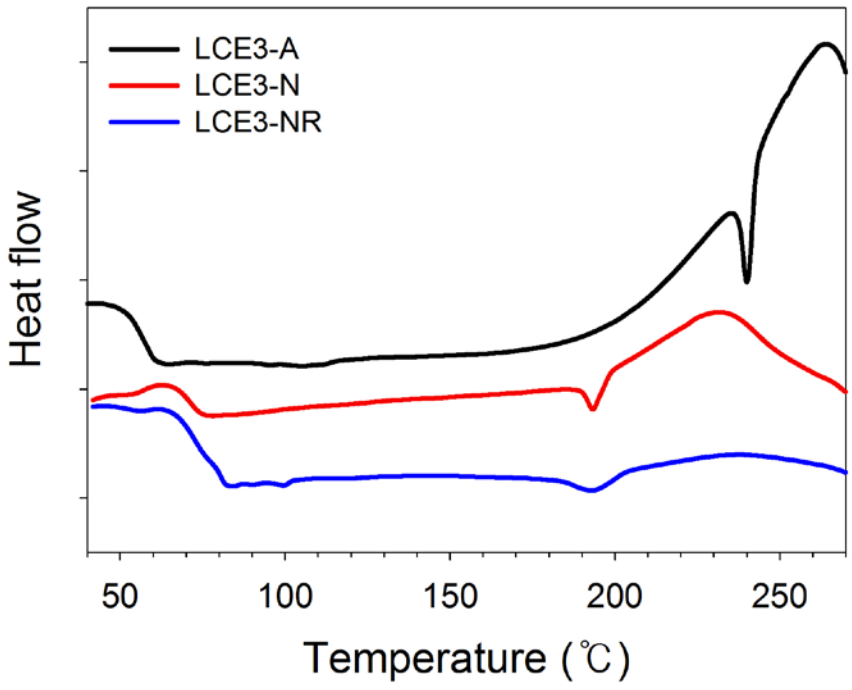

(b)

Figure 4.4 DSC first heating thermogram curves of LCE/amine LCPs. (a) LCE1/amine LCPs (b) LCE3/amine LCPs

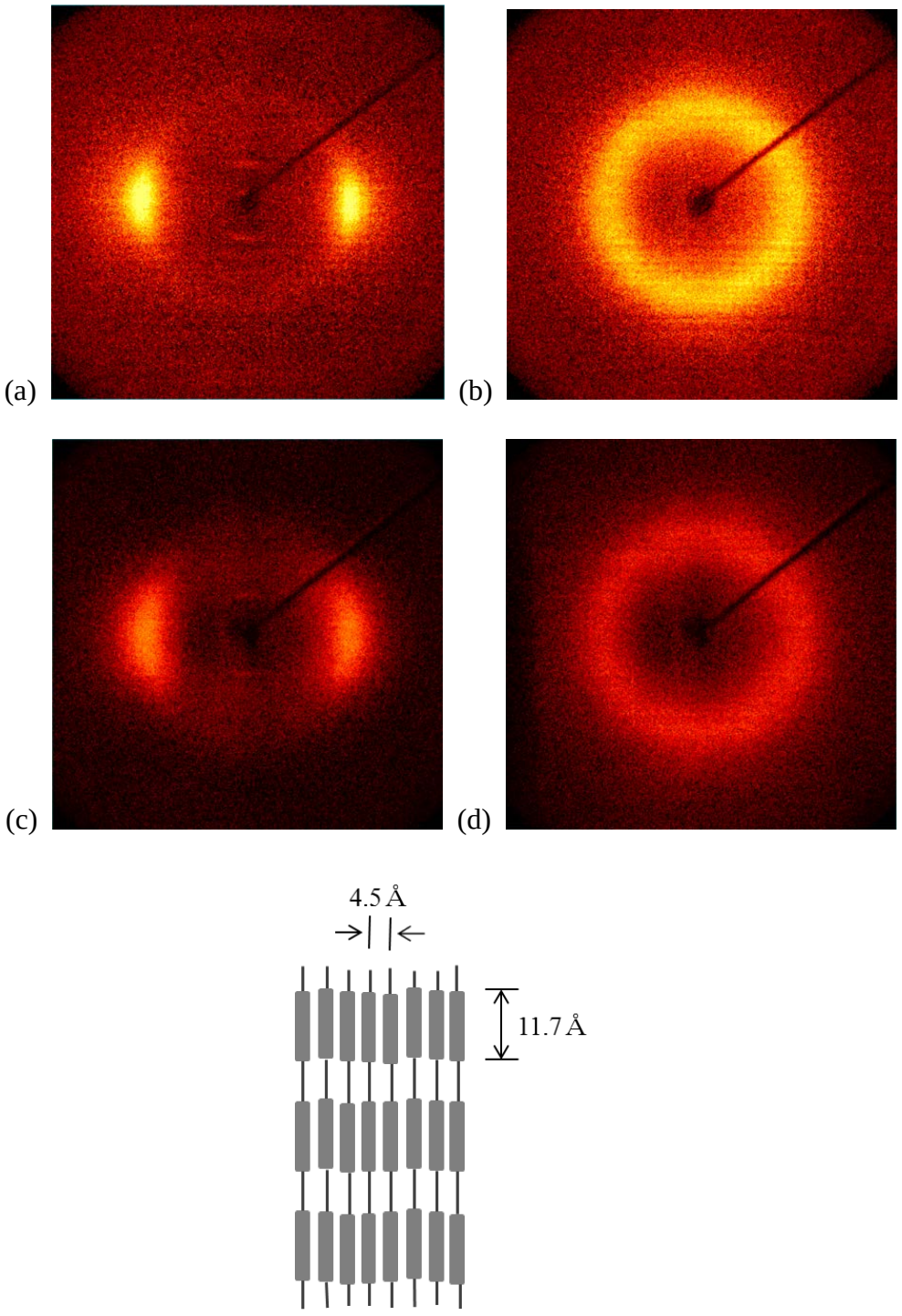

Figure 4.5 2-D XRD patterns. (a) LCE1-A at 180℃ (b) LCE1-A at 230℃ (c) LCE1-N 170℃ (d) LCE1-N at 230℃

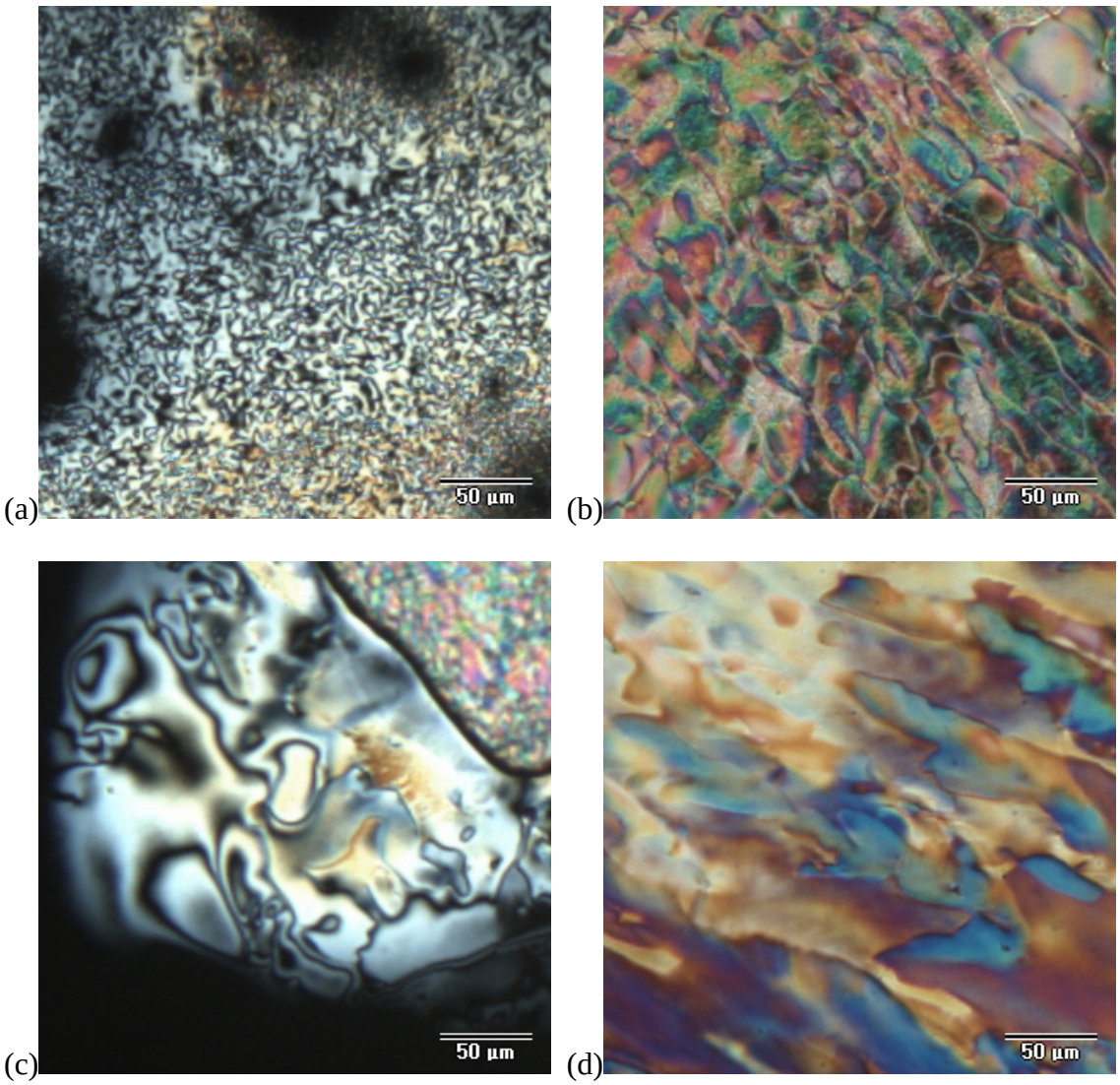

Figure 4.6 POM images of LCE/amine LCPs (X100). (a) LCE1-A at 180℃ (b) LCE1-N at 170℃ (c) LCE3-A at 220℃ (d) LCE3-N at 190℃

4.4 Conclusion

In this study, we successfully produced thermoplastic LCE based LCPs with various monoamine through bulk polymerization and REX. Epoxy groups of LCE had been reacted with amine, forming OH groups. It was observed by IR and NMR experiments. We suggested the expected chemical structures of main chain LCPs, C-NMR spectra supported it. Molecular weights of LCPs were 8,000 ~ 25,000 g/mol depending on the polymerization condition and reactants. But, there were some oligomers and low molecular weight LCP existed, even LCPs which had been polymerized by REX had low molecular weight. However, It is worth that we suggested the possibility of manufacturing LCPs through in-situ REX.

All the LCPs in our study did not show any multi-phase transition, but exhibited glassy nematic mesophase. We investigated LC behaviors of LCPs by DSC, XRD and POM. LC behaviors were affected by the chemical structures of LCP that were length of flexible alkyl chain and bulkiness of pendant groups. But, the relationship between LC behaviors and chemical structure was not identified clearly. So the further researches are needed to get high molecular weight low PDI LCP and identify the LC behavior.

4.5 References

[1] MacDonald, W. A., Liquid crystal polymer: from structures to applications. 1992; p 407.

[2] Finkelmann, H. Angew Chem Int Edit 1987, 26, (9), 816-824.

[3] Dobb, M. G.; Mcintyre, J. E. Adv Polym Sci 1984, 60-1, 61-98.

[4] Noel, C.; Navard, P. Prog Polym Sci 1991, 16, (1), 55-110.

[5] Ober, C. K.; Jin, J. I.; Lenz, R. W. Adv Polym Sci 1984, 59, 103-146.

[6] Kricheldorf, H. R.; Doring, V. Polymer 1992, 33, (24), 5321-5327.

[7] Bilibin, A. Y.; Tenkovtsev, A. V.; Piraner, O. N.; Pashkovsky, E. E.; Skorokhodov, S. S. Makromol Chem 1985, 186, (8), 1575-1591.

[8] Griffin, B. P.; Cox, M. K. British Polymer Journal 1980, 12, 147.

[9] Jin, J. I.; Chang, J. H.; Jo, B. W.; Sung, K. Y.; Kang, C. S. Makromol Chem-M Symp 1990, 33, 97-115.

[10] Ignatious, F.; Lu, C. X.; Kantor, S. W.; Lenz, R. W. Macromolecules 1994, 27, (26), 7785-7793.

[11] Antoun, S.; Lenz, R. W.; Jin, J. I. J Polym Sci Pol Chem 1981, 19, (8), 1901-1920.

[12] Bilibin, A. Y.; Piraner, O. N. Makromol Chem 1991, 192, (2), 201-214.

[13] Lenz, R. W. Polym J 1985, 17, (1), 105-115.

[14] Lenz, R. W.; Furukawa, A.; Bhowmik, P.; Garay, R. O.; Majnusz, J. Polymer 1991, 32, (9), 1703-1712.

[15] Shaffer, T. D.; Percec, V. Polymer Preprint (American Chemical Society) 1986, 27, (1), 369.

[16] Blumstein, A. Polym J 1985, 17, (1), 277-288.

[17] Zhou, Q. F.; Lenz, R. W. J Polym Sci Pol Chem 1983, 21, (11), 3313-3320.

[18] Batzer, H.; Lohse, F.; Schmid, R. Angew Makromol Chem 1973, 29-3, 349-411.

[19] Oleinik, E. F. Pure Appl Chem 1981, 53, (8), 1567-1580.

[20] Chien, L. C.; Lin, C.; Fredley, D. S.; Mccargar, J. W. Macromolecules 1992, 25, (1), 133-137.

[21] Zentel, R. Polymer 1992, 33, (19), 4040-4046.

[22] Zentel, R.; Jungbauer, D.; Twieg, R. J.; Yoon, D. Y.; Willson, C. G. Makromol Chem 1993, 194, (3), 859-868.

[23] Bormann, S.; Brossas, J.; Franta, E.; Gramain, P.; Kirch, M.; Lehn, J. M. Tetrahedron 1975, 31, (22), 2791-2793.

[24] Klee, J. E.; Grutzner, R. E.; Horhold, H. H. Macromol Chem Phys 1996, 197, (7), 2305-2323.

[25] Blanco, M.; Corcuera, M. A.; Riccardi, C. C.; Mondragon, I. Polymer 2005, 46, (19), 7989-8000.

[26] Kawakami, H.; Yamanaka, H.; Nanzai, Y. Polymer 2005, 46, (25), 11806-11813.

[27] Lee, J. Y.; Jang, J. S. Polymer 2006, 47, (9), 3036-3042.

[28] Chang, S.; Han, C. D. Macromolecules 1997, 30, (6), 1670-1684.

[29] Watanabe, J.; Hayashi, M. Macromolecules 1989, 22, (10), 4083-4088.

[30] Kantor, S. W.; Sung, T. C.; Atkins, E. D. T. Macromolecules 1992, 25, (11), 2789-2795.

[31] Long, T. M.; Swager, T. M. J Mater Chem 2002, 12, (12), 3407-3412.

Summary

High-performance polymers were successfully synthesized by in-situ REX process. Compared to typical extrusion, REX process made it possible that melt blending as well as chemical reactions such as polymerization of monomers or modification of homopolymer. However, it have been not reported yet that both polymerization and modification occurred at the same time. In this study, both anionic polymerization and coupling reaction were simultaneously carried out in extruder successfully by adopting new reaction system, resulted in manufacture the enhanced PA6 polymer. Various kinds of multi-functional molecules such as epoxy and amine had been adopted to react with different position in PA6 chain.

In Chapter 2 and 3, high performance PA6 composites were synthesized successfully by coupling reaction between bifunctional chain extenders with the PA6 in REX. Synthesized chain extenders had bifunctional reactive end group such as diepoxy or diamine so that they could react with PA6 matrix polymer. In-situ REX process was used to blend chain extending additives with PA6 polymer, simultaneously chain extenders connected the PA6 polymer chains each other resulted in enhancing the PA6 properties. In reactive extrusion, diepoxy chain extender reacted with amide linkage of PA6 chain and extended it by crosslinking. On the other hand, diamine chain extender reacted with lactamate end group of PA6 chain and extended it linearly. As a result, physical properties were improved because increasing molecular weight of PA6 based nanocomposites due to chain extenders. But, there are some difficulties due to narrow reaction window for anionic polymerization which was sensitive to reaction condition.

It is necessary that control the composition of reactants and reaction condition to obtain high performance PA6 based composites. Another challenge is that the structure of organic additive did not affect remarkable to the properties of nanocomposites. So it was needed that effective design of chain extending molecules for further works.

In Chapter 4, we discover the possibility of producing thermoplastic LCE based LCPs with various monoamines through bulk polymerization and REX. Epoxy groups of LCE had been reacted linearly with primary monoamine, and successfully polymerized thermoplastic LCPs. But, there were some oligomers and low molecular weight LCP existed, and LCPs showed glassy nematic transition behavior. The relationship between LC behaviors and chemical structure was not identified clearly. However, it is worth that we suggested the possibility of manufacturing LCPs through in-situ REX. And further researches are needed to get high molecular weight low PDI LCP and identify the LC behavior.

국 문 초 록

반응압출 공정(REX)은 고분자의 블렌딩(blending) 외에 중합, 그래프팅(grafting), 브랜칭(branching), 기능화 등의 다양한 화학반응을 동시에 진행할 수 있는 효과적이고 효율적인 고분자 가공 공정이다. 또한, 반응성 작용제(agent)를 반응 공정에 도입하여 분산을 균일하게 하고 반응시간을 감소시킬 수 있다. 따라서, 단순히 블렌딩을 하는 일반적인 압출 공정과 비교해 볼 때, 반응압출 공정은 블렌딩과 화학반응을 압출기 내에서 동시에 진행할 수 있다는 큰 장점이 있다. 결과적으로 반응압출공정의 도입을 통해 고분자의 중합과 반응을 한 단계의 공정으로 간소화 하는 것이 가능하다.

반응압출 공정의 이러한 특유의 장점을 이용하여, 단량체로부터 고분자 중합, 크래프팅이나 가교를 통한 고분자의 개질, 고분자끼리의 커플링 반응과 같은 다양한 화학반응에 응용할 수 있다. 고분자의 중합 반응은 반응 온도나 조성, 시간 등의 조건에 매우 민감하게 반응하기 때문에, 고기능성 고분자를 단량체로부터 중합하는 연구는 매우 어려운 일이다. 따라서, 이러한 중합이나 개질에 대해 많은 연구들이 진행되어 왔지만, 중합과 개질을 동시에 반응압출 공정을 통해서 가능하게 한 연구는 아직 보고된 바가 없다.

본 연구에서는, 반응압출 공정과 새로운 이작용기(bifunctional) 첨가제의 도입으로 단량체로부터 폴리아미드 6 복합체를 in-situ로 중합하였다. 기존에 보고된 이작용기 첨가제들의 경우 단량체로부터 in-situ 중합이 불가능하였으

나, 에폭시와 아민 작용기를 갖는 첨가제를 합성하여 사용한 새로운 반응 시스템의 도입으로 in-situ 중합을 가능하게 하였고, 더 나아가 반응압출을 통해 단일공정으로 복합체를 제조하였다. 이작용기 첨가제의 경우 고분자 체인 증량제(chain extender)로 작용하여 분자량을 증가시키고 물성을 향상시켰다. 하지만 반응 조건에 따른 고분 복합체의 성능이 차이를 보이므로 첨가제의 양과 반응조건에 대한 미세한 조종이 필요했다.

또한 본 연구에서는, 액정성을 띄는 열가소성 고분자를 반응압출로 중합하였다. 액정에폭시와 모노아민을 반응압출기 내에서 선형으로 반응시켜 성공적으로 액정고분자를 중합하였다. 하지만 높은 분자량의 액정고분자를 얻기 위해서는 추가 연구가 필요하다.

주요어: 폴리아미드 6, 나일론 6, 개환중합, 음이온 중합, in-situ, 반응압출, 에폭시, 아민, 체인증량제, 액정 에폭시, 1차 단일아민, 액정고분자

학번: 2007-20723

List of Publications

1. SM Hong, SS Hwang, CM Koo, HG Cho, YS Seo, KH Oh. “Thermoplastic elastomer composite composition with high dimentional stability for noise and EMI shielding and use thereof”, Patent KR 1009634340000

2. Kyunghwan Oh, Youngwook P. Seo, Soon Man Hong, Atsushi Takahara, Kyoung Hwan Lee, Yongsok Seo. “Dispersion and reaggregation of nanoparticles in the polypropylene copolymer foamed by supercritical carbon dioxide.”, *Physical Chemistry Chemical Physics*, 2013, 15, 11061-11069

3. Kyunghwan Oh, Soon Man Hong, Yongsok Seo. “Effect of crosslinking reaction on the electromagnetic interference shielding of a Fe–Si–Al alloy (Sendust)/polymer composite at high frequency.”, *Polymers for Advanced Technologies*, 2014, 25, 1366-1370

4. Youngwook P. Seo, Kyounghwan Oh, Yongsok Seo, Soon Man Hong. “Develpment of a manufacturing process for an organic-inorganic nanocomposite and its physical property characterization.”, *International Journal of Material Forming*, 2010, 3, 1, 691–694

5. Kyunghwan Oh, Wei Huan Chua, Sung Eun Park, Jihun Kim, Soon jong Kwak, Sehyun Kim, Yongsok Seo. “Nonisothermal crystallization behaviors of nanocomposites prepared by in-situ polymerization of high-density polyethylene on tungsten oxide particles.”, *Macromolecular Research*, 2015, in press

Appendix

Introduction – polymer nanocomposites

Appendix A

Effect of crosslinking reaction on the electromagnetic interference shielding of a Fe-Si-Al alloy (Sendust)/polymer composite at high frequency.

A.1 Introduction

A.1.1 Electromagnetic wave absorption

A.1.2 Snoek's limit and flake EMI absorption materials

A.1.3 Polymer matrix for EMI absorption

A.2 Experimental

A.2.1 Materials

A.2.2 Sample preparation

A.2.3 Characterization

A.3 Results and discussion

A.3.1 Thermal stability

A.3.2 Morphology

A.3.3 Electromagnetic wave absorption properties

A.4 Conclusion

A.5 References

Appendix B

Dispersion and reaggregation of nanoparticles in the polypropylene copolymer foamed by supercritical carbon dioxide.

Appendix C

Nonisothermal crystallization behaviors of nanocomposites prepared by in-situ polymerization of high-density polyethylene on tungsten oxide particles.

Introduction - polymer nanocomposites

Polymer nanocomposites are materials which consist of a polymer or copolymer having nanoparticles or nanofillers dispersed in the polymer matrix. These nanosize-additives may be of different shape (platelets, fibers, rods and spheroids), at least one dimension must be in the range of nanometer. The transition from micro- to nano-particles leads to change in its physical as well as chemical properties. The major factor in this is the increase in the ratio of the surface area to volume by the decreased size of particles. The increase in surface area-to-volume ratio, which increases as the particles get smaller, leads to an increasing dominance of the behavior of atoms on the surface area of particle over that of those interior of the particle. This affects the properties of the particles when they are reacting with other particles. Because of the nano-sized scale, the interaction with the other particles within the mixture is more significant than micro-sized scale. Thus, this affects to improvement of the various properties such as mechanical, chemical, electrical, optical and so on.

Polymer nanocomposites belong to the category of multi-phase systems such as blends, composites and foams. These systems require controlled mixing, blending, compounding and stabilizing in order to achieve dispersion and orientation of the fillers because dispersion and orientation of fillers affects to the properties critically. There are various kinds of methods to modify the micro structure and morphology either chemically and physically. For example, high shear applied processing, adopting the compatibilzer, applying electric and/or magnetic field, control the shape and size of the fillers and introducing chemical reactive functional group on the fillers are the well-

known methods. These methods have been used alone or together to improve the properties of polymer nanocomposites.

In most cases, it has been focused on the microstructure of additives in polymer nanocomposites such as dispersion orientation and morphology so that it has been developed in functional fillers and/or processing. In this Appendix chapter, we controlled the microstructure of nanocomposites by adopting various kinds of chemical and physical processing methods in order to improve the physical properties.

Appendix A

Effect of crosslinking reaction on the electromagnetic interference shielding of a Fe-Si-Al alloy (Sendust)/polymer composite at high frequency.

A.1 Introduction

A.1.1 Electromagnetic wave absorption

In recent years, the use of microwave in GHz frequency, especially 0.5~5 GHz range, has been rapidly increased with the development of advanced electronic devices and communication instruments.[1,2] High frequency microwave generates undesired noise with complicated microwave environment which can affect the proper operation of commercial, military and scientific electronic devices as well as the health of our human body.[3,4] This in turn has led to increased demand for electromagnetic interference (EMI) shielding. When electromagnetic wave is incident on the shielding material, it can be transmitted (T), reflected (R) or absorbed (A) (Figure A.1). The EMI shielding is done by the reflection or absorption of the wave energy.[5~15] When an electromagnetic wave encounters a discontinuity (boundary surface of the shielding material), it can be reflected or absorbed depending on the impedance difference at the

boundary.[6~8] If the magnitude of the air impedance is quite different from the intrinsic impedance of the shielding material, most of the electromagnetic wave will be reflected, and very little will be transmitted across the boundary. However, less energy is reflected and more is absorbed for low impedance materials such as the metals. Highly dielectric materials induce more reflection than absorption whereas materials of high permeability are more suitable for absorption.[6,11] In the small electronics, noise removal within a close distance from the source is very important. This implicates that EMI shielding in the equipment should be done by the absorption of the energy rather than the reflection.[10,14]

Electromagnetic wave absorption materials can be categorized into three groups; conducting absorbers, dielectric absorbers and magnetic absorbers.[1,2] Conducting absorbers containing conductive powder can induce electric field loss by the resistance heat, but thick layer is needed to get efficient EMI absorption.[6] Dielectric absorbers including dielectric powder of high permittivity can lead to strong electromagnetic energy loss but at low frequency range.[8] In the magnetic absorbers, a strong electromagnetic energy loss occurs by the resistant heat by the induced current from the spin of small magnetic domains at high frequency range.[14]

When incident electromagnetic wave absorbed into magnetic EMI absorption materials, the spin momentum of magnetic material resonates with the change of external magnetic field which is induced by incident electromagnetic wave. So an induced current was generated, subsequently the absorbed energy of incident electromagnetic wave was transformed to resistant heat, emitting out. Therefore, soft magnetic materials are the most effective EMI absorbers because of its high permeability and ease of magnetization. But, there are some obstacles disrupt the

magnetization such as eddy current loss, hysteresis loss and resonance loss. When an induced current generated under the high frequency region, opposite direction current also induced which called eddy current. By Lenz's law, an eddy current creates a magnetic field that opposes the magnetic field that created it, and thus eddy currents react back on the source of the magnetic field. So it declines the magnetization of EMI absorption materials.

A.1.2 Snoek's limit and flake EMI absorption materials

The eddy current losses (P_e) can be expressed as below.

$$P_e \propto \frac{f^2 {B_M}^2 d^2}{\rho}$$

In this formula d is the thickness of the sample, B_M is magnetic flux density, f is frequency and ρ is electrical resistivity. The miniaturization and rapid increase in frequencies of electronic devices require that magnetic materials possess high resonance frequency, large permeability, and low magnetic loss. Because the product of the static spin susceptibility and the spin resonance frequency regarded as the upper limit frequency of magnetic materials is proportional to the magnetization, because P_e is proportional to square of the frequency. Therefore, eddy current loss is drastically increases at high frequency, simultaneously permeability decreases extremely. This phenomenon have been known as 'Snoek's limit', expressed as below.

$$f_r \cdot \mu_i \leq 5.6\ GHz$$

μ_i is the initial permeability of material and f_r is half frequency of permeability. So it is a great challenge to increase both resonance frequency and permeability simultaneously.

One way enhancing the resonance frequency is to introduce additional magnetic anisotropies, including shape anisotropy or strain induced anisotropy. Because of their large saturation magnetization and low eddy current loss coming from the effects of particle shape, ferromagnetic metal particles of thin flake shape is known to have a high magnetic permeability in GHz frequencies above Snoek's limit.[17] The ferromagnetic metal particles can be easily flattened into thin flakes by a facile mechanical milling method (attrition milling).[12,13]

A.1.3 Polymer matrix for EMI absorption

In general, most of the polymeric materials are transparent to electromagnetic wave or weak absorption occurs in the polymers because the polymer molecules are very low dielectric or ferromagnetic. The electromagnetic wave absorbers can get a strong electromagnetic energy loss by dispersing conductive, dielectric or magnetic metal powder into the polymer matrix. Thus, it is possible to make thin electromagnetic wave absorbers from the ferromagnetic metal particles such as ferrite, perm alloy (Fe-Ni) or Sendust (Fe-Si-Al) dispersed in polymer resins.[9~13] In this case, the metal particles take more than 70 wt% of the composite so that the blending polymers play the role of a binder rather than a matrix.[3~10] Halogenated polyolefins or other elastomers such as acryl rubber, polyurethane and silicon rubbers are frequently used for this purpose.[2] Though halogenated polymers show good flame retardancy, their halogen components can be easily separated by combustion, aging or hardening process.[16] Also they can produce dioxine or furan; both are fatal compounds for human body or instruments. Meanwhile, the rubber compounds or thermoplastic elastomers are flexible and easily

processible but have poor or weak thermal stability. For the practical application purpose, diverse polymeric materials of good thermal stability and easy processibility have been investigated as a binder for magnetic absorbers.[2]

A triblock copolymer (poly(styrene-block-(ethylene-1-buthylene)-block-styrene) (SEBS) is a thermoplastic elastomer which is physically crosslinked by both ends of hard segment block. In this study, we designed and fabricated EM wave absorbers using Sendust and SEBS triblock copolymer with good thermal and dimensional stabilities. In order to get the high permeability, we used roll-milling technique to align the flake-shape metal powder into the rolling direction. The effect of crosslinking of SEBS molecules on the orientation of flake particles and on the EMI shielding of the composite are characterized.

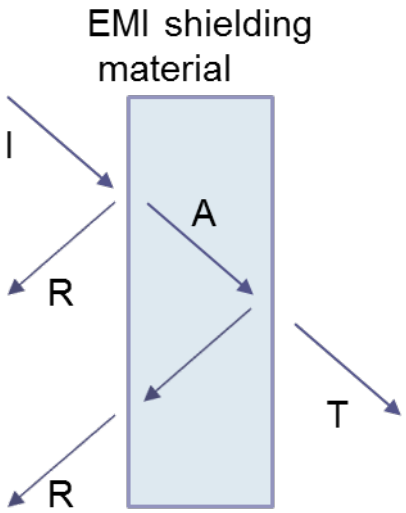

Figure A.1 EMI shielding mechanism.

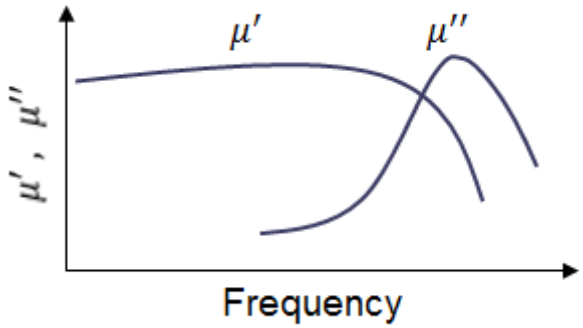

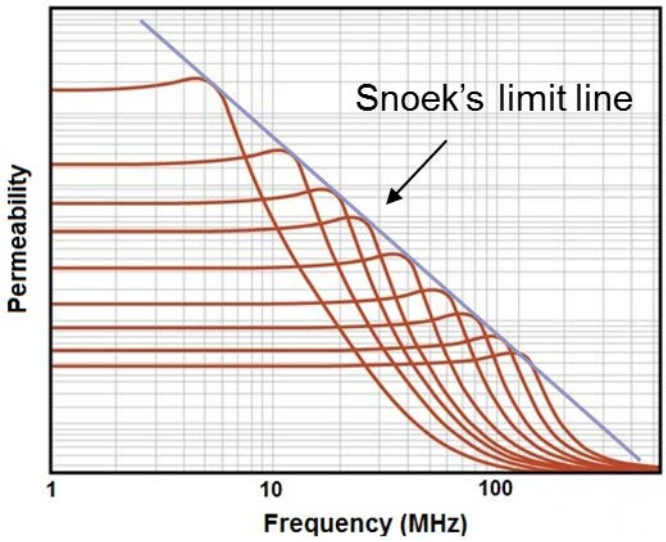

Figure A.2 Snoek's limit.

A.2 Experimental

A.2.1 Materials

As a polymer binder, maleic anhydride grafted SEBS (SEBS-g-MA, Kraton FG1901X from Shell Co.) was used after blending with polypropylene (PP, Y120 + PP-g-MA, PH200 from Honam Petroleum Co., T_m of PP = 165℃). For the ferromagnetic metal powder, two different types of Sendust (Fe-Si-Al alloy), bulk and flake provided by Changsung Co. (Korea), were used. Stearic acid from Aldrich was used for the lubrication in the preparation process. Dicumyl peroxide (DCP, Aldrich) was used for the crosslinking reaction. Since the leakage of incident radiation from the patches of microwave transparent host matrix (empty spaces devoid of filler phase) results in deterioration of radiation blocking efficiency, well dispersed composition is very important. Herein, we added a small amount of sodium dodecylbenzenesulfonate (NaDBSA from Merck), 0.7%, to achieve uniform dispersion of metal fillers without affecting their intrinsic properties.

A.2.2 Sample preparation

Blends of SEBS-g-MA and PP were done in an athermal mixer (HAAKE, Polydrive mixer) at 180℃, 100 rpm for 5 minutes. Maleic anhydride grafted polypropylene (MAPP) mixed polypropylene (PP+MAPP from Honam Petrochemical CO., Korea),

stearic acid and DCP was then added into the internal mixer. They were mixed for 3 minutes at the same temperature as before. Sendust particles and NaDBSA were added and mixed for 5 minutes. The blend was then fabricated into 1 mm thin film by using two roll miller. The roll milling was done for 1 hour at 150℃ and 100 rpm.

A.2.3 Characterization

Complex permeability ($\mu = \mu' - j\,\mu''$) and complex permittivity ($\varepsilon = \varepsilon' - j\,\varepsilon''$), where j is $\sqrt{-1}$, were evaluated by measuring the reflection coefficient (S_{11}) from the sample backed by a copper strip and transmission coefficient (S_{21}) with the frequency range from 50 MHz to 10 GHz using an HP8510 C network analyzer.[1] The reflection loss, RL, of the composite was evaluated by the following well-known equations with measured complex permeability and permittivity,

$$RL(dB) = 20\ log_{10}\left|\frac{Z_{in} - Z_0}{Z_{in} + Z_0}\right| \qquad (1)$$

$$Z_{in} = Z_0\sqrt{\frac{\mu}{\varepsilon}}\ \tanh\ \left(j\frac{2\pi\ fd}{c}\sqrt{\mu\,\varepsilon}\ \right) \qquad (2)$$

where Z_{in} is the absorber impedance, Z_0 is the impedance of free space, μ and ε represent complex permeability and complex permittivity, d is the thickness of the absorber, and f is the input frequency.[6~14]

Dimensional stability was checked by TMA (TA 2940) in the temperature range of -80~200℃. Heating rate was 10 ℃/min. Morphology was observed using scanning electron microscopy (SEM, Hitach S 2200C). Fractured sample surface in the liquid nitrogen was coated Pt/Pd before SEM observation.

A.3 Results and discussion

A.3.1. Thermal stability

Considering the practical application, tough and strong film with good thermal stability is required. While the thermoplastic elastomer SEBS-g-MA is a flexible rubbery polymer showing high impact strength and elongation, its tensile strength is not so high whereas polypropylene (PP) is a semi crystalline polymer of high tensile strength and good dimensional stability but weak impact strength. Addition of polypropylene to SEBS-g-MA can enhance the tensile strength as well as the dimensional stability of the composite film, though the elongation decreases. After taking into consideration of all these, the composition of SEBS/PP blended film was decided as 75 to 25 wt% ratio. Figure A.3 shows the dimensional change with the temperature measured by TMA. Addition of DCP leads to partial crosslinking between SEBS-g-MA molecules to increase thermal stability of the composite films below 150℃. The PP phase in the composite film acts as the organic filler to improve the dimensional stability, but dimension change of the blended temperature increased rapidly above 160℃ temperature due to the melting of PP. Dimensional stability improves with the addition of DCP. Because excessive crosslinking impedes uniform blending and impels phase separation, DCP amount was set as 0.3 phr for electromagnetic wave absorption film.

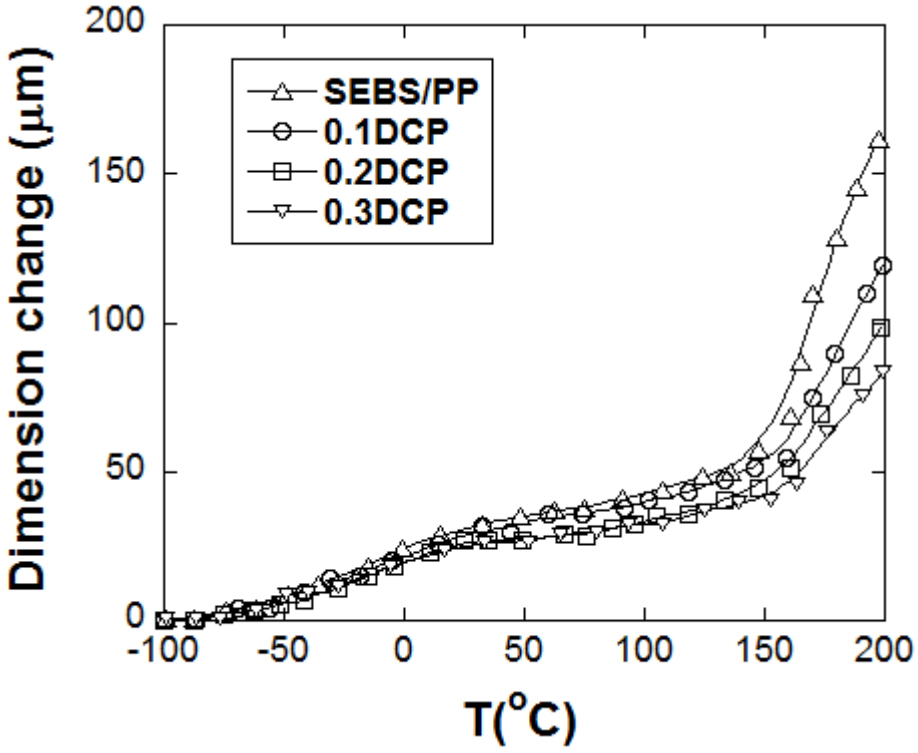

Figure A.3 Dimension change of crosslinked SEBS/PP– Sendust (400 phr) electromagnetic absorber.

A.3.2 Morphology

Figure A.4 shows SEM micrographs of sieved bulk Sendust particles of 30~40 μm, microforged Sendust flakes and aligned structure of Sendust in the absorption film after roll-milling. The Sendust bulk powder has a random shape, but after the micro forging they were deformed as flat flakes with the average aspect ratio of ~80. Figure A.4 (c) shows the orientation of flake particles after roll milling. By the roll-milling, the flakes were aligned along the rolling direction. Hence, they are orderly aligned without empty spaces devoid of filler phase and deterioration of the radiation blocking efficiency.[4,9] The crosslinking reaction increases the melt viscosity which helps the orientation of flakes more in the rolling direction. Besides, this orientation of flakes can contribute to three facts; 1) the electrical charge of flake polarization can be more easily polarized, 2) the space-charge polarization and the exchange coupling reaction of the magnetic moment between particles are enhanced with the increase of the surface area, 3) the eddy current loss is reduced with the particle shape change from bulk particles to thin flakes.[14]

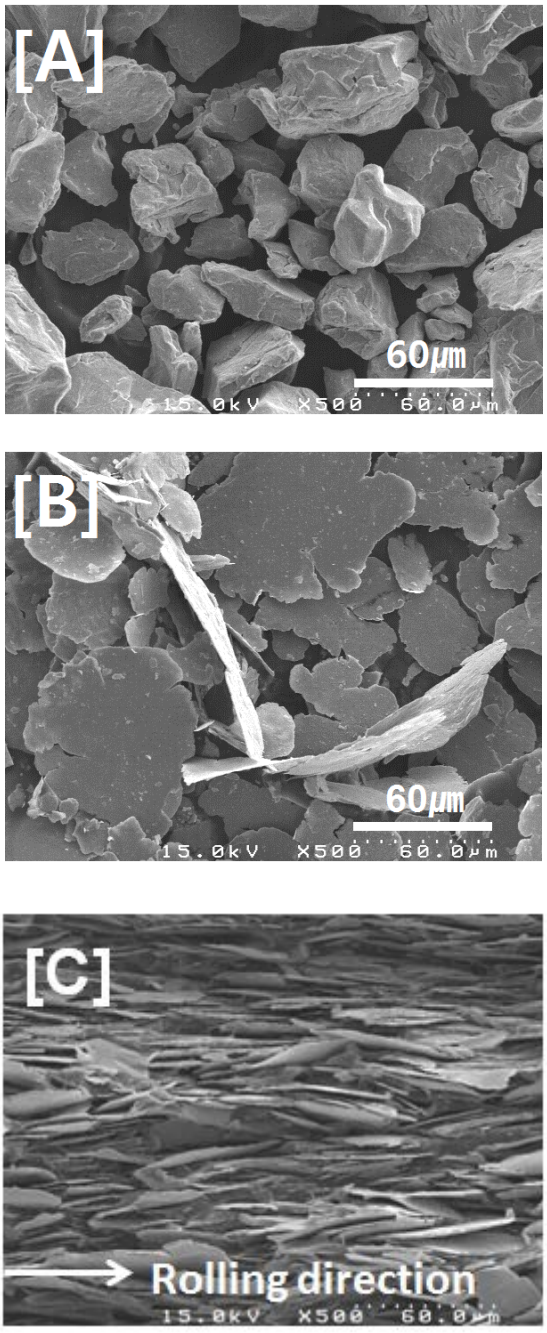

Figure A.4 SEM photographs of (a) bulk Sendust, (b) microforged Sendust, and (c) fractured surface of the composite absorber after roll-milling (containing 400 phr of Sendust).

A.3.3 Electromagnetic wave absorption properties

Variation of the complex permeability of the Sendust composite films formed are represented in Figure A.5. Flake composites show 5~6 times higher permeability than Sendust bulk particle composites. As the Sendust amount increases, the permeability gradually increases. This is more prominent for flake composites. Here a few facts are worthy of note. First, μ_r' of the bulk Sendust composite is almost constant in the low frequency region but weakly decreasing in the high frequency region whereas that of Sendust flake shows maximum in the low frequency region and rapid decrease in the high frequency region. Addition of more Sendust particles vividly enhances the μ_r' values, especially for Sendust flake composite. Secondly, μ_r" values of the flake composites display obvious two maxima, one in the low frequency and the other at around 1 GHz. After then, it rapidly decreased. On the other hand, the bulk composites exhibit weak maximum at ca. 900 MHz. The peak maximum of the flake composites appeared in the lower frequency range is correlated to a shape anisotropy of the flakes while the second maximum is attributed to a magnetoelastic effect in the surface layer where intensive stress caused by forging remains.[9] By doing the annealing of the flakes, Yoshida et al found out that the surface layer of the annealed flakes was paramagnetic in which Fe is dispersed in the Si and Al.[9] Since the second peak is enhanced with increase of the surface area, the second peak is believed to be caused by a magnetoelastic effect near the surface. Imaginary permeability was also increased with the amount of Sendust particles, but flake composite shows more prominent increase. In general, the real part of permeability abruptly decreases and the imaginary part of

permeability has maximum value at a frequency higher than the resonance frequency, so that the magnetic loss is maximized.[6] Because of the Snoek's limit, flake composites exhibit rapid decrease of the complex permeability.[7,16] Sendust composites obviously follow this general behavior of magnetic loss which indicates that the wave absorption phenomenon is mainly due to magnetic resonance. Thirdly, the loss tanδ ($=\mu_r'/\mu_r''$) increases with the frequency for all composites, but the magnitude of the loss tanδ for the flake composites was almost one order larger (Figure A.6). This means that oriented flake composites absorbs the wave energy more efficiently than the bulk composites at high frequency of GHz region. All these reflect that aligned anisotropic flake composites are way better efficient to absorb the wave energy and to shield EMI.

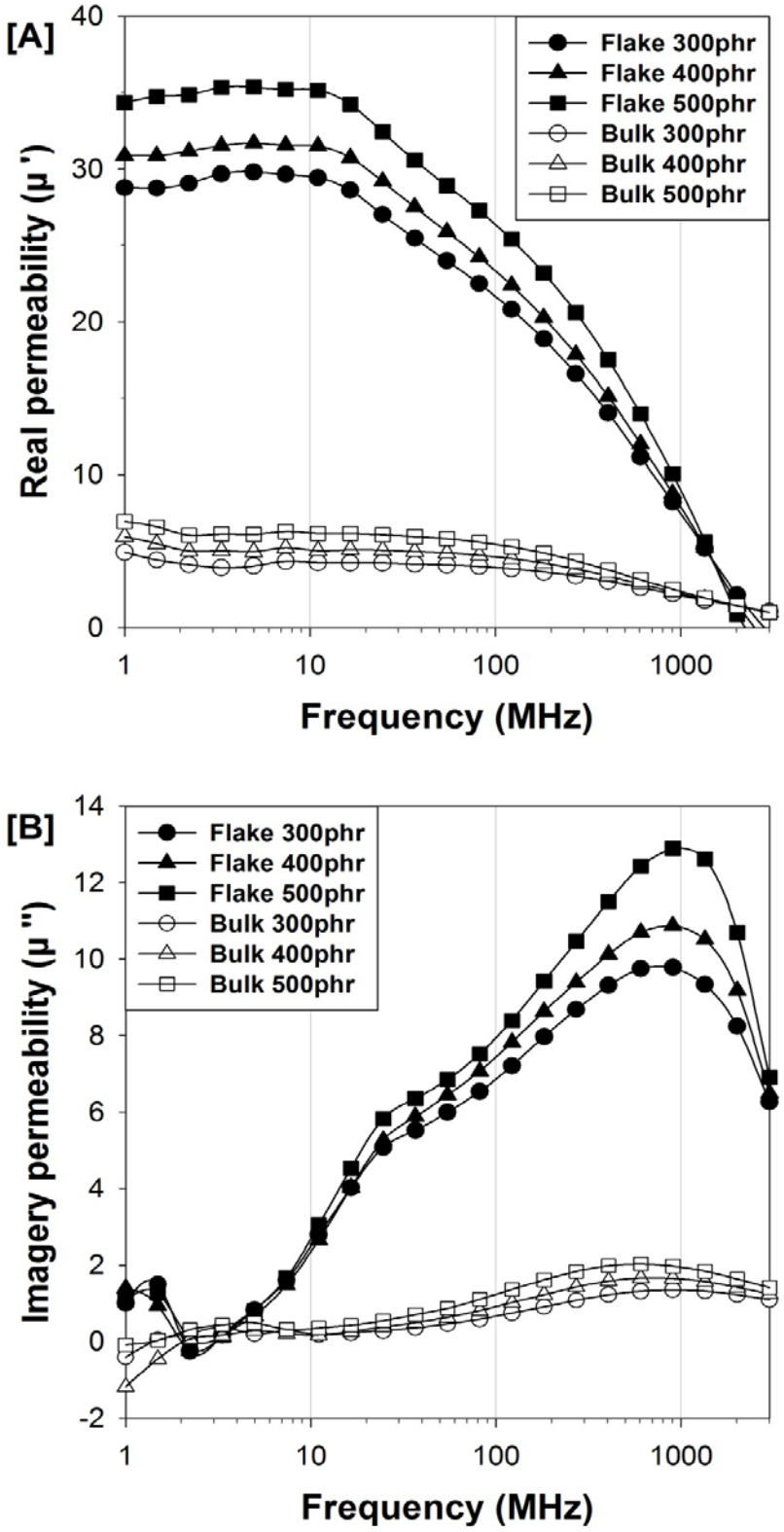

Figure A.5 Complex permeability of electromagnetic wave absorbers. (A) real permeability (B) imaginary permeability

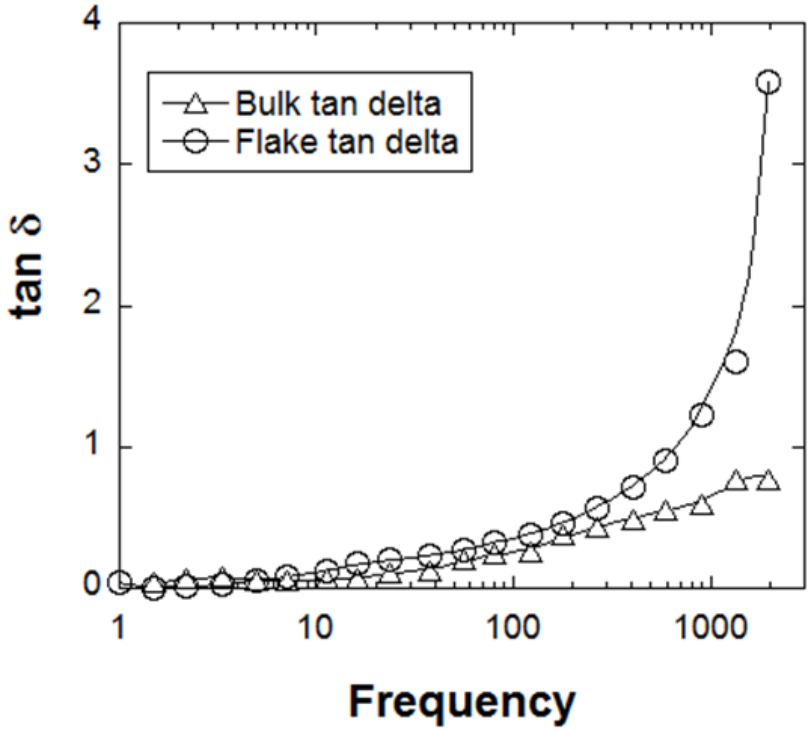

Figure 1.6 The tanδ values of the electromagnetic wave absorbers containing 400 phr Sendust.

Figure A.7 and A.8 show the reflection loss, RL, and the transmission power loss which was deduced from the equation of $P_{loss}/P_{in} = 1 - (|\Gamma|^2 + |T|^2)$ where Γ is the reflection coefficient and T is the transmission coefficient obtained from the reflection (S_{11}) and transmission (S_{21}) scattering parameters, $S_{11} = 20 \log|\Gamma|$ and $S_{21} = 20 \log|T|$.[4,19] The microwave absorbing characteristics increases as the reflection loss increases. It is evident that the intensity of RL peak increases significantly for thin flakes while the RL peak moves to lower frequency with the amount of the Sendust. These are attributed to the increase of the complex permeability. The larger μ" led to higher magnetic loss to increase the adsorption of the EM wave.[16] When 500 phr flake powder was added, the minimum of reflection loss reached -9.6 dB which is 30 times lower than the irregular shape particle composites. The natural resonance frequency (f_r) was increased with the increase of anisotropic flake amount. The microwave-absorbing characteristics also increased as the reflection loss increased. The ratio of P_{loss}/P_{in} was drastically increased over 2 GHz and reached over 90 % up to 10 GHz. This result indicates that the sheet works effectively as an electromagnetic wave absorber for frequencies higher than 1 GHz. Difference in the power loss between flake composite and bulk composite are quite noticeable in the frequency range of 1~2 GHz which coincides with the 2nd peak appearance frequency in Figure 1.5. Comparison of our imaginary part of permeability data with Yoshida et al's shows clearly that present flakes have superior absorbing properties than Yoshida et al's due to better deformation (anisotropy) though their specimen was thinner (0.3 mm) than ours.[9]

Although SEBS/PP - Sendust composite has good dimensional stability as well as excellent EMI shielding performance, its film processing by roll-milling shows some detaching instability. This can be further improved by using linear low density

polyethylene which can undergo the crosslinking reaction to provide the dimensional stability as well as the alignment of the flakes along the rolling direction. Further works are underway to be reported in the future.

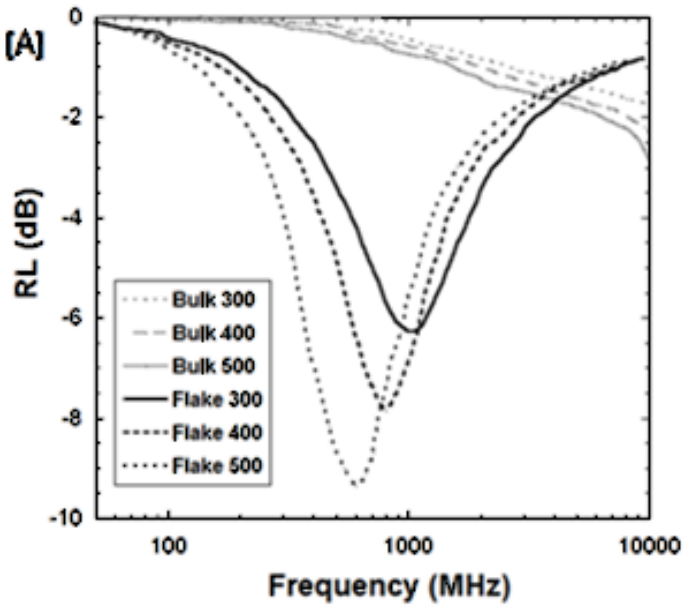

Figure A.7 Reflection loss (RL) of the SEBS/PP - Sendust composite films.

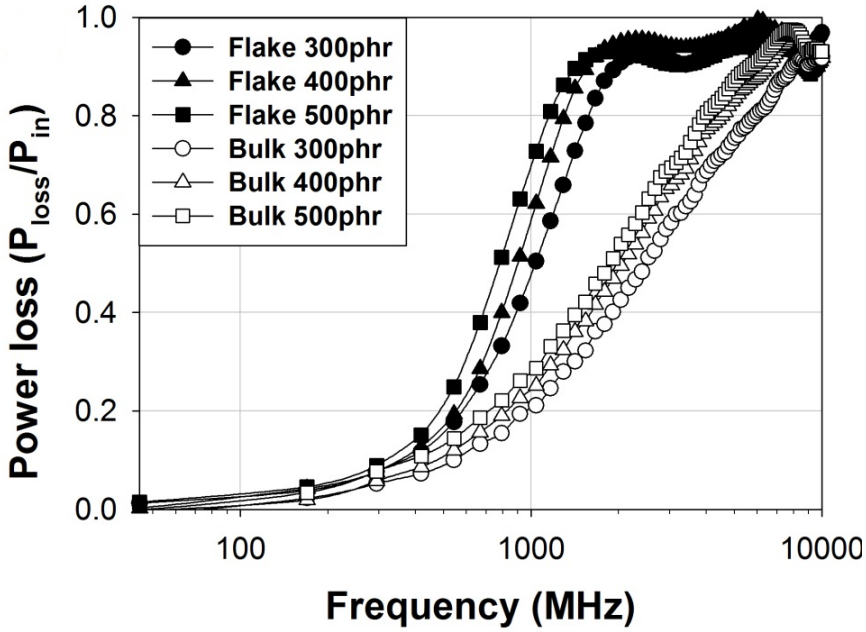

Figure A.8 Power loss of the SEBS/PP - Sendust composite films.

A.4 Conclusion

Addition of the microforged Sendust flakes as the absorbent fillers in SEBS/PP matrix could enhance EMI shielding efficiency significantly in comparison to that of Sendust bulk particle added composites. This is very prominent in the frequency range of 1~5 GHz. High value of magnetic permeability could be obtained in the composites containing Sendust flake particles. When the amount of Sendust flake was 500 phr, the reflection loss was peak reached -9.6 dB. Addition of PP and occurrence of crosslinking reaction between SEBS molecules help to improve the dimensional stability as well as the orientation of flake particles along the rolling direction by the increase of the viscosity, which provides additional performance improvement by the overlapping of flat flakes without any vacancy of fillers in the composite. The power loss reached almost 1 at 5~6 GHz which means that the materials can be industrially useful for EMI shielding.

A.5 References

[1] Tong K.C, Advanced Materials and Design for Electromagnetic Interference Sheilding. CRC Press: New York, 2009.

[2] Geetha, S.; Kumar, K. K. S.; Rao, C. R. K.; Vijayan, M.; Trivedi, D. C. J Appl Polym Sci 2009, 112, (4), 2073-2086.

[3] Shen, B.; Zhai, W. T.; Tao, M. M.; Ling, J. Q.; Zheng, W. G. Acs Appl Mater Inter 2013, 5, (21), 11383-11391.

[4] Saini, P.; Choudhary, V.; Vijayan, N.; Kotnala, R. K. J Phys Chem C 2012, 116, (24), 13403-13412.

[5] Hu, M. J.; Gao, J. F.; Dong, Y. C.; Li, K.; Shan, G. C.; Yang, S. L.; Li, R. K. Y. Langmuir 2012, 28, (18), 7101-7106.

[6] Lim, K. M.; Kim, M. C.; Lee, K. A.; Park, C. G. Ieee T Magn 2003, 39, (3), 1836-1841.

[7] Kim, S. S.; Kim, S. T.; Yoon, Y. C.; Lee, K. S. J Appl Phys 2005, 97, (10).

[8] Li, N.; Huang, Y.; Du, F.; He, X. B.; Lin, X.; Gao, H. J.; Ma, Y. F.; Li, F. F.; Chen, Y. S.; Eklund, P. C. Nano Lett 2006, 6, (6), 1141-1145.

[9] Yoshida, S.; Ando, S.; Shimada, Y.; Suzuki, K.; Nomura, K.; Fukamichi, K. J Appl Phys 2003, 93, (10), 6659-6661.

[10] Nam, I. W.; Lee, H. K.; Jang, J. H. Compos Part a-Appl S 2011, 42, (9), 1110-1118.

[11] Liu, Z. F.; Bai, G.; Huang, Y.; Ma, Y. F.; Du, F.; Li, F. F.; Guo, T. Y.; Chen, Y. S. Carbon 2007, 45, (4), 821-827.

[12] Wang, X.; Gong, R. Z.; Li, P. G.; Liu, L. Y.; Cheng, W. M. Mat Sci Eng a-Struct

2007, 466, (1-2), 178-182.

[13] Qiao, L.; Wen, F. S.; Wei, J. Q.; Wang, J. B.; Lia, F. S. J Appl Phys 2008, 103, (6).

[14] Cho, H. S.; Kim, A. S.; Kim, S. M.; Namgung, J.; Kim, M. C.; Lee, G. A. Phys Status Solidi A 2004, 201, (8), 1942-1945.

[15] Maiti, S.; Shrivastava, N. K.; Suin, S.; Khatua, B. B. Acs Appl Mater Inter 2013, 5, (11), 4712-4724.

[16] Choi, C. M.; Il Kim, D.; Je, S. H.; Choi, Y. S. Curr Appl Phys 2007, 7, (5), 586-589.

[17] Dionne, G. F. Ieee T Magn 2003, 39, (5), 3121-3126.

[18] Lee, J. W.; Hong, Y. K.; Kim, K.; Joo, J.; Yoon, Y. W.; Kim, S. W.; Kim, Y. B.; Kim, K. Y. J Korean Phys Soc 2006, 48, (6), 1534-1538.

[19] Yoshida, S.; Ando, S.; Ono H.; Shimada, Y., J Magn Soc Japan, 2002, 26, 843

Appendix B

Dispersion and reaggregation of nanoparticles in the polypropylene copolymer foamed by supercritical carbon dioxide.

B.1 Introduction

During the last decade, nanocomposites have attracted great interest at an unprecedented level both in industry and in academia, due to their extraordinary potential to overcome the limit of conventional composite materials.[1–15] They can achieve high performance in mechanical properties[1,2,10] as well as various physical properties such as flame retardance,[11] decreased gas permeability[3,12] and thermal resistivity[6,7,10] to name a few. The most heavily used filler materials are the aluminum silicate clays; one of them is montmorillonite (MMT). Besides its intrinsic potential due to a high aspect ratio and a high surface area, it is a naturally abundant, environmentally desirable material.[1,2,5] However, preparations of montmorillonite for nanocomposites meet the obstacle of dispersion, because the aluminum silicate clays are hydrophilic whereas most engineering polymers are hydrophobic; thus, they are intrinsically incompatible with each other. High performance nanocomposites are possible when the nanoparticles are fully dispersed in the polymer matrix. The solution to this incompatibility has been sought via the ion exchange reaction by replacing the

interlayer cations with quarternary alkylammonium or alkylphosphonium cations, though full dispersion of the clays in the polymer matrix has not been accomplished yet.[2–5]

This was the same for polypropylene (PP) nanocomposite foams. Because of the nanoparticles' dual role as a nucleus for foaming and crystallization as well as its role as a filler for the improvement of mechanical properties, nanoclay particles blended with the PP matrix have attracted a lot of attention.[1–19] Polymer foams based on PP have been considered as a substitute for other thermoplastic materials or other foams due to their outstanding physical properties and low material cost, which are of practical and significant interest to the automotive, packaging and furniture industries.[4,8,14,17] However, inhomogeneous cell nucleation due to crystallization of PP and a low melt strength hamper the foaming of PP. In addition, foaming a nanocomposite with polyolefin polymers such as PP was not easy because of PP's nonpolarity.[15] A direct-melt blending method using a compatibilizer like a maleic anhydride grafted polypropylene (MAPP) or in-situ polymerization method was also tried.[2–5] Some success was obtained with some room for improvement. Although the melt blending method did not require solvent, addition of MAPP did not induce full exfoliation; rather they facilitated the intercalation of clay particles.[3,6] A large amount of MAPP was necessary in order to get more exfoliation which was not favorable due to the loss of other properties, as well as high costs for MAPP.[2,4] An in-situ polymerization process was environmentally unfavorable and required purification, which was impractical for industrial application. As an alternative to overcome these difficulties in PP foaming, supercritical CO_2 ($scCO_2$) has been used since the 1990s over gaseous CO_2 because $scCO_2$ has a much higher solubility and diffusivity in polymers.[2,5,15,17] Okamoto et

al. have shown that the MAPP/clay nanocomposite foams had higher cell density and thicker walls than the pure MAPP foams.[14,18] Zhao et al. investigated the role of clay layers in the foaming of PP/clay nanocomposites.[19] They observed that better-dispersed clay platelets could provide more nucleating sites and lead to uniform cell structure. Nguyen and Baird investigated the effect of $scCO_2$ on the exfoliation and dispersion of nanoclay into the PP.[2] They observed the exfoliation of clay after the pressure of the mixing chamber of the nanoparticles and $scCO_2$ was released, but the exfoliated nanoparticle partially collapsed and re-aggregated after further compounding in a single-screw extruder. In this study, we investigated the foamability of a PP copolymer rather than the PP itself because the copolymer, including ethylene and 1-butene units, has less crystallinity than PP which is expected to induce easy foaming. We also explored the role of nanoclay particles in the foaming of PP copolymer/clay nanocomposites. We tried to figure out the detailed relationship between the clay particles' dispersion and the processing variables. The influence of the blowing agent (CO_2) over the exfoliation of clay layers was also examined.

B.2 Experimental

B.2.1 Materials

Instead of pure PP, we used a copolymer with an expectation of easier foaming due to its higher melt strength and lesser crystallinity. PP copolymer (poly(propylene-co-ethylene-co-1-butene), with a composition of 94.5 wt% of PP unit, 3 wt% of ethylene unit, and 2.5 wt% 1-butene unit, was obtained from Honam Petrochemicals Co. (Korea). Its number and weight molar masses were 42,000 and 230,000 g/mol, respectively. The melting temperature of the terpolymer was 148℃, slightly lower than pure PP. In order to aid the compatibilization between PP terpolymer and the nanoclay particles, a small amount of maleic anhydride grafted polypropylene (MAPP including 1 wt% maleic anhydride, Aldrich) was added. The clay used was a montmorillonite (Cloisite 20A) purchased from Southern Clay Products Inc. It was a surface modified montmorillonite through a cation exchange reaction, in which the sodium cation was replaced by dimethyl, dehydrogenated tallow and quarternary ammonium cation (40 wt% of the clay).[2,15] The individual platelets are typically 1 nm in thickness, with an aspect ratio larger than 50.[16] For the master batch preparation, MAPP and clay were premixed with different proportions of clay in the internal mixer (HAAKE) at 210℃, 50 rpm for 10 minutes. Terpolymer and premade master batch were mixed in a twin screw extruder (Prism). The temperature in the extruder was maintained at 160, 170 and 180℃ for the hopper, mixing zone and die. The weight ratio between the matrix polymer and the

master batch compound was controlled to set the clay amount as 0.2 wt% and 1 wt%. We also prepared 3 wt% and 5 wt% clay containing nanocomposites, but in this study we focused mainly on the samples containing 0.2 wt% and 1 wt% clay.

B.2.2 Nanocomposite foam preparation

For better and more uniform foam fabrication, a batch foaming process was applied (Figure B.1). An autoclave of 300 mL was used for the high pressure vessel. The autoclave was immersed in a silicone oil bath. A given amount of CO_2 was fed into the reactor. The samples were saturated with CO_2 under controlled pressure and temperature for 10 minutes; during that time the dissolution of CO_2 in the PP reached an equilibrium state. The vessel was then rapidly opened to release the CO_2 gas and induce cell nucleation and foamed samples.

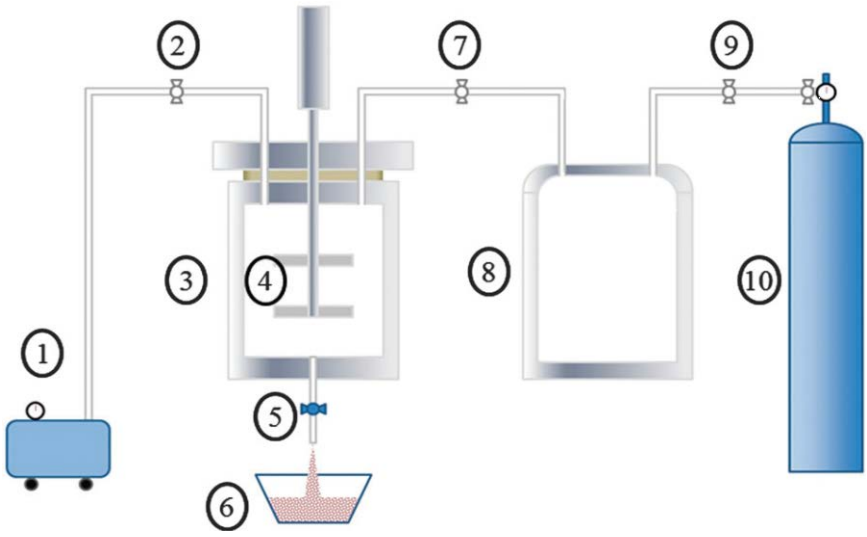

Figure B.1 Schematic of the batch foaming reactor.

(1) vacuum pump, (2) vacuum valve, (3) main reactor, (4) screw, (5) release valve, (6) product collector, (7) high pressure valve, (8) sub reactor, (9) CO_2 valve, (10) CO_2 cylinder

B.2.3 Characterization

The thermal properties of the terpolymer samples were analyzed using differential scanning calorimetry (DSC), performed on a Mettler DSC 823 e. Prior to the analysis, samples were dried at 80℃ in a vacuum oven for 24 hours. About 50 mg of the dried samples was used in each run. To examine nonisothermal crystallization, samples were heated from 25℃ to 200℃ at a heating rate of 10 ℃/min, and then cooled at different cooling rates. A polarized optical microscope (Olympus BX 51) equipped with a Mettler FP82 HT hot stage and a CCD camera was used to measure the growth rate of the crystallites. Transmission electron microscopy (TEM) images were obtained using a JEM 1010 microscope with an accelerating voltage of 100 kV. Ultrathin sections, 60–80 nm in thickness, were cryogenically microtomed with a diamond knife at ca. -100℃. Sections were collected on copper TEM grids. Small-angle X-RAY scattering (SAXS) was carried out at the BL40B2 beamline of Spring-8 (Hyogo prefecture, Japan) using an incident X-RAY with a wavelength $\lambda = 0.1$ nm. A surface and interface cutting analysis system (SAICAS) NN-04 (Daipla Wintes Co., Ltd.) was used to cut the sample obliquely and measured the stress-strain relationship. More than 50 measurements were averaged for each specimen. The tensile strength was measured using an Instron Universal Testing Machine (model 4204) at room temperature. A crosshead speed of 10 mm/min was used. All the reported results are averages of at least 10 measurements.

B.2.4 Cell density calculation and the nonisothermal crystallization kinetics

The cell density (N_0) is the number of cells per cubic centimeter of unfoamed polymer determined from SEM micrographs using the following equation

$$N_0 = [n\, M^2/A]^{3/2}\, \varphi \qquad (1)$$

where n is the number of cells in the SEM micrographs, M is the magnification factor, A is the area of the micrograph (cm^2) and φ is the volume expansion ratio of the polymer foam which is ρ/ρ_j, where ρ and ρ_j are the mass densities of the sample before and after foaming, respectively. To calculate the nuclei concentration for the nanocomposite crystallization using the kinetic model, the following equation was used

$$n_{nuclei} = 3K/(4\pi G^2) \qquad (2)$$

where G is the radial growth rate of the crystalline phase, obtained from the polarized optical microscopy (POM). K is the rate constant which was calculated from the experimental value as $K = (K_{exp})^{3/n}$ where $K_{exp} = \ln 2/(t_{1/2})^n$, $t_{1/2}$ is the half crystallization time and n is the Avrami constant. The nuclei density, n_{nuclei}, can be obtained once the Avrami constant value, n, is provided. To determine the Avrami constant, n, nonisothermal crystallization kinetics model that we proposed sometime ago was applied.[20–23] Here, we briefly present the basic equations from our earlier report. For the nonisothermal crystallization process, the Avrami equation is expressed using a cooling rate

$$\ln[-\ln(1-X_v(T)_U)] = \ln K(T) - n \ln U \qquad (3)$$

where $X_v(T)$ is the volume fraction of the polymer transformed at a temperature T and the cooling rate U, and K(T) is the so-called cooling function, which only varies as a function of the temperature. As suggested by the theory, a linear dependence between ln K(T) and the temperature T is assumed, ln K(T) = aT + b.[20] When the temperature

reaches the peak of the exothermal curve, T_{max}, for a given cooling rate (U), n ln U = aT_{max} + b - ln[-ln(1-$X_v(T_{max})_U$)]. Therefore, eqn (3) can be rewritten as

$$\ln[-\ln(1-X_v(T)_U)] = a\,(T-T_{max}) + \ln[-\ln(1-X_v(T_{max})_U)] \qquad (4)$$

Hence the value of the parameter a can be estimated from the slope of a plot of ln[-ln(1-$X_v(T)_U$)] against T-T_{max}. Also, plotting T_{max} versus ln U gives a straight line whose slope is n/a and intercept is (ln[-ln(1-$X_v(T_{max})_U$)]-b)/a; thus, all the parameter values can be determined without resorting to any numerical process.[21–23]

B.3 Results and discussion

B.3.1 Foamed cell morphology

As displayed in Figure B.2, there are four steps involved in a foaming process: (1) dissolution of gas into a polymer; (2) cell nucleation (driven by heterogeneous nucleation of clay nanoparticles); (3) cell growth (a combination of mass and heat transfer); and (4) cell stabilization via a cooling process of the system.[4,24] The cell growth process is stopped by a natural or an imposed ending of the driving force for cell growth and a cellular foam is obtained.[14] The cell nucleation and growth are controlled by the process parameters such as foaming temperature, saturation pressure, depressurization rate and saturation time. After much trial-and-error, we could optimize the processing conditions. Representative samples are exemplified here. PP copolymer was foamed easily at lower pressure and temperature (5~7 MPa and 120~140 ℃) than pure PP (for e.g. 7~30 MPa and 155~165 ℃).[3,19,25] This is mainly attributed to the copolymer moieties other than PP which induced easy deformation due to their less ordered structure (the crystallinity of the terpolymer was 35%, lower than general PP which was about 45%). More free volume in the amorphous phase could accommodate more CO_2.

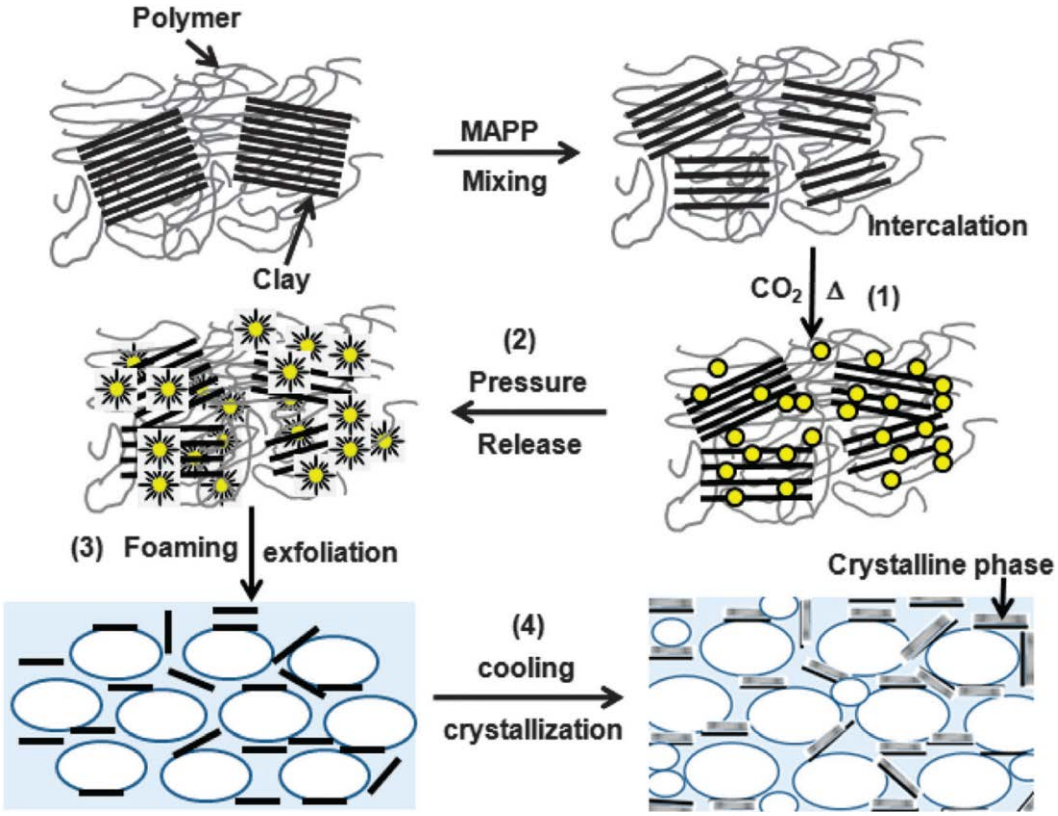

Figure B.2 Schematic figure of the foaming process.

The volume expansion ratio of the foamed PP copolymer, R_v, was defined as the ratio of the bulk density of the virgin PP (ρ_p) to that of the foamed one (ρ_f), $R_v = \rho_p/\rho_f$. For a given cell size, an increase in cell density necessarily leads to a decrease of foam density and an increase in the volume expansion ratio. Figure B.3 shows the effect of the saturation pressure on the volume expansion ratio at different foaming temperatures for the PP copolymer and nanocomposites. The volume expansion ratio increased almost linearly with the saturation pressure.[2,4] The temperature showed an opposite effect to the volume expansion ratio and foam density. Compared to pure PP foams, the terpolymer foaming was possible at much lower temperature.[4,5] Addition of the clay increased the foam density as well as the modulus; hence it could hinder the expansion of the cell while it also acted as the nuclei for the foaming. Though addition of the clay increased cell density, its effect on the expansion ratio was not remarkable due to the small amounts of added clay. The cell morphologies were well defined (uniform cell distribution).

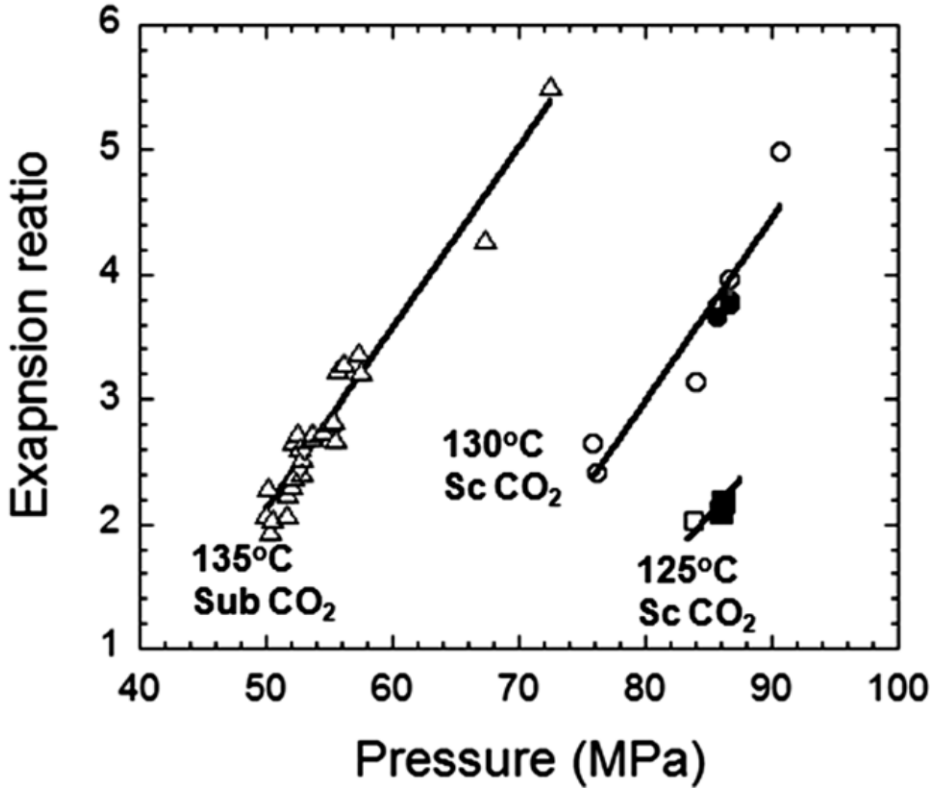

Figure B.3 Foam expansion ratio versus the reaction pressure.

△ (135℃, subcritical CO_2), ○ ● (130℃, supercritical CO_2), □ ■ (125℃, supercritical CO_2). Open symbols are 0.2 wt% clay nanocomposites and filled symbols are 1 wt% clay nanocomposites.

Figure B.4 shows the cell morphology of the foamed structure of PP copolymer and two composite samples including 0.2 wt% and 1 wt% clay. Regardless of the foaming temperature, the PP copolymer foam had bigger cells than the nanocomposite foams. While the cell size was large for the PP copolymer foamed at 135℃ with subcritical CO_2 (subCO_2), it was noticeably decreased for the foams processed with supercritical CO_2 (scCO_2). It was very clear from the morphologies that scCO_2 dissolved and diffused more CO_2 molecules into the terpolymer than sub CO_2. Since the foaming temperature was below the melting temperature of the terpolymer, the crystalline phase of the terpolymer could not be disrupted. Foaming by scCO_2 was done at higher pressure than the one by subCO_2 (Figure B.3) under which conditions more CO_2 molecules permeated into the polymer amorphous phase. More dissolved CO_2 evolved into more cells later to increase the cell density and decrease the cell size. Nanoparticles were generally added to induce heterogeneous nucleation of foaming.[7,26–29] Nanocomposites showed a more uniform cell size due to more heterogeneous nuclei of the clay nanoparticles. However, the morphologies of the nanocomposites revealed that a lower foaming temperature and a higher saturation pressure were more favorable for obtaining a uniform foam than a higher foaming temperature and a lower saturation pressure process, similar to other PP foaming.[4,7] Opposite effects of the temperature and pressure were observed; increasing the foaming temperature was equal to decreasing the saturation pressure in terms of foamability. Higher temperature decreased CO_2 dissolution into the polymer to reduce the cell density and increased the cell size. The samples foamed at 135℃ by subCO_2 had a bigger cell size and lower cell density. Like the PP foams, it was obvious that scCO_2 dissolved and diffused more into the terpolymer than sub CO_2. The samples foamed by scCO_2 at a temperature of 125℃

showed more uniform and smaller cell morphology than those foamed at a temperature of 130℃, though the pressures were almost the same for both cases. This indicates that the cell growth is very sensitive to temperature change as well as the CO_2 pressure.

Introduction of a small amount of clay greatly improved the foamability of PP terpolymer and cell morphology. They were heterogeneous nuclei for the foaming and for the matrix polymer crystallization. The cell density calculated by a simple equation (eqn (1)) with previous SEM images is presented in Table 2.1. A higher density implies more heterogeneous foaming nuclei and thus better dispersion of the nanoclay particles. About 4–5 times more cells were formed for the lower temperature (125℃) samples than those foamed at 130℃, because of the greater dissolution of CO_2 molecules. Also, more clay addition (1 wt%) provided more cell nucleation sites during foaming and provided a higher cell density.

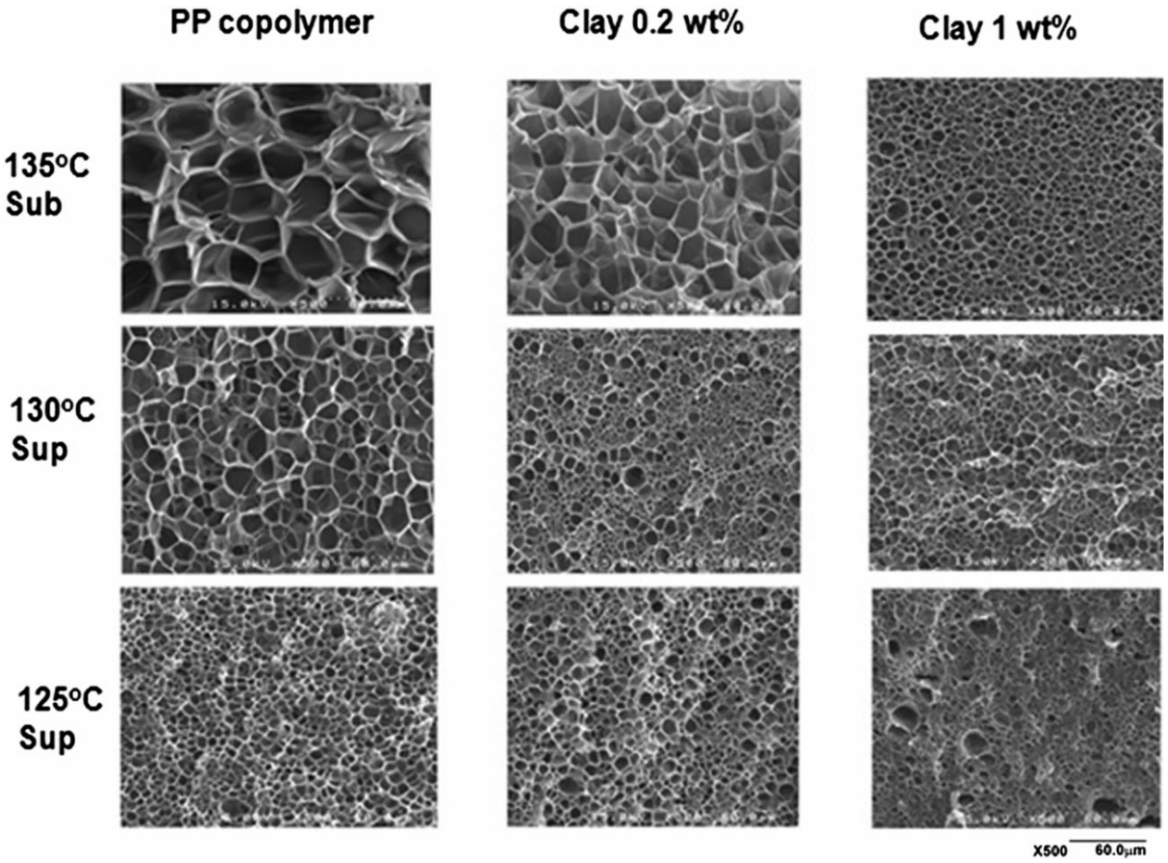

Figure B.4 SEM images of foams. (X500 magnification) first row: foamed at 135℃ with subcritical CO_2; second row: foamed at 130℃ with supercritical CO_2; third row: foamed at 125℃ with supercritical CO_2.

Temperature	Cell density of foam (N_0/cm^3)		Crystallization nuclei density of foamed nanocomposite (1 wt% clay) (N_0/cm^3)	
	0.2 wt% clay	1 wt% clay	1st scan	2nd scan
135℃ ($subCO_2$)	9.5×10^7	1.5×10^8	2.1×10^7	0.9×10^7
130℃ ($scCO_2$)	1.4×10^8	4.7×10^8	3.0×10^8	1.0×10^8
125℃ ($scCO_2$)	3.3×10^8	8.1×10^8	3.3×10^8	2.0×10^8

Table B.1 Cell density and crystallization nuclei density of foamed nanocomposites.

B.3.2 Dispersion of clay in nanocomposites

Small angle X-RAY scattering (SAXS) patterns for the noncompatibilized sample, the MAPP-added blend, and two $scCO_2$ foamed nanocomposites are illustrated in Figure B.5. The noncompatibilized sample (Figure B.5 (a)) demonstrated the characteristic diffraction peak of montmorillonite. The peak of the unfoamed MAPP-added sample (Figure B.5 (b)) was shifted to lower angle compared to that of the noncompatibilized sample, indicating that unfoamed MAPP added samples had an intercalated morphology, i.e., some separation of the clay gallery. This separation was attributed to the compatibilizer polymer chains (MAPP) in the clay galleries. On the other hand, SAXS patterns of all foamed samples of 0.2 wt% and 1 wt% clay, foamed under subcritical conditions (135℃, 56 MPa) (Figure B.5 (c) and (e)) as well as supercritical conditions (125℃ and 130℃ at 86 MPa) (Figure B.5 (d) and (f)), showed no peak at low angles, indicating the highly dispersed state (possibly full exfoliation) of the nanoclay particles. The crystalline phase of PP copolymer matrix was not in the full melt state under these conditions. It is quite obvious that the high dispersion and/or exfoliation of the clay platelets was not because of the penetration of MAPP polymer molecules into the gallery, but was mostly due to the CO_2 molecules dissolved into the clay galleries as well as the interface between the clay and the polymer molecules and the amorphous phase of the polymer matrix. Later they grew into foams by the release of pressure (Figure B.2). Foamed nanocomposites by $scCO_2$ showed very uniform and smaller cells than PP copolymer and $subCO_2$ foamed samples (Figure B.4). The greater cell formation (increased cell density) by $scCO_2$ is primarily due to the fact that more

CO_2 molecules permeated into the clay gallery which served as the nucleating sites during the foaming process. The SAXS spectra of the nanocomposite foams demonstrate that most clay platelets are in the highly dispersed state (possibly the full exfoliated state as shown later). Baird et al. also noticed that a great improvement in the exfoliation of the clay was possible by allowing the clay to be in direct contact with the $scCO_2$, and injecting the mixture into the polymer melt (PP).[2] In the supercritical state, CO_2 behaves like a polar organic solvent that readily penetrates into the galleries of the nanoclay treated with alkyl quarternary ammonium salt.[17–19] When the pressure was released, CO_2 molecules expanded the galleries to separate them. The penetration of CO_2 molecules into the clay galleries can be indirectly checked by foaming the binary blend of PP terpolymer and clay (Figure B.2). Without the compatibilizer (MAPP), most clay particles are in stacks without much intercalation. However, the foams of the binary blends without the compatibilizer show good dispersion (intercalation as well as some exfoliation) of clay platelets. The characteristic peak of the clay also disappeared.

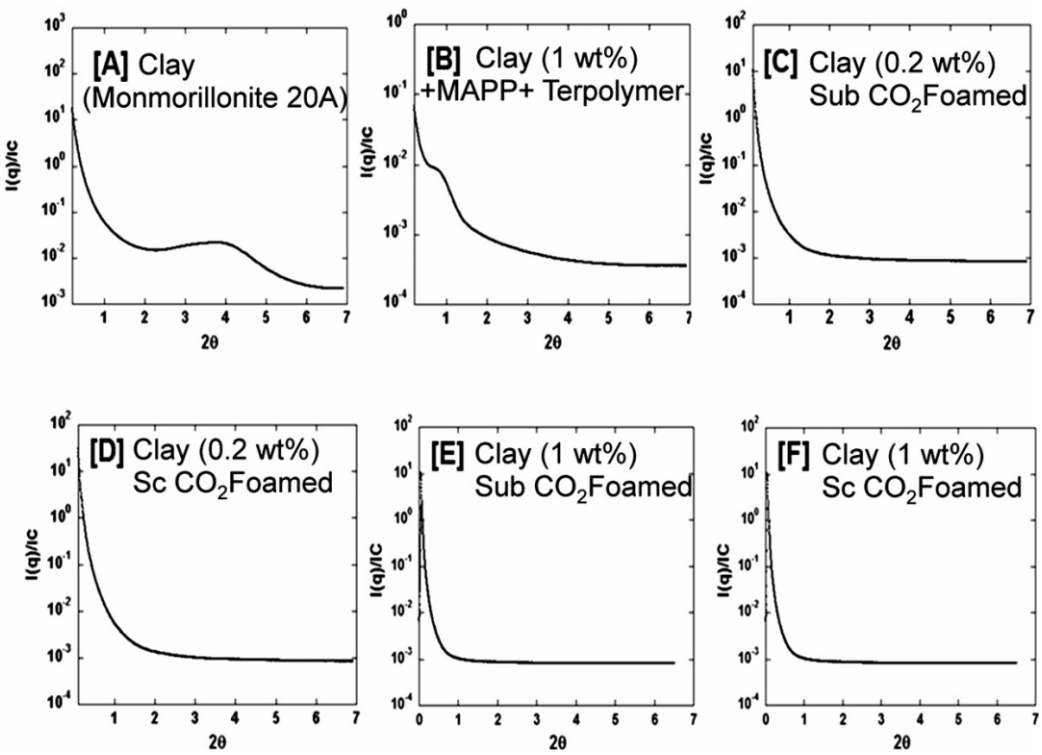

Figure B.5 SAXS patterns for the clay, unfoamed and foamed nanocomposites.

The high dispersion and/or full exfoliation of the clay nanoparticles provided more nuclei for foaming. Hence the foam size became smaller and the cell density increased (Figure B.3). The dispersion state (possible exfoliation) of the clay nanoparticles can be directly seen by TEM. Though TEM allows only observation limited to a very small area, it can give a qualitative understanding of the spatial distribution of the clay in the matrix. Regardless of their limitations, TEM and SAXS together are essential tools for evaluating the nanocomposite structures. TEM micrographs of nanocomposites prepared under different conditions are presented in Figure B.6. Figure B.6 (a) shows an enlarged micrograph of a clay particle. It is obvious that the clay particle is an aggregate of thousands of layers. The compatibilized one (Figure B.6 (b)) has much smaller particles of a thin intercalated structure. Mixing with MAPP, the clay particles were partially separated and dispersed. The compatibilizing action of MAPP induced the intercalation of the nanoparticles, but it was not enough to lead to full exfoliation of the particles. On the other hand, nanocomposite foams demonstrate that clay platelets were well dispersed (some are fully exfoliated) in the polymer with little aggregates. Better dispersion of clay platelets were observed for $scCO_2$ foams (Figure B.6 (d) and (f)), indicating that $scCO_2$ was more effective to derive further exfoliation. Most clay components existed as separated layers in nanocomposites in direct contact with the matrix copolymer, which provided much larger interfacial area for CO_2 adsorption and cell nucleation later. TEM observation confirmed the SAXS patterns of nanoclay dispersion. Also, the low foaming temperature demanded a higher CO_2 pressure, leading to more dissolution and permeation of CO_2 molecules into the nanocomposites, and it helped to induce more cell formation. Therefore, foamed nanocomposites could have a higher cell density and smaller cell size.

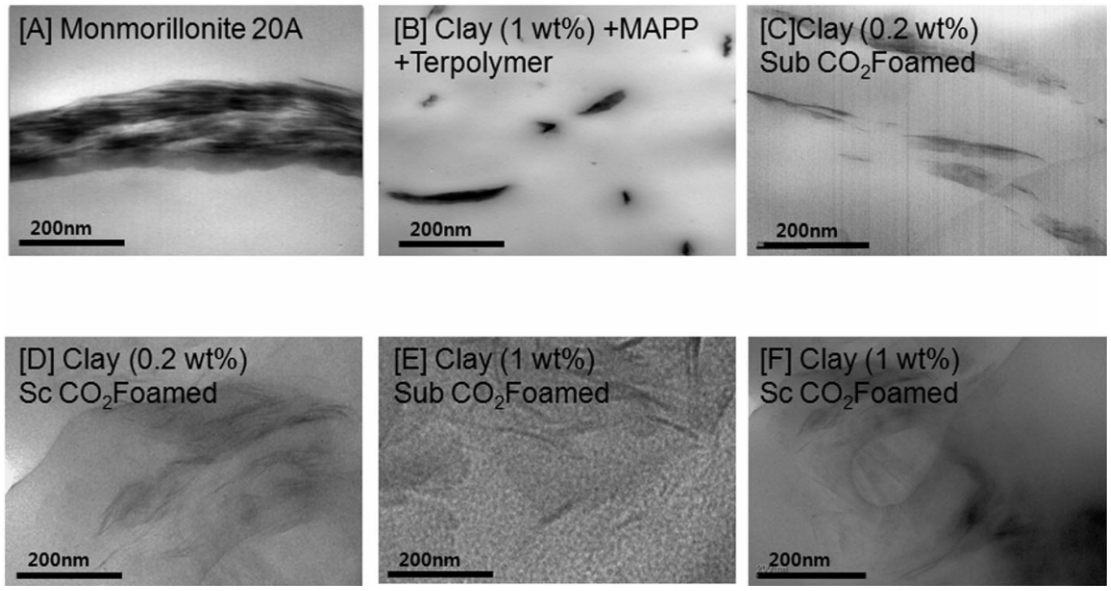

Figure B.6 TEM images of the clay and nanocomposites.

B.3.3 Further processing and reaggregation of platelets

Though a high degree of dispersion and/or full exfoliation of the clay galleries were achieved by the foaming process, they were not thermodynamically stable.[24] When the foams were used as the master batch for mixing with the PP copolymer in the twin-screw extruder, the SAXS patterns for the extrudate showed the characteristic peak of the clay (Figure B.7). All reprocessed ones displayed the reappearance of the characteristic peak of intercalated platelets which was unseen in the foam (Figure B.5 and B.7). If we look into 2-D SAXS spectra, this becomes more prominent. Figure B.8 shows the 2-D SAXS spectra demonstrating that all reprocessed ones had a long range ordered structure by the aggregation of some platelets close to one another (the second row in Figure B.8) while the foams did not show any sign of it (the first row in Figure B.8). Reappearance of the characteristic peak after extrusion is the sign of the aggregation of the highly dispersed/exfoliated clay platelets during the extrusion (the last row in Figure B.8). Similar phenomena were observed by Baird et al.[2] The PP copolymer has no or little attractive interaction with the clay platelets.[24] Reaggregation of clay platelets can be indirectly checked by DSC. Using the nonisothermal crystallization kinetics (eqn. (2)–(4)), the number of nuclei for the crystallization of foamed nanocomposites were calculated in Table B.1. The number of nuclei after the 1st scan, which was done by cooling down the sample as soon as it reached 160℃, means the number of nuclei in the foamed nanocomposites before the reaggregation occurs. The 2nd scan was done after the sample was heated to 180℃ and stayed there for 3 minutes. All the numbers of nuclei were decreased after the 2nd scan,

indicating that the clay platelets were aggregated in the melt state. We speculate that platelets at closer distances or exposed on the inner surface of the foam cell could reaggregate in the melt state while those at further distance could not aggregate because of the high viscosity of the matrix polymer. With the assumption of the uniform dispersion of clay particles both in the amorphous phase and in the crystalline phase (~35%), total number of heterogeneous nuclei (clay platelets) can be approximated as 3 times the crystallization nuclei because the crystallization occurs after the pressure release (Figure B.2). The orders of nuclei number obtained from the cell density and from the crystallization kinetics are in agreement (Table B.1). This implies that most clay particles were well dispersed (possibly fully exfoliated) in the foamed nanocomposites.

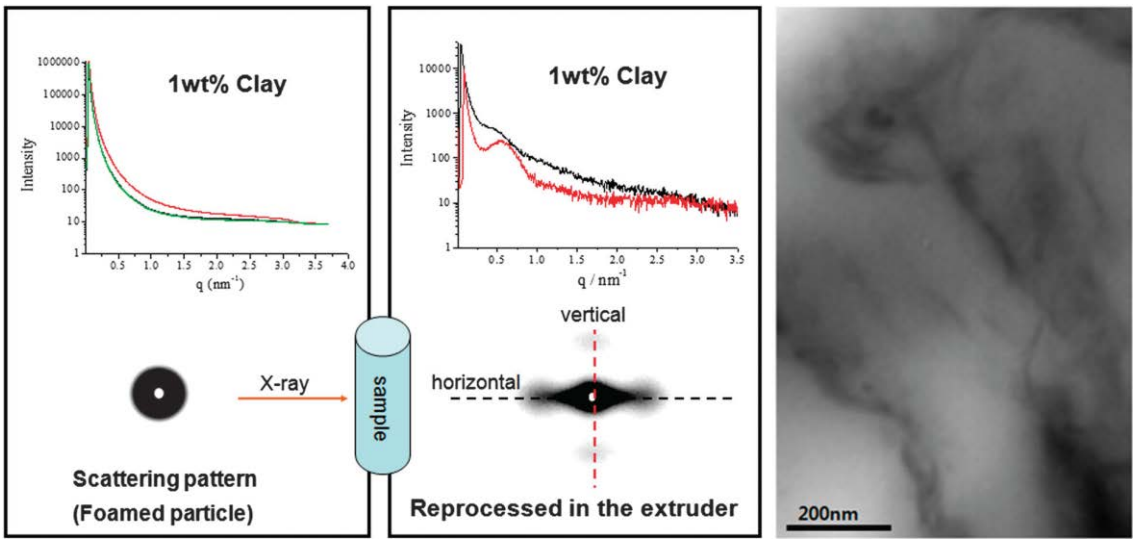

Figure B.7 SAXS patterns for foamed (125℃ ($scCO_2$)) and reprocessed nanocomposites (including 1 wt% clay). The TEM Figure shows the aggregation of platelets in the reprocessed composite.

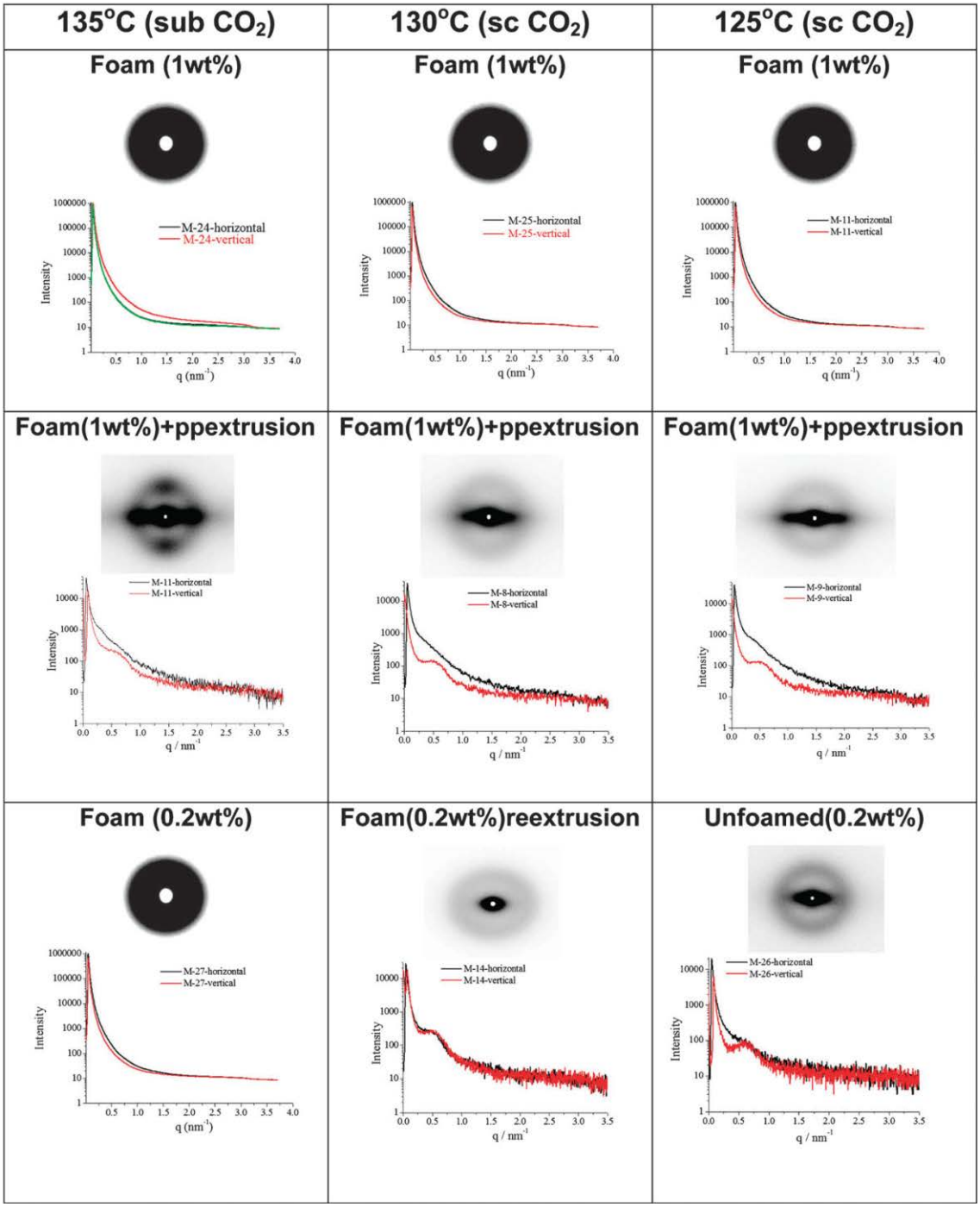

Figure B.8 2-D SAXS patterns for foamed and reprocessed nanocomposites (1 wt% clay).

B.3.4 Mechanical properties

Using the surface and interface cutting analysis system (SAICAS), we measured the cutting resistance of the foamed nanocomposites. The SAICAS is a low angle gradient cutting instrument that uses a diamond knife.[29] Like TEM, SAICAS detects over a very small area which does not represent the microstructure of the nanocomposite as a whole. Regardless of its limitations, it can give a glimpse of the mechanical properties of nanocomposites. The nanocomposites are obliquely cut from the surface randomly with constant speed and at a constant cutting angle. The resistant stress detected by the piezoelectric actuators was recorded against the moving distance. Figure B.9 shows the stress against distance. Constant velocities were maintained throughout the whole cutting edge moment. The results suggest that the unfoamed sample was harder than the foamed samples. A linear relationship between the stress and the distance indicates a constant movement of the diamond knife. A steep slope means that it has cut through a hard material whereas a less-steep slope implies that it passed through soft material. While passing through the composites, the more uniformly dispersed clay particles are in the highly dispersed state (or exfoliated), the less resistance the blade experienced. The intercalated clay or aggregated platelets are harder than the highly dispersed or fully exfoliated samples. The slope may be decreased with the dispersion of the clay nanoparticles. As mentioned before, exfoliated and uniformly dispersed clay platelets aggregate again if they undergo further processing.[2,30] This is because the well-dispersed alumina silicate is thermodynamically unstable, especially in the nonpolar polypropylene.[24] Two different samples, unfoamed and scCO_2 foamed, containing 0.2

wt% clay were used for mechanical property measurement. The samples were prepared by a Mini-Max molder at a temperature of 200℃ and a tensile test was conducted. The modulus of the foamed samples showed a 10% increase compared to the unfoamed one (450 MPa to 500 MPa), but the tensile strengths were almost the same regardless of the foaming (30.2 MPa to 30.6 MPa). As Nguyen and Baird observed, this could be due to the formation of big agglomerates in the nanocomposites which results in marginal enhancement of the mechanical properties.[2]

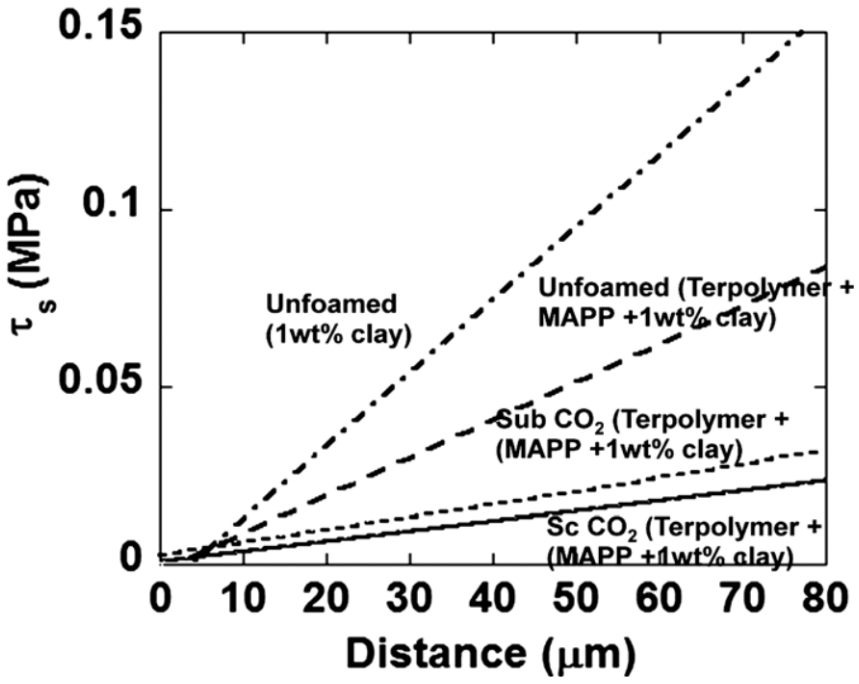

Figure B.9 SAICAS measurement of the resistant stress versus the forwarding distance.

B.4 Conclusion

The effect of foaming the PP copolymer blends with a clay by subCO_2 and scCO_2 on the dispersion and exfoliation of nanoclay particles was investigated. The terpolymer blends were foamed well under milder condition than pure PP. The processing temperature window was wider than the one applied for the general PP foam. The SAXS analyses showed that the foaming process facilitated a high degree of dispersion of the clay particles. Fully exfoliated structures were obtained for some foamed nanocomposite samples. scCO_2 facilitated more permeation of CO_2 into the clay gallery, and thus produced more cells of smaller size. A higher saturation temperature under the same pressure reduced CO_2 adsorption in the polymer matrix and in the clay gallery. Hence, higher saturation temperature produced less uniform foams and bigger cells. Since the clay layers were heterogeneous nucleating sites for foaming and later for crystallization, nanocomposites with better dispersion of clay platelets raised more cells and more uniform structures. We could confirm the dual role of clays for foaming and crystallization. A direct use of the produced nanocomposites may be best to exploit the exfoliated structure. Further processing to take advantage of the well dispersed or fully exfoliated structure at a temperature above the melting temperature of the PP copolymer was not advantageous because it led to reaggregation of clay platelets which was not helpful to improve the mechanical properties of the reprocessed sample.

B.5 References

[1] Zeng, C. C.; Han, X. M.; Lee, L. J.; Koelling, K. W.; Tomasko, D. L. Adv Mater 2003, 15, (20), 1743-+.

[2] Nguyen, Q. T.; Baird, D. G. Polymer 2007, 48, (23), 6923-6933.

[3] Xu, Z. M.; Jiang, X. L.; Liu, T.; Hu, G. H.; Zhao, L.; Zhu, Z. N.; Yuan, W. K. J Supercrit Fluid 2007, 41, (2), 299-310.

[4] Jiang, X. L.; Bao, J. B.; Liu, T.; Zhao, L.; Xu, Z. M.; Yuan, W. K. J Cell Plast 2009, 45, (6), 515-538.

[5] Shen, J.; Zeng, C. C.; Lee, L. J. Polymer 2005, 46, (14), 5218-5224.

[6] Bhattacharya, S.; Gupta, R. K.; Jollands, M.; Battacharya, S. N. Polym Eng Sci 2009, 49, (10), 2070-2084.

[7] Lee, Y. H.; Park, C. B.; Wang, K. H.; Lee, M. H. J Cell Plast 2005, 41, (5), 487-502.

[8] Kawasumi, M.; Hasegawa, N.; Kato, M.; Usuki, A.; Okada, A. Macromolecules 1997, 30, (20), 6333-6338.

[9] Zhai, W. T.; Yu, J.; Wu, L. C.; Ma, W. M.; He, J. S. Polymer 2006, 47, (21), 7580-7589.

[10] Giannelis, E. P. Adv Mater 1996, 8, (1), 29-&.

[11] Gilman, J. W.; Jackson, C. L.; Morgan, A. B.; Harris, R.; Manias, E.; Giannelis, E. P.; Wuthenow, M.; Hilton, D.; Phillips, S. H. Chem Mater 2000, 12, (7), 1866-1873.

[12] Bharadwaj, R. K. Macromolecules 2001, 34, (26), 9189-9192.

[13] Fu, X.; Qutubuddin, S. Polymer 2001, 42, (2), 807-813.

[14] Nam, P. H.; Maiti, P.; Okamoto, M.; Kotaka, T.; Nakayama, T.; Takada, M.;

Ohshima, M.; Usuki, A.; Hasegawa, N.; Okamoto, H. Polym Eng Sci 2002, 42, (9), 1907-1918.

[15] Bao, J. B.; Liu, T.; Zhao, L.; Barth, D.; Hu, G. H. Ind Eng Chem Res 2011, 50, (23), 13387-13395.

[16] Han, X. M.; Zeng, C. C.; Lee, L. J.; Koelling, K. W.; Tomasko, D. L. Polym Eng Sci 2003, 43, (6), 1261-1275.

[17] Ibeh, C. C.; Bubacz, M. J Cell Plast 2008, 44, (6), 493-515.

[18] Taki, K.; Yanagimoto, T.; Funami, E.; Okamoto, M.; Ohshima, M. Polym Eng Sci 2004, 44, (6), 1004-1011.

[19] Jiang, X. L.; Liu, T.; Xu, Z. M.; Zhao, L.; Hu, G. H.; Yuan, W. K. J Supercrit Fluid 2009, 48, (2), 167-175.

[20] Seo, Y. Polym Eng Sci 2000, 40, (6), 1293-1297.

[21] Seo, Y.; Kim, S. Polym Eng Sci 2001, 41, (6), 940-945.

[22] Hong, S. M.; Seo, Y. J Phys Chem B 2007, 111, (14), 3571-3575.

[23] Seo, Y.; Kim, J.; Kim, K. U.; Kim, Y. C. Polymer 2000, 41, (7), 2639-2646.

[24] Ray, S. S.; Okamoto, M. Prog Polym Sci 2003, 28, (11), 1539-1641.

[25] Ma, J.; Peijs, T. Polypropylene, ed. F. Dogan, Intech, Rijeka, 2012, ch.20.

[26] Nowacki, R.; Monasse, B.; Piorkowska, E.; Galeski, A.; Haudin, J. M. Polymer 2004, 45, (14), 4877-4892.

[27] Manias, E.; Touny, A.; Wu, L.; Strawhecker, K.; Lu, B.; Chung, T. C. Chem Mater 2001, 13, (10), 3516-3523.

[28] Zhai, W. T.; Park, C. B.; Kontopoulou, M. Ind Eng Chem Res 2011, 50, (12), 7282-7289.

[29] Narayama, I.; Baba, D.; Takahara, A.; Tanaka, K. Appl Surf Sci 2010, 257, (3),

1145-1148.

[30] Fu, J.; Naguib, H. E. J Cell Plast 2006, 42, (4), 325-342.

Appendix C

Nonisothermal crystallization behaviors of nanocomposites prepared by in-situ polymerization of high-density polyethylene on tungsten oxide particles.

C.1 Introduction

C.1.1 Polyethylene/CNT composites

The properties of the polymer nanocomposites are strongly affected by the dispersion of fillers in the polymer matrix and their adhesion with the polymer molecules.[1] This is no exception for carbon nanotubes (CNTs) because they show a strong tendency for aggregates.[2-4] Uniform dispersion of CNTs has been a critical issue for CNT nanocomposites due to the large surface area of CNTs.[5-7] Recently the polyethylene (PE)/CNT nanocomposites have been the subject of many studies due to its variety of useful applications.[1,8,9] In-situ ethylene polymerization on the CNT surface was proven to be an effective method to grow PE chains on the surface of the nanotubes that allowed breakup of the CNT bundles. Produced PE/CNT composites can be further melt-blended with matrix molecules to provide improved high-performance nanocomposites. Li and coworkers reported that high density polyethylene (HDPE)

molecules formed nanohybrid shish-kebabs or similar structures when crystallized from the solution and the melt.[10,11] Their experimental results showed that PE chains oriented preferentially along the CNT axis. The -CH group of the HDPE allows for the CH-π interaction to successively attach the HDPE molecules onto the surface, leading to parallel chain adsorption.[11] The large aspect ratio and the curvature of CNTs decisively control the morphology development of HDPE-grown HDPE/CNT nanocomposites. In our recent study, we also investigated the properties of nanocomposites of HDPE/multiwalled carbon nanotubes (MWNT) prepared by in-situ metallocene polymerization.[9,12] We could also observe the shish-kebab structure in the melt crystallized nanocomposites. The HDPE/MWNT nanocomposite in which HDPE was in-situ polymerized on the MWNT surface showed different crystallization behavior from the pristine HDPE: the Avrami exponent of the pristine HDPE was close to 3 indicating that the crystallites had a spherulite structure whereas that of the HDPE/MWNT nanocomposites was close to 2 depending on the amount of CNTs, indicating the growth mechanism of 2-dimensional rod shape.[9] We ascribed this to the CH_2-π interaction and successive -CH_2 groups gradually attachment to the CNT surface, leading to parallel chain adsorption as noted by Li et al.[10,11] The curvature of the CNTs let the HDPE molecules preferentially align themselves parallel to the nanotube axis, later grow perpendicularly to MWNT surface to exhibit the shish of shish-kebab morphology of melt spun PE fibers.[9] Thus, we confirmed that templating on CNT is quite effective for producing aligned PE morphologies.[9,12]

C.1.2 HDPE/tungsten oxide (WO_3) composites

In this study, we investigated the effect of interaction between the dispersed fillers and the polymer molecules that decides the emerging morphology. This was explored by studying the HDPE/tungsten oxide (WO_3) nanocomposites where tungsten oxide does not have interaction with the HDPE molecules, but has attached HDPE molecules on the surface due to the metallocene catalysis adsorbed on the tungsten surface. By comparing the HDPE/MWNT nanocomposite morphology development, we could verify the effect of interaction on the emerging nanocomposite morphology during the cooling process. For the analysis of the HDPE/MWNT crystallization kinetics, we applied Seo's method which was devised for nonisothermal crystallization kinetics to provide supplementary information about the crystal structure produced during the cooling process. Though crystallization kinetics is generally analyzed using Avrami's equation, it is for isothermal crystallization process which poses some difficulties in maintaining the polymer melt in an amorphous state while cooling to the crystallization temperature.[7,8] Also the crystallization processes encountered in nature tend to be nonisothermal. Hence we applied Seo's method with a focus on the morphological changes.

C.2 Experimental

C.2.1 Materials

Tungsten oxide (WO_3, Inframat Advanced Materials) was employed as a filler. They were dried in a vacuum oven for more than 24 hours at 100℃ before use. The mean particle size of tungsten powder was 1 μm. The same synthesis scheme we used before was applied for the preparation of HDPE modified WO_3 composite, i.e., the in-situ Ziegler-Natta polymerization of PE on tungsten nanoparticles whose surfaces were impregnated by the metallocene catalyst.[9] Details of the synthesis process are as follows: ethylene (Dong-A Co., 99.9%) was used as a polymerization monomer, and titanium tetrachloride ($TiCl_4$, 1 $mol \cdot L^{-1}$ solution in toluene, Aldrich Chemical Co.) was used as a catalyst. Triethylaluminium (Et_3Al, 1.9 $mol \cdot L^{-1}$ solution in toluene, Aldrich Chemical Co.), a commonly used cocatalyst in metallocene-based olefin polymerization, was also used.

C.2.2 Sample preparation

C.2.2.1 Polymerization of PE/WO_3 composite

Fixation of catalyst on the surface of tungsten nanoparticles and polymerization of ethylene were consecutively carried out in a 1 L high-pressure reactor equipped with a magnetic drive. Dried tungsten powder (40g) was charged into the reactor and added to

purified toluene. The tungsten particles dispersion was done by an ultrasonic treatment for 1 hour at room temperature. At the same time, argon gas bubbling was conducted to purge completely the residual oxygen and water vapor from the mixture. $TiCl_4$ (1.95 mol) was injected into the slurry after the ultrasonic treatment. The fixation reaction of added $TiCl_4$ was performed for 1 hour at 50℃. Then, 38.96 mol of Et_3Al (20.5 mL) was introduced into the reactor. The polymerization reaction was carried out as soon as the ethylene gas was injected into the reactor under a constant pressure of 0.5 bar of ethylene at 50℃. After a predetermined reaction time, the polymerization was quenched with a diluted HCl solution. The polymer was precipitated in methanol, filtered, and dried in a vacuum oven.

C.2.2.2 Manufacturing of HDPE/WO_3 composites

HDPE homopolymer which was later blended was obtained from Honam Petrochemicals; its weight average molar mass was 97K Dalton and its PDI value was 12.3. Modified WO_3 composite with HDPE were melt blended in a twin screw internal mixer (Haake Rheomix model 600p) with mixing speed of 100 rpm at 150℃ for 10 minutes. The blended samples were named 0.5 wt% WO_3-HDPE and 1.0 wt% WO_3-HDPE including 0.5 wt% and 1.0 wt% of tungsten oxide, respectively.

C.2.3 Characterization

Differential scanning calorimetry (DSC) and thermogravimetric analysis (TGA) were performed on a Mettler 30 DSC and TGA to characterize the thermal properties of

the nanocomposite samples. Prior to DSC analysis, samples were dried first at 80℃ in a vacuum oven for 24 hours. Three different samples, homo HDPE, 0.5 wt% WO_3-HDPE and 1 wt% WO_3-HDPE, were used in the test. The nonisothermal crystallization was done by heating the samples from 25℃ to 200℃ at a heating rate of 20 ℃/min and then holding at 180℃ for 10 minutes, prior to be cooled at 4 different cooling rates. In the test, the samples were cooled in a temperature range from 180℃ to 80℃ at the cooling rate of (-1, -3, -5, -7) ℃/min and were heated up again from 80℃ to 180℃ at a heating rate of 10 ℃/min for further tests. A polarized optical microscope (POM) (Olympus BX-51) equipped with a Mettler FP82 HT hot stage and a CCD camera was used to observe the growth of the crystallites. The morphological observations were executed by scanning electron microscopy (SEM, Hitachi S-4700) for the samples coated with platinum in a C-1045 ion sputter coater.

C.2.4. The Seo's method for the nonisothermal crystallization

Since details of the Seo's method for nonisothermal crystallization kinetics analysis were fully explained in our previous publications,[9,13-15] and also briefly explained in Chapter 2. Thus, we omit the detailed explanation in this chapter.

C.3 Results and discussion

C.3.1 Polymerization of HDPE/WO_3 composites

Figure C.1 shows the SEM photos of WO_3 particles, binary mixed composites and in-situ metallocene polymerized composite containing 1 wt% tungsten particles. Tungsten particles are aggregated in the PE matrix for the binary blend due to the heterogeneity between the metal powder and the PE molecules whereas in-situ metallocene polymerized composite shows more uniform distribution of WO_3 particles in HDPE matrix and good adhesion at the interface. EDS analysis was done to check how much HDPE molecules were generated on the WO_3 surface. Figure C.2 shows the EDS element analysis of HDPE modified WO_3 particles. Blue region denotes the presence of carbon element on the surface of the sample. The sample consists of 65.95 wt% of tungsten, 21.04 wt% of oxygen and 13.02 wt% of carbon. Since the carbons are from HDPE polymer, it is easily conjecturable that more than 13.7 wt% of the modified WO_3 particles was HDPE molecules.

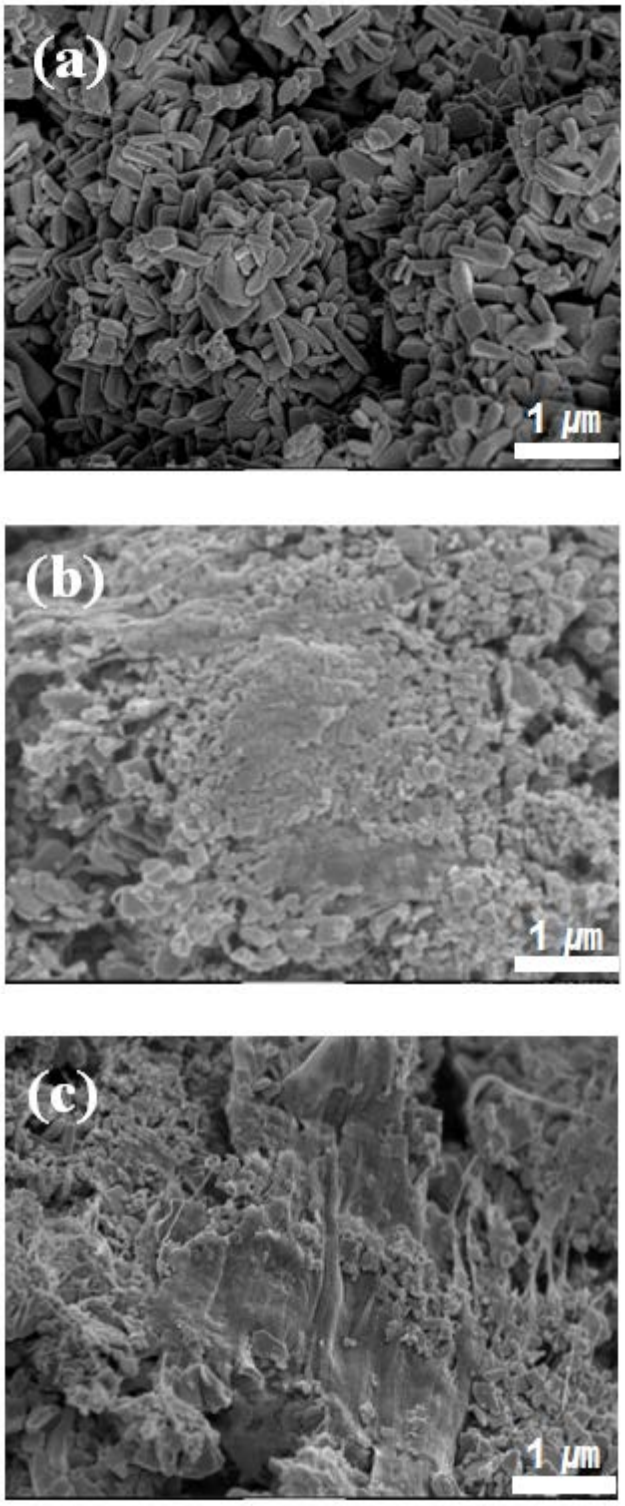

Figure C.1 SEM images of (a) WO_3 particles (b) HDPE-WO_3 binary blend (c) Blend of HDPE and polymerized HDPE-WO_3 (1 wt%) (X20000).

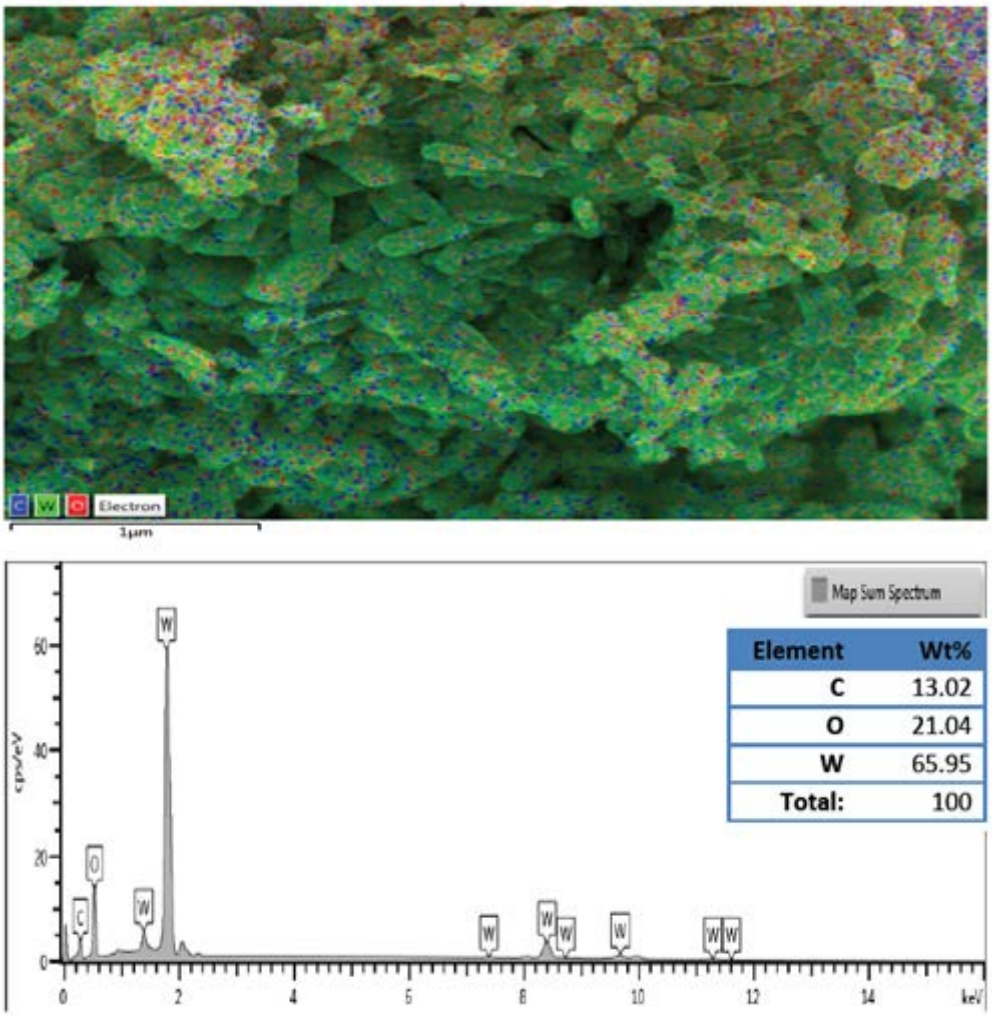

Figure C.2 EDS element analysis of HDPE modified WO_3 particles.

Thermal degradation characteristics of HDPE/WO_3 nanocomposites by TGA are shown in Figure C.3. Although it is known that the thermal degradation of PE that occurs by chain scission can be delayed by adding the fillers,[16] the HDPE/WO_3 composites and the pure HDPE polymer followed almost the same degradation trajectories. On the other hand, the degradation temperature was increased as high as 50℃ for HDPE/MWNT (1.5 wt%) in N_2 atmosphere.[9] A similar result regarding the stabilities of HDPE/MWNT nanocomposites was reported by Li et al.[14] Uniform dispersion and enhanced interfacial adhesion between carbon fillers and the matrix polymer molecules were ascribed to hinder the flux of degradation product and delay the onset of degradation.[9] Though thermal energies were well transferred to metal particles by the strong adhesion between PE molecules and the metal fillers (WO_3), it was not enough to delay the onset of the composite's degradation because of less volume of tungsten due to the high density of the tungsten metal compared to CNT. Its volume portion in the composite was far way down than that of CNT at the same weight of inclusion.

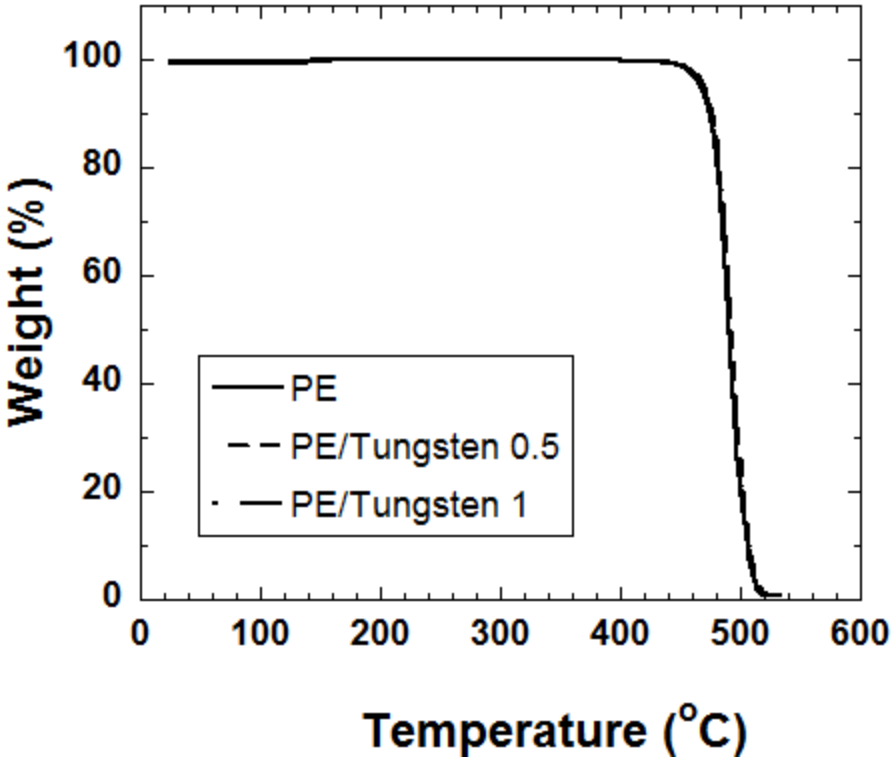

Figure C.3 TGA graphs for homo PE, 0.5 wt% HDPE/WO_3, 1 wt% HDPE/WO_3.

C.3.2 Nonisothermal crystallization of HDPE/WO_3 composites

DSC scans can be seen in Figure C.4. All the samples were cooled from the melt (180℃) with various cooling rates. They exhibit a single crystallization exotherm. However, the onset and peak crystallization temperatures, related to the values of the associated enthalpies as well as the peak broadening effects in nanocomposites, were different from those of neat HDPE.[9] The onset temperatures of the nanocomposites are higher than that of neat HDPE. It is clear that the supercooling needed for the crystallization was much smaller for all in-situ polymerized nanocomposite samples and the crystallization occurred much faster for the composites. This is a direct consequence of the nucleation effect caused by the WO_3. Also, T_{max} of the nanocomposites is higher than that of homo HDPE in all cooling rates implicating that WO_3 act as the nuclei to induce heterogeneous nucleation.[1-9] Since Seo's analysis scheme select the relative crystallinity at the same cooling rate and does not include values from other rates, we can safely exclude the possibility of comparison at different stages, which was applied in the Ozawa analysis.[13,15]

All curves in Figure C.5 display a linear variation of the maximum temperature of the HDPE and nanocomposites crystallization isotherm, T_{max}, with the logarithm of the cooling rates (ln*U*). This is observed in all nonisothermal crystallization process as long as the cooling rate is low (< 7 ℃/min). T_{max} of the nanocomposites was higher than that of the neat PE at the same cooling rate, indicating a faster crystallization for the nanocomposites. The relative crystallinity development of neat PE and nanocomposites of 0.5 wt% WO_3 and 1 wt% WO_3 was obtained after the normalization by dividing the

heat flow axis by the weight of HDPE content in the sample. Figure C.6 shows the changes in the HDPE crystallinity. As the cooling rate goes up, a large fraction of the relative crystallinity occurs after the most rapidly increasing point in the heat flow curve where the kinetics are going to change to a slower process.[9] The presence of WO_3 markedly influences the crystallization behavior of HDPE since PE chains were grown on the surface of the WO_3. The crystallinity of the composites increased with the amount of WO_3. In Table C.1, the melting temperatures of the composites are presented after the second heating. In spite of the content of WO_3 increase, T_m does not show any noticeable changes. This indicates that the presence of WO_3 does not have influence on the lamellar thickness of PE chains but affects the kinetics.[17]

As we expected, the plot of $\ln[-\ln(1-X_v(T)_U)]$ versus $(T-T_{max})$ shown in Figure C.6 gives a straight line with a slope of n/a. The calculated values of the Avrami exponent, *n*, for neat PE are between 2.7 and 3.3, with an average value of 2.98. (Table C.2). This value is close to the characteristic value for spherulitic development arising from athermal instantaneous nucleation.[18] As the cooling rate goes up, the Avrami exponent becomes smaller due to less crystallization time.[18] As shown below, this is consistent with the morphological data. Consistent with the behavior of T_{max} showing a good linear relationship between T_{max} and lnU at low cooling rates, the half crystallization time data, $t_{1/2}$, again indicates that the nanocomposites crystallize faster than the neat PE. The calculated average value of Avrami exponent, *n*, from Figure C.7 is *ca* 4.0 for 0.5 wt% HDPE/WO_3 nanocomposite and 4.1 for 1 wt% HDPE/WO_3 nancomposite. The *n* values approaching 4 means that the encapsulation of WO_3 by in-situ polymerization obviously causes heterogeneous nucleation and creates the growth mechanism of 3-dimensional shape.[18] The result shows a marked contrast to the

Avrami exponent values of HDPE/MWNT composites.[9] For HDPE/MWNT nanocomposites, the calculated average value of the Avrami exponent was 2.56 including 1.5 wt% MWNT, 1.99 including 2.4 wt% MWNT and 1.78 including 7.3 wt% MWNT, respectively. The *n* values approaching 2 means that the encapsulation of MWNT by in-situ polymerization obviously causes heterogeneous nucleation and creates the growth mechanism of the 2-dimensional rod shape while that of HDPE/WO_3 implies heterogeneous nucleation and creates the growth mechanism of 3-dimensional shape.[9,18] As explained below, this is ascribable to the difference of interactions between the filler and HDPE molecules.

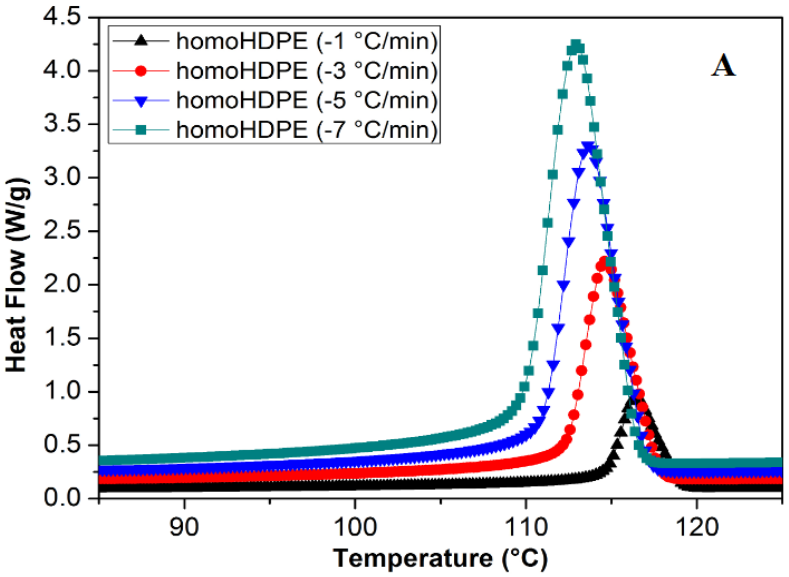
homoHDPE (-1 °C/min)
homoHDPE (-3 °C/min)
homoHDPE (-5 °C/min)
homoHDPE (-7 °C/min)
A
Heat Flow (W/g)
Temperature (°C)
4.5
4.0
3.5
3.0
2.5
2.0
1.5
1.0
0.5
0.0
90
100
110
120

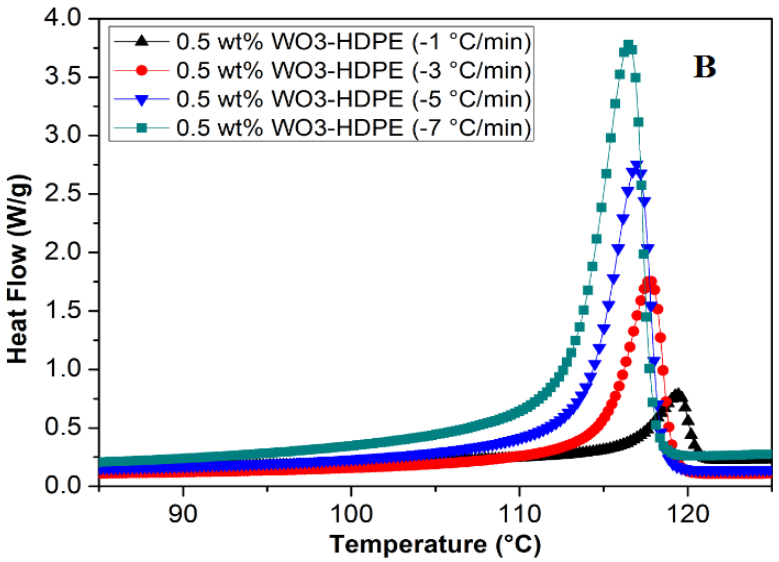
0.5 wt% WO3-HDPE (-1 °C/min)
0.5 wt% WO3-HDPE (-3 °C/min)
0.5 wt% WO3-HDPE (-5 °C/min)
0.5 wt% WO3-HDPE (-7 °C/min)
B
Heat Flow (W/g)
Temperature (°C)
4.0
3.5
3.0
2.5
2.0
1.5
1.0
0.5
0.0
90
100
110
120

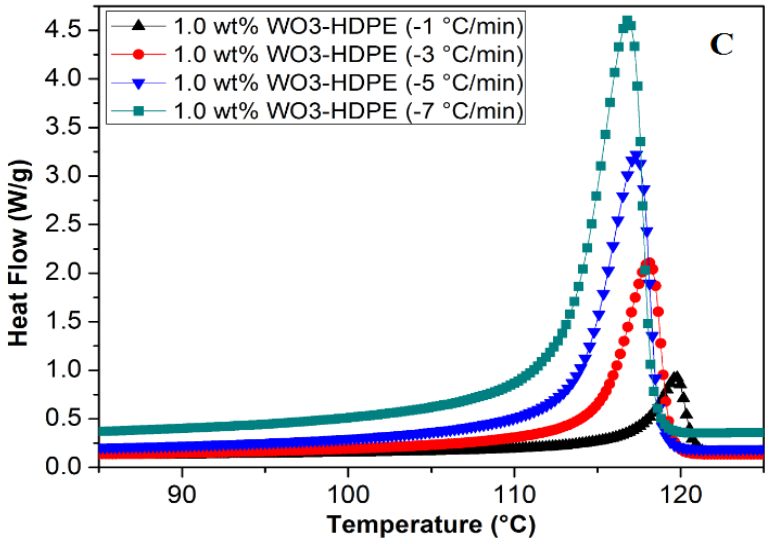

Figure C.4 DSC curves of nonisothermal crystallization at different cooling rates (a) Homo HDPE, (b) 0.5 wt% HDPE/WO_3 composite and (c) 1.0 wt% HDPE/WO_3 composite.

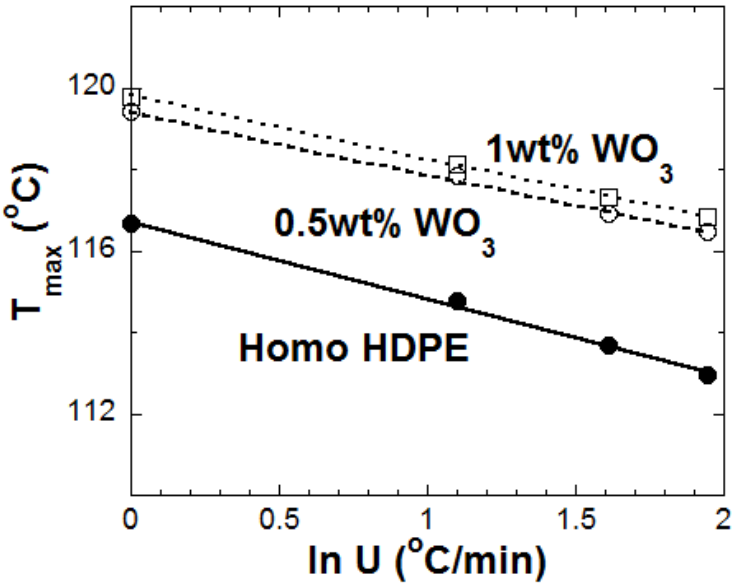

Figure C.5 Evolution of T_{max} as a function of ln*U* (a) homo PE, (b) 0.5wt% PE/WO_3 nanocomposite and (c) 1wt% PE/WO_3 nanocomposite. T_{max} decreases as the cooling rate increases because less time is needed for faster cooling rates.

Sample	T_m (℃)	Crystallinity (%)
Homo PE	128.5	54.8
0.5 wt% PE/WO_3	128.6	62.9
1 wt% PE/WO_3	128.9	68.2

Table C.1 Values of melting temperature and crystallinity of homo PE, 0.5 wt% PE/WO_3 and 1 wt% PE/WO_3.

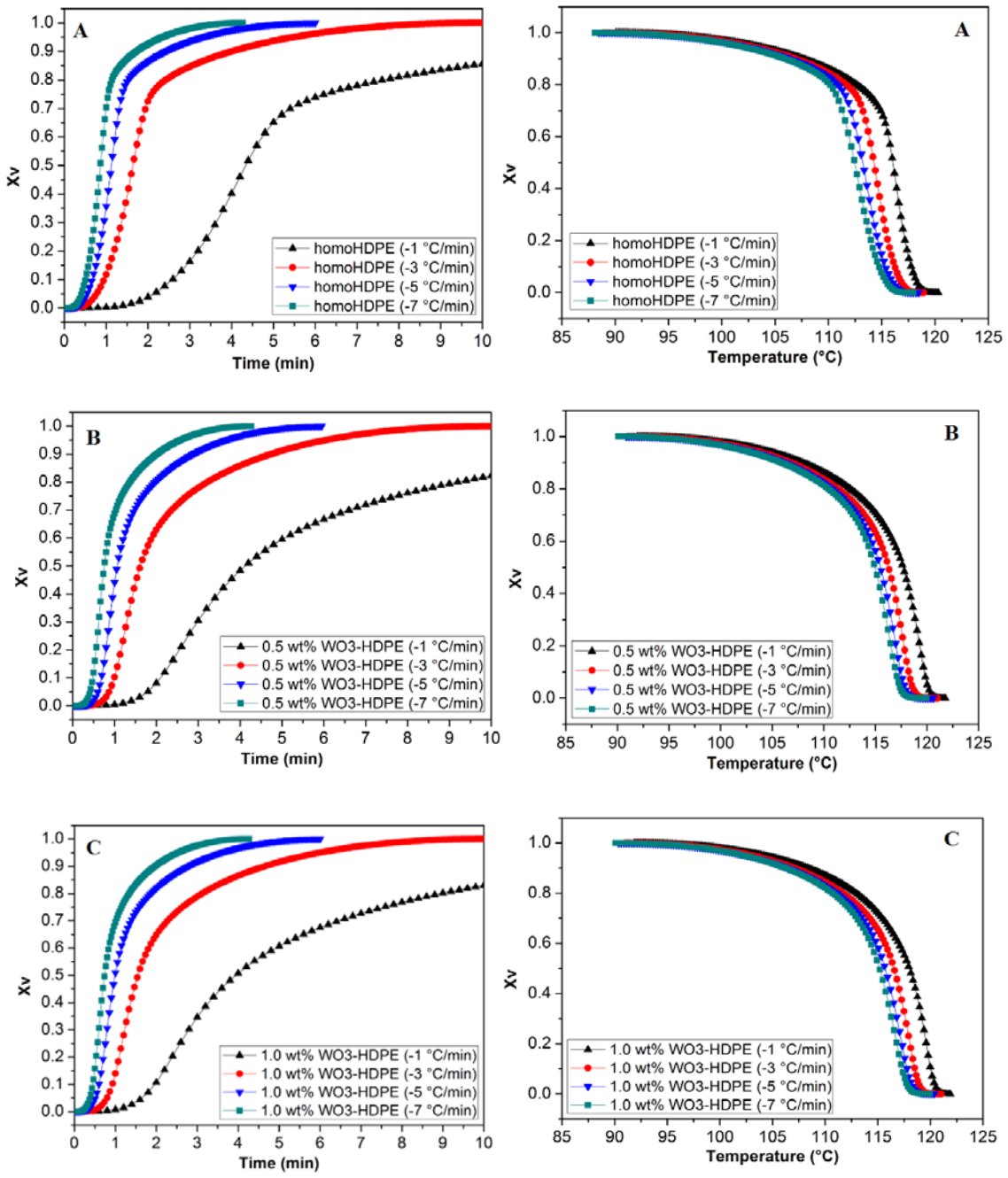

Figure C.6 Development of relative crystallinity, X_v as a function of time and temperature at different cooling rates (a) homo PE, (b) 0.5 wt% PE/WO_3 nanocomposite and (c) 1 wt% PE/WO_3 nanocomposite.

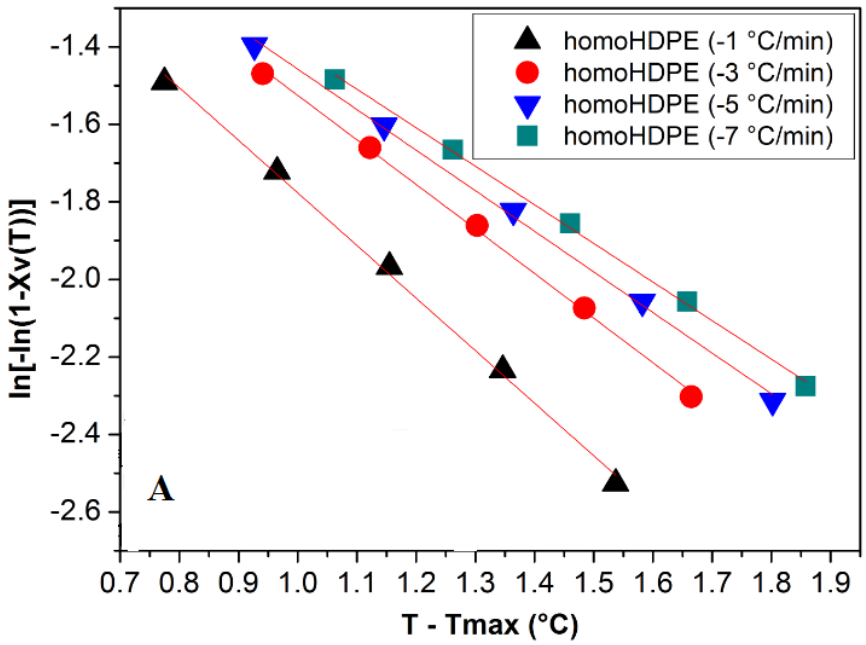
homoHDPE (-1 °C/min)
homoHDPE (-3 °C/min)
homoHDPE (-5 °C/min)
homoHDPE (-7 °C/min)
A
ln[-ln(1-Xv(T))]
T - Tmax (°C)

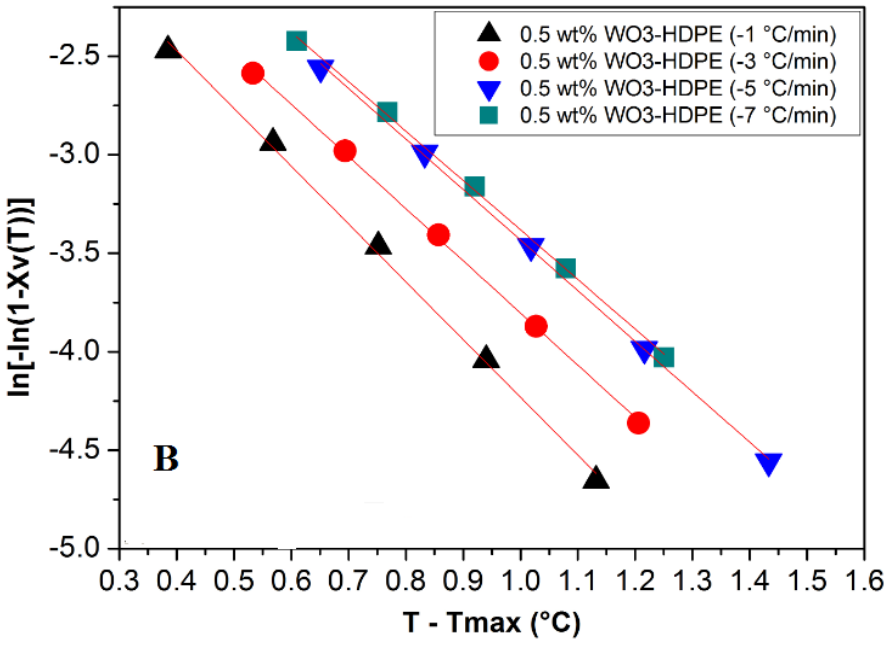
0.5 wt% WO3-HDPE (-1 °C/min)
0.5 wt% WO3-HDPE (-3 °C/min)
0.5 wt% WO3-HDPE (-5 °C/min)
0.5 wt% WO3-HDPE (-7 °C/min)
B
ln[-ln(1-Xv(T))]
T - Tmax (°C)

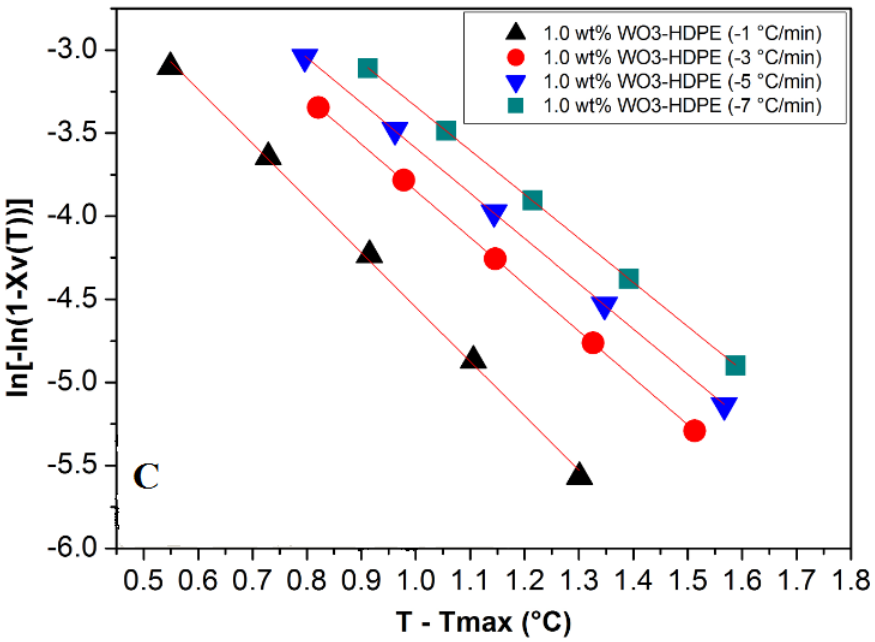

Figure C.7 Plot of ln[-ln(1-X_v(T))] versus T-T_{max} at different cooling rates. (a) homo PE, (b) 0.5 wt% PE/WO_3 composite and (c) 1 wt% PE/WO_3 composite.

Cooling rate (℃/min)	Homo PE		0.5 wt% PE/WO_3		1 wt% PE/WO_3	
	$t_{1/2}$	*n*	$t_{1/2}$	*n*	$t_{1/2}$	*n*
1	4.34	3.3	4.12	4.3	3.94	4.4
3	1.64	3.0	1.62	4.1	1.55	4.2
5	1.12	2.9	1.06	3.9	0.99	4.0
7	0.86	2.7	0.76	3.8	0.74	3.9
average		2.98		4.0		4.1

Table C.2 The half crystallization time,$t_{1/2}$ and Avrami constant, *n*.

C.3.3 Morphology of the HDPE/WO_3 composites

The presence of WO_3 metal particles dramatically increases the number of nucleation sites and thereby decreases the average crystallite size as detected by polarized optical microscopy (Figure C.8 for neat HDPE and Figure C.9 for 1 wt% HDPE/WO_3). HDPE forms large spherulites (20~50 μm) with slightly twisted lamellae in the absence of WO_3. In contrast, the crystal structure in 1 wt% HDPE/WO_3 composites consists of much smaller crystallites (1~5 μm). The crystallites of the HDPE/WO_3 composites did not grow as large as neat HDPE molecules due to the excessive nucleation sites in HDPE/WO_3 composites. This is general to the morphology of heterogeneous nucleated composites.[7,18] Recent experiments about the HDPE/CNT crystallization kinetics have shown that, in addition to the nucleating effect, CNTs were very efficient in templating polymer lamellae to grow perpendicular to the CNT surface in a shish-kebab fashion even under quiescent conditions.[3,9,19] For both in-situ polymerized HDPE/MWNT and in-situ polymerized HDPE/WO_3 nanocomposites, HDPE chains were rooted on the nuclei (MWNT and WO_3) surfaces. However, the CH_2-π interaction between the -CH_2 group of the HDPE polymers in the HDPE/MWNT composites made successive -CH_2 groups gradually attach themselves to the surface, leading to parallel chain adsorption.[11] The PE crystallites then nucleate on the MWNT upon crystallization and grow parallel to the nanotubes whose shape is similar to shish of a shish-kebab morphology of melt-spun PE fibers.[9] On the other hand, the HDPE molecules grown on the WO_3 surface in the HDPE/WO_3 composites do not have much interaction with the tungsten oxide surface nor its preferential orientation

of growth. Rather they try to take the free conformation in the off space from the tungsten surface. Upon crystallization, they take the 3 dimensional chain folding by heterogeneous nuclei to show the Avrami constant values close to 4.[18] As the cooling rate increases, the Avrami index decreases (Table C.2). The faster is the cooling rate, the less time is provided for a molecule to be relaxed and ordered. Thus, high cooling rates means that crystallization occurs at an earlier stage than that for low cooling rates. The chain's movement becomes much slower in later stages due to cooling. Because the number of HDPE roots on the MWNT and WO_3 surface is very high, the crowded HDPE molecules cannot grow to form large crystallites, different from that of neat HDPE (Figures C.8 and C.9). It was similar for HDPE/MWNT nanocomposites that more HDPE molecules have ordered conformation with slow cooling and more HDPE-wrapped MWNTs were formed with increasing concentrations of MWNTs.[9] The other molecules off the wrapped MWNT were still in amorphous state to become involved into the ordered state in later stages by growing vertically on the MWNT surface to form the kebab. Early stage behavior was the same to HDPE/WO_3 nanocomposites that more HDPE molecules have ordered conformation with slow cooling, but the conformation of the ordered molecules does not change much with the cooling time: the morphology of HDPE molecules grown up vertically on the WO_3 surface in the lamellar form in its infant stage stays the same form in its later stages and with higher concentration of WO_3. Hence, the Avrami index values are close to 4, without much variation. The half-crystallization time that increased with the MWNT concentration in HDPE/MWNT nanocomposites because of the ordering difficulties, decreased for HPDE/WO_3 composites due to the high density of tungsten by which the number of tungsten oxide nuclei was not so many as to cause congestion of the HDPE

lamellar growth. However, slight increase of the Avrami exponent with the concentration of WO_3 possibly indicates the appearance of crystalline sheaf formation (Table C.2).[15] From these results, it can be plausibly concluded that polymer chains do not go through conformation adjustment and orientation transformation in the process of the nonisothermal crystallization unless there are interactions between the filler surface and the molecules, though their crystalline size becomes reduced with the foreign nuclei.[3,19,20]

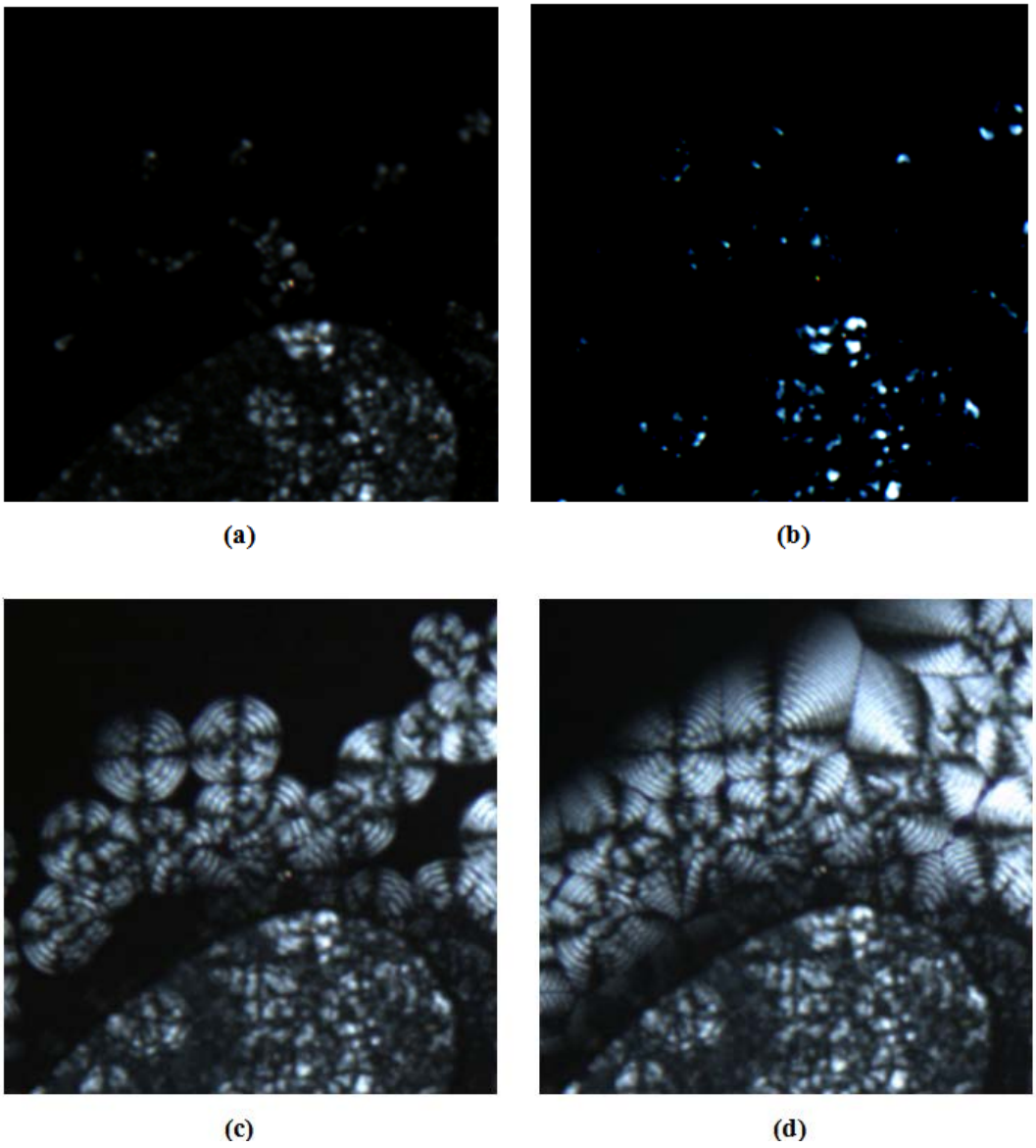

Figure C.8 POM images of homo PE at cooling rate, 3 ℃/min. (a) 118℃ (b) 117℃ (c) 116℃ (d) 115℃ (magnification X400)

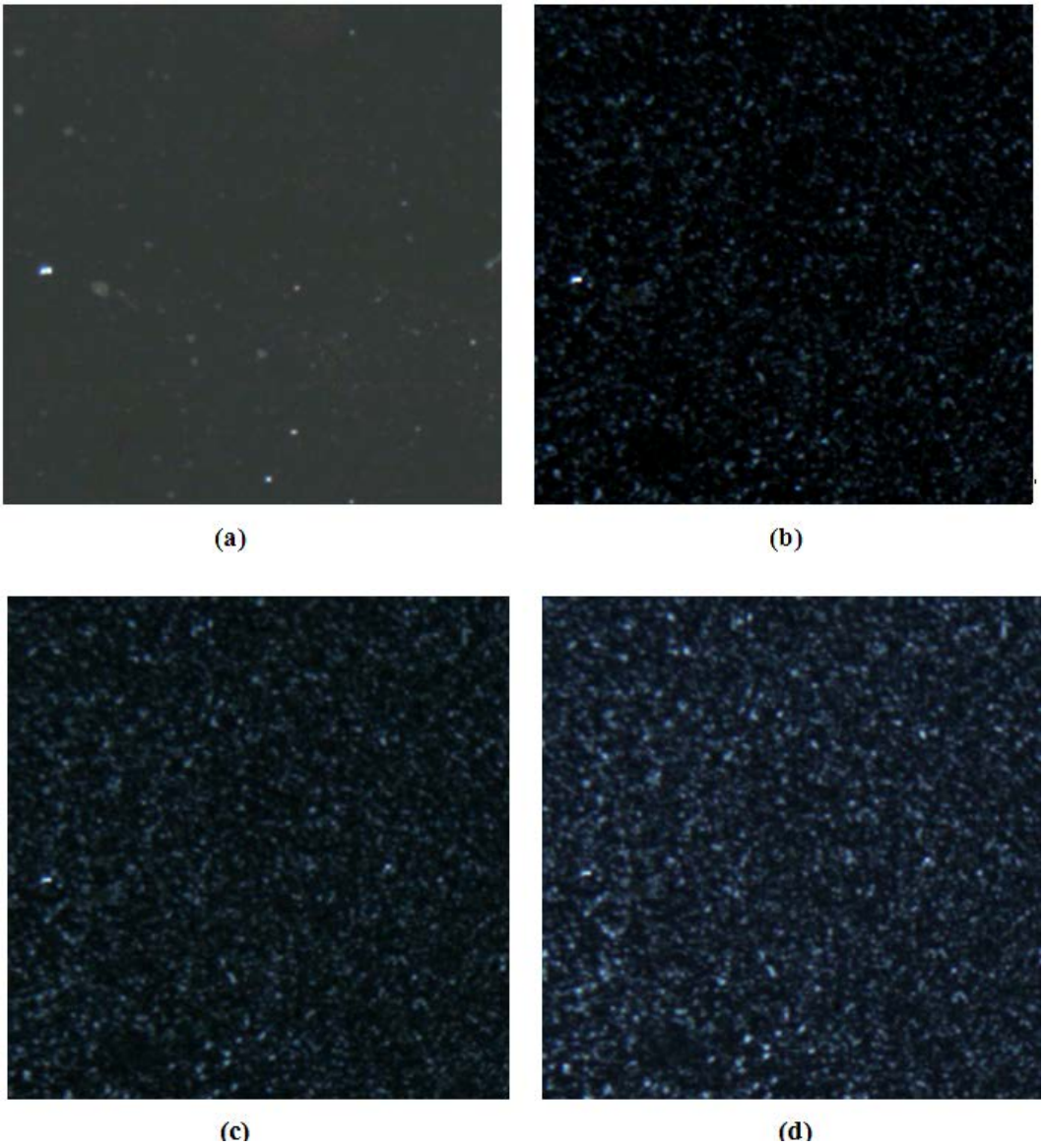

Figure C.9 POM images of 0.5 wt% PE/WO_3 at cooling rate, 3 ℃/min. (a) 118℃ (b) 117℃ (c) 116℃ (d) 115℃ (magnification X400).

C.4 Conclusion

Nonisothermal crystallization analysis of a HDPE and its WO_3 nanocomposites provides some important information that the interaction between the polymer molecules and the heterogeneous nuclei surface decides the crystalline structures of these materials. The Avrami exponent of the pure HDPE was close to 3 indicating that the crystallites had a spherulite structure whereas that of the HDPE/WO_3 composites was close to 4, indicating the heterogeneous nucleation due to encapsulation of WO_3 by HDPE in-situ polymerization and the growth mechanism of 3-dimensional shape. Though the morphology looked similar to that of HDPE/MWNT composites, its detailed morphology development was different from that of HDPE/MWNT nanocomposites. HDPE/MWNT nanocomposites showed HDPE molecules' ordering change with the cooling rates and the concentration of MWNT by the CH_2-π interaction whereas anchoring of HDPE molecules on the WO_3 surface rendered free conformational ordering in the early stage due to no interaction between HDPE and WO_3 surface. This ordering was kept in the same form until the late stages. The Avrami exponent values decreased with the cooling rate, but did not change with the concentration of WO_3. The half crystallization time decreased with the WO_3 amount whereas that was increased for HDPE/MWNT nanocomposites due to the nuclei density difference. The nonisothermal crystallization analysis provides the clue of morphological development history as well as molecular ordering in the nanocomposites.

C.5 References

[1] Vega, J. F.; da Silva, Y.; Vicente-Alique, E.; Nunez-Ramirez, R.; Trujillo, M.; Arnal, M. L.; Muller, A. J.; Dubois, P.; Martinez-Salazar, J. Macromolecules 2014, 47, (16), 5668-5681.

[2] Yang, B.; Ni, H. K.; Huang, J. J.; Luo, Y. Macromolecules 2014, 47, (1), 284-296.

[3] Li, L. Y.; Li, B.; Hood, M. A.; Li, C. Y. Polymer 2009, 50, (4), 953-965.

[4] Li, L. Y.; Li, C. Y.; Ni, C. Y. J Am Chem Soc 2006, 128, (5), 1692-1699.

[5] Uehara, H.; Kato, K.; Kakiage, M.; Yamanobe, T.; Komoto, T. J Phys Chem C 2007, 111, (51), 18950-18957.

[6] Srinivas, S.; Babu, J. R.; Riffle, J. S.; Wilkes, G. L. Polym Eng Sci 1997, 37, (3), 497-510.

[7] Cebe, P.; Hong, S. D. Polymer 1986, 27, (8), 1183-1192.

[8] Seo, Y.; Kim, S. Polym Eng Sci 2001, 41, (6), 940-945.

[9] Kim, J.; Kwak, S.; Hong, S. M.; Lee, J. R.; Takahara, A.; Seo, Y. Macromolecules 2010, 43, (24), 10545-10553.

[10] Hu, X.; An, H. N.; Li, Z. M.; Geng, Y.; Li, L. B.; Yang, C. L. Macromolecules 2009, 42, (8), 3215-3218.

[11] Li, L. Y.; Wang, W. D.; Laird, E. D.; Li, C. Y.; Defaux, M.; Ivanov, D. A. Polymer 2011, 52, (16), 3633-3638.

[12] Kim, J.; Hong, S. M.; Kwak, S.; Seo, Y. Phys Chem Chem Phys 2009, 11, (46), 10851-10859.

[13] Seo, Y. Polym Eng Sci 2000, 40, (6), 1293-1297.

[14] Seo, Y.; Kang, T.; Hong, S. M.; Choi, H. J. Polymer 2007, 48, (13), 3844-3849.

[15] Seo, Y. P.; Oh, K.; Seo, Y.; Hong, S. M. Int J Mater Form 2010, 3, 691-694.

[16] Watts, P. C. P.; Fearon, P. K.; Hsu, W. K.; Billingham, N. C.; Kroto, H. W.; Walton, D. R. M. J Mater Chem 2003, 13, (3), 491-495.

[17] Peacock, A. J. Handbook of Polypropylene: Structures, Properties and Applications, Marcel Dekker, Inc: New York 2000, 376-382

[18] Wunderlich, B. Thermal Characterization of Polymeric Materials (Ed. Turi, A.), Academic Press 1997, Ch. 2

[19] Anand, K. A.; Agarwal, U. S.; Joseph, R. Polymer 2006, 47, (11), 3976-3980.

[20] Haggenmueller, R.; Fischer, J. E.; Winey, K. I. Macromolecules 2006, 39, (8), 2964-2971.